Structures and Properties of Metalloid Al and Ga Clusters Open Our Eyes to the Diversity and Complexity of Fundamental Chemical and Physical Processes during Formation and Dissolution of Metals[†]

Hansgeorg Schnöckel*

Karlsruhe Institute of Technology (KIT), Institute of Inorganic Chemistry, Engesserstrasse 15, Bldg. 30.45, 76131 Karlsruhe, Germany

Contents

1. Preliminary Remarks

Very recently, we have prepared some reviews about metalloid Al/Ga clusters. However, in every case a special topic has been addressed:

1. Metalloid clusters and the renaissance of main group chemistry.[1,2]
2. Metalloid clusters and the development of organometallic chemistry.[3]
3. Metalloid clusters and the structure of the elements.[4−7]

Furthermore, a comprehensive chapter in a book about molecular clusters of the main group elements has been published in 2004.[8] A further comprehensive review presenting the results up to 2008 will be published in a book about

[†] Dedicated to R. Ahlrichs.
* Tel ++49 (0) 721 608 2981, fax ++49 (0) 721 608 4854, e-mail hansgeorg.schnoeckel@kit.edu.
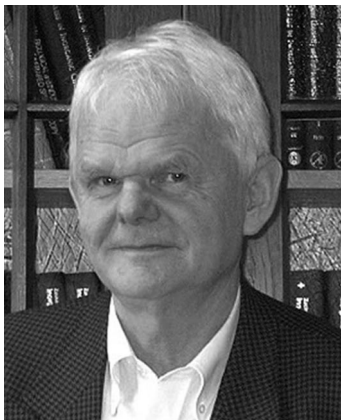
Hansgeorg Schnöckel studied chemistry at the University of Münster, where he gained his Ph.D. under H. J. Becher in 1970. Subsequently, he started spectroscopic matrix investigations of reactive high-temperature molecules, which were the basis for later synthetic work. In 1987, he became professor, and in 1989, he moved to the University of Munich. From 1993 to 2007, he has held the chair for analytical chemistry at the University of Karlsruhe; retired from professional life, he is professor emeritus.

the chemistry of group 13 elements in the near future.[9] Therefore, the aim of this contribution is not to present a further comprehensive review but to address the following points.

By combining selected former results with very recent ones, we will try to bring across the following message: because of the thermodynamical instability of metalloid clusters as intermediates toward the bulk base metals as well as to their reaction products with fragments of the ligand shell to, for example, salt-like $[AlN]_n$ or $[AlO]_n$ clusters, a classical synthesis could not be expected to be successful. Even now, a successful generation of metalloid clusters via a highly sophisticated disproportionation and trapping method introduced by us more than 20 years ago seems, also in a retrospect, to be a miracle. Therefore, (a) the low yield from this cluster formation process is not unexpected, and (b) the chemistry of metalloid clusters as any research for application cannot be in the center of interest at the moment; however, the discussion of structure, bonding, mechanism of formation, and properties of metalloid clusters is most challenging today. These results will open our eyes to the complexity and the fundamental principles of a simple-seeming chemistry, for example, the dissolution and the formation of metals. Moreover, many results obtained so far (e.g., the electrical behavior of crystalline compounds containing metalloid clusters) may be essential topics for the next decades, in order to prepare novel metal-rich materials with unusual properties and also in the area of nanosciences.

2. Introduction

Most elements of the periodic table are metals. Their chemistry and especially their formation and dissolution belong to the oldest chemical technology, which has played a central role in the evolution of mankind. In general, however, only the bulk metals themselves, on the one hand, and their stable compounds (e.g., salts, oxides, or sulfides in solution or in bulk), on the other hand, are well-known. Thus, it seems strange that intermediates in the formation and breaking of metal−metal bonds are mostly unknown, although, as mentioned above, this process has had a vital role in the evolution of the planet in general and of human life in particular. These fundamental processes of formation

as well as dissolution of metals and of identification of molecular intermediates exhibiting metal−metal bonding are central to this review.

These molecular intermediates are mostly addressed as "metal atom clusters".[10,11] However, since Cotton's original definition is not restricted to species containing mainly metal−metal bonding, we have introduced the term "metalloid clusters".[6,12,13] Such clusters contain more metal−metal contacts than metal−ligand bonds and mostly show similarities with respect to the topology of the arrangements of atoms in the elements themselves. How these clusters are integrated in the whole field of classical and modern inorganic chemistry will be presented in section 3.

In section 4, we will describe the relation of metalloid clusters to isolated naked metal atom clusters in the gas phase under high vacuum conditions; the discussion extends to some reactions of the naked Al_{13}^- metal atom cluster, which as a singular model for the bulk metal sheds a new light on the dissolution process of metals. A suitable tool that provides snapshots of elementary steps during these metal−metal bond cleavage processes in the gas phase is Fourier transform ion cyclotron resonance (FT-ICR) mass spectrometry.

After discussing the dissolution process of metals via investigations on naked Al clusters, we turn in section 5 to the formation process of metals: metalloid clusters as intermediates on the way from the salts to the metals provide snapshots for this fundamental process. Most investigations on metalloid cluster species have been and are still performed in the field of precious metals (e.g., Au, Pd, etc.).[14−16] This is due to their relatively straightforward synthesis, their stability, and their inertness, even in air and sometimes also in water. However, it seems to be extremely difficult to obtain crystalline materials in order to characterize these compounds via crystal structure analysis. The metalloid cluster compounds of precious metals are not the subject of this review. However, in view of the many synthetic results for these clusters, with few detailed structure determinations on the one hand and the failure previously to synthesize clusters of base metals on the other hand, it came as a great surprise when in 1997 a metalloid cluster $[Al_{77}\{N(SiMe_3)_2\}_{20}]^{2-}$, **1**, was discovered containing 77 Al atoms, of which 57 were "naked" and only 20 were ligand-bearing (Figure 1).[17]

This result was first assumed to be a singularity or a curiosity.[18] However, as this review seeks to make clear, such is not the case. Rather an exciting story has developed from
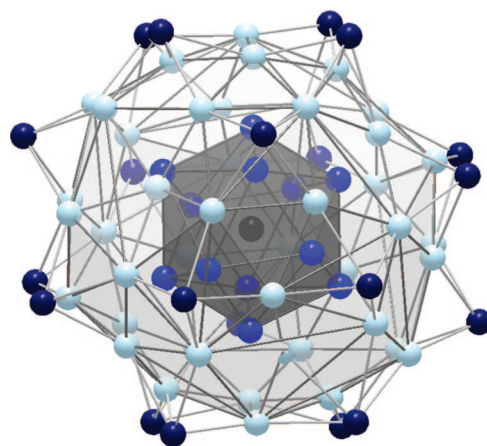
Figure 1. Shell-like representation of the arrangement of the 77 aluminum atoms inside the metalloid cluster $[Al_{77}\{N(SiMe_3)_2\}_{20}]^{2-}$ (**1**).

this starting point and one that is likely to have a significant impact on the development of chemistry in general.

In section 5 are also discussed the formation of an AlAl σ bond (section 5.1) and the preparation of metalloid Al and Ga clusters, that is, of clusters of base metals (section 5.2). However, because details have been presented in other reviews, we will concentrate on fundamental points as well as on some recently published investigations on an alternative thermodynamically favored decomposition route of Al(I) and Ga(I) compounds (section 5.3). Furthermore, the significance of the metalloid cluster $Al_{50}Cp^*_{12}$, **2**,[19] as an intermediate on the way from the textbook molecule $Al_4Cp^*_4$, **3**,[20] to bulk Al, which has been shown recently, is also discussed in section 5.

In section 6, we will present some selected metalloid Al and Ga clusters in order to show the most important aspects: similarities and differences from the structure of the metals, hints to hypothetical Al/Ga modifications, drastic changes caused by doping, that is, by addition of electrons or substitution by atoms of neighbor elements, and metalloid clusters as hints for the importance of the jellium model to understand the bonding in these clusters.

Finally, in section 7, interactions of metalloid Al/Ga clusters in the crystalline state, for example, the unexpected electrical conductivity and superconductivity, are discussed.

In order to show the relation of metalloid Al/Ga clusters to similar clusters of the other elements a short section (section 8) about recently published Ge clusters and the giant $Au_{102}R_{44}$ cluster has been included.

After the summary and outlook (section 9), all compounds and clusters discussed here are collected in a table including their references as an appendix, section 12.

3. Metalloid Clusters and Their Relation to Classical and Modern Inorganic Chemistry and to Zintl-like Clusters

We have described clusters that contain both ligand-bearing and naked metal atoms that are bonded only to other metal atoms as *metalloid*[6,7,12,13] or, more generally, *elementoid*, to express, in accordance with the Greek word ειδος (ideal, prototype), the notion that the ideal form or the motif of the solid structure of the metal or element can be recognized in the topology of the metal atoms in the cluster. The original limits of the term *metalloid*, used, for example, for the elements silicon and germanium, which are metal-like with respect to certain macroscopic properties (e.g., metallic luster), were extended to include the metalloid clusters, thus accessing an additional structural level, which can be gained only by crystal structure analysis. In general, such metalloid clusters contain more direct metal−metal contacts than metal−ligand contacts. This means that metalloid clusters represent a subgroup of the extensive metal-atom cluster group in which, according to Cotton's definition,[11] nonmetal atoms may also be present, and therefore molecular clusters like $Cu_{146}Se_{73}(PPh_3)_{30}$[21] and similar very large clusters can be regarded as metal atom clusters, though "salt-like" clusters might be a more appropriate term.

Thus, there are three different types of metal atom clusters: the naked metal atom clusters that are present under ultrahigh vacuum conditions (see section 4), the metalloid clusters, which are the main subject of this review, and finally the giant "salt-like" clusters described, for example, by the groups of Fenske and Müller.[22,23] The topological relations
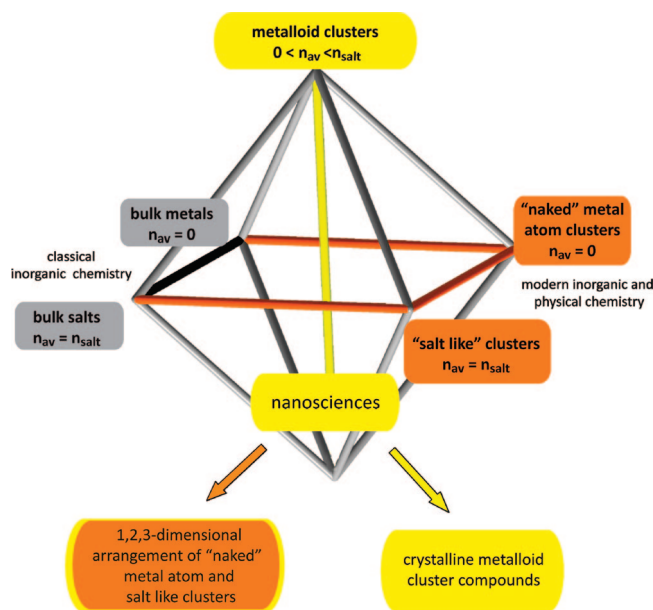
Figure 2. Interrelation among the three different types of metal atom cluster, the bulk phase of the metals and their salts, and nanosciences; n_{av} is the average oxidation state of the metal atoms.

of all these types of metal atom clusters are collected and illustrated in a very recent review.[24] Figure 2 visualizes the relation between these three types of clusters and presents a correlation with classical inorganic chemistry of the bulk phases of the metals and their salts.[25]

Consequently, the three types of metal atom clusters can be regarded as intermediates of a cyclic process between the metals and their salts. The metalloid clusters represent the most complex type of cluster, because a highly mixed valence situation exists for the metal atoms, resulting in an average oxidation number between zero and the oxidation number of the salts. This falls between the much "simpler" situations of naked metal atom clusters (oxidation number 0) and the "salt-like" metal atom clusters (oxidation number n_{salt}). How the three types of metal atom clusters relate to the wider field of nanoscience is also visualized in Figure 2. However, it should be mentioned that, because of the sophisticated methods needed for the preparation of metalloid clusters, the great majority of published results on nanosized metal atom clusters are based on investigations with either naked metal atom clusters or salt-like clusters.[26]

Though the metal cluster species of Zintl ions are excluded in this contribution, because the formation of metalloid molecular cluster compounds shows clear differences from that of Zintl-like phases, which have been investigated so successfully in recent years by Corbett and others,[27] a few aspects and some recently published results should be mentioned here. Although there is a certain topological similarity to metalloid clusters, as described herein, the Zintl-like metal cluster units (e.g., $Tl_{13}{}^{10-}$ in $Na_4K_6Tl_{13}$[28]) carry high negative charges that are stabilized in a "sea" of positive cations. The preparative method established for the Zintl-like phases begins typically with the elemental metal, which is reduced with an electropositive metal (often an alkali metal), leading to the "extraction" of small parts from the infinite crystal lattice structure of the metal. This reduction process is responsible for the negative values of the average oxidation state of the clusters in which the chemical bonding and electron count can mostly be explained by Wade's rules

Scheme 1. The MOs of Al_4^{2-} and $Al_4H_4^{2-}$ Showing the HOMOs (a_{2u}) down to the HOMO-5 and HOMO-8 (both a_{1g}) with the Relation between the Lone Pairs of Al_4^{2-} and the Localized AlH Bonds of $Al_4H_4^{2-}$ Visible
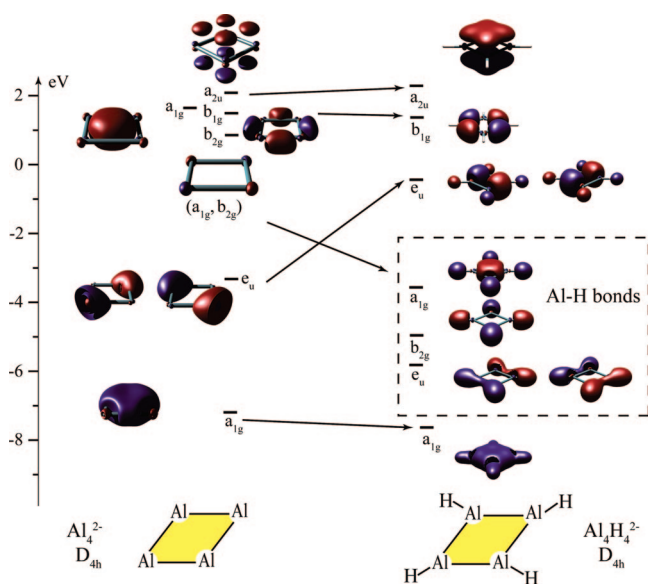
or the Zintl–Klemm concept.[29−31] Thus, oxidation of Zintl anions proceeds by coupling of clusters[32,33] toward the bulk element[34−37] and via further oxidation to metalloid clusters and finally to the salt-like species. In addition, the cations located in the immediate vicinity of the anionic units lead to physical properties[38] for these Zintl phases differing significantly from those of the molecular, ligand-protected metalloid clusters.

In order to get a deeper feeling for the differences between these two types of cluster compounds, we extended our efforts after the detection of Al_4H_6[39,40] and during the investigations on an Al_4R_6 cluster.[41]

The $Ga_4R''_4^{2-}$ cluster[42] (Ga oxidation state +0.5) and the hypothetical Zintl-like Al_4^{2-} species[43,44] (Al oxidation state −0.5) provide two experimentally detected simple examples to make visible the similarities and differences between the chemistries of the Zintl ions (mostly stabilized in ionic solids with an overall negative oxidation state of the metal atoms) and the metalloid clusters (exhibiting oxidation states between 0 and +1). The similarities seem plausible via the bonding descriptions of Al_4^{2-} and the hypothetical $Al_4H_4^{2-}$ (Scheme 1).[45]

The sequence and the shape of MOs with respect to the AlAl bonds are similar for $Al_4H_4^{2-}$ and Al_4^{2-} (Scheme 1). However, the important difference between these two species is the high energetic position of the two additional lone pairs (a_{1g} and b_{2g}) for the Zintl ion, Al_4^{2-}, in contrast to the low-energy position of the four electrons localized in the four AlH bonds of $Al_4H_4^{2-}$. Therefore, it is not surprising that the calculated reaction of Al_4^{2-} with four H atoms is strongly exothermic ($\Delta E \approx -1300$ kJ mol^{-1}).

Thus, though the negative oxidation numbers in Zintl-like metalloid clusters (e.g., −0.5 in Al_4^{2-}) and the slightly positive oxidation numbers in the molecular metalloid clusters protected by bulky ligands seem to be only a formal aspect, comparison of the MOs of Al_4^{2-} and hypothetical $Al_4H_4^{2-}$ and the energy relation between these species convincingly shows the higher stability of the ligand-protected clusters, which, in accordance with the presented bonding type, can be handled in solution, even with nonpolar

solvents. In contrast, Zintl clusters have a high reduction potential, with a negative unprotected charge on the surface of the ions, causing a high reactivity (e.g., the strong association with positively charged species in any equilibrium solution). Thus, though there are similarities between Zintl ions and metalloid clusters with respect to bonding between the metal atoms, there are not only formal differences (oxidation number) but also differences in principle between the two kinds of metalloid clusters. Consequently, it seems to be a highly ambitious challenge for further investigations to stabilize "naked" pure Al_n^- cluster ions such as the Al_4^{2-} anion and the prototypical jellium cluster Al_{13}^{-46} as salt-like compounds. Therefore, supported by the above-mentioned stabilization via ligand bonding, the chance to observe clusters of this kind experimentally, for example, as crystalline compounds, increases in going from Al_4^{2-} to $Al_4H_4^{2-}/Al_4R_4^{2-}$, and finally to the Al_4H_6[39]/Al_4R_6 molecules,[41] that is, stability increases via step by step oxidation.

At the end of this introduction, some short remarks on very recent ongoing investigations on an $Al_{12}K_8R_{18}$[47] cluster may be allowed. This cluster may represent the common link between metalloid clusters on the one hand and Zintl/Wade clusters (a molecular $Al_{12}K_8$ Zintl phase?) on the other hand; that is, perhaps this latest result may be the starting point for investigations to a novel unified concept for the description of bonding within the entire field of metal-to-metal atom clusters.

4. Reactions of the Al_{13}^- Cluster As a Model for the Dissolution of Bulk Al

Because of its outstanding electronic and topological situation among all the other elements and within the field of Al_n clusters, the Al_{13}^- cluster and its chemistry are outlined here in a separate section. Its relation to metalloid clusters and to the bulk phase is discussed first, before two selected gas-phase reactions are described in more detail.

4.1. The Relation to Metalloid Clusters[48,49]

To understand the bonding and structure within the group of metalloid cluster compounds calls first for some introduction to naked metal atom clusters in the gas phase and how they relate to metalloid cluster compounds. This relation between metalloid and naked metal atom clusters became evident for the first time in a study of the successive fragmentation of the structurally characterized metalloid cluster anion $Ga_{19}R_6^-$ [R = $C(SiMe_3)_3$], **4**,[12] in the gas phase:[48]

$$[Ga_{13}(GaR)_6]^- \rightarrow [Ga_{13}]^- + 6GaR \qquad [R = C(SiMe_3)_3]$$

It was possible to study this reaction as the crystalline compound containing the metal atom cluster $Ga_{19}R_6^-$, **4** (Figure 3), stands out from other metalloid cluster compounds in being soluble in organic solvents without decomposition.[12] Additionally, solubilized $Ga_{19}R_6^-$ can be transferred intact to the gas phase through the mild method of electrospray ionization. For the first time, then, fragmentation reactions of a *structurally characterized metalloid cluster* (see section 6) could be investigated in the gas phase.

Hence it emerged that collisions between the gaseous molecules induce fragmentation reactions, where the car-benoid GaR units are split off one after another, until only the naked Ga_{13}^- core is left (Figure 4). This demonstrates
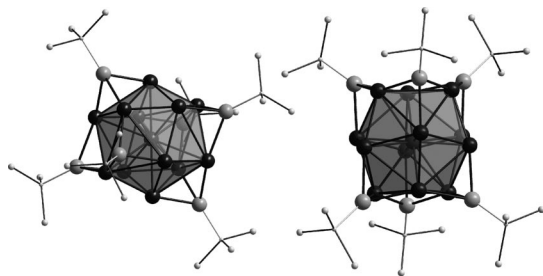
Figure 3. Two different representations of the $[Ga_{13}(GaR)_6]^-$ cluster $[R = C(SiMe_3)_3]$ (**4**) and its Ga_{13} core based on a cuboctahedral or an icosahedral geometry. The six ligand-bearing Ga atoms are gray; the central Ga atoms are black.
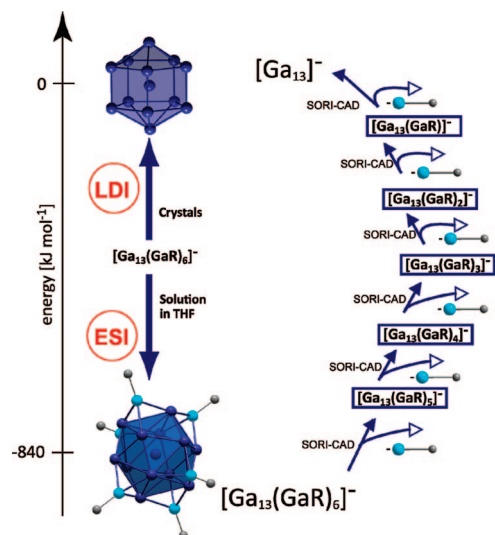
Figure 4. By electrospray ionization (ESI), $[Ga_{13}(GaR)_6]^-$ clusters (**4**) can be transferred entirely to the gas phase; the fragmentation pattern of the $[Ga_{13}(GaR)_6]^-$ cluster after collisionally induced dissociation (SORI-CAD) is displayed. Ga_{13}^- can also be obtained by laser desorption ionization (LDI) of crystals containing $[Ga_{13}(GaR)_6]^-$.

that the ensemble of GaR units containing oxidized Ga atoms (oxidation state +1) must be considered as a protecting ligand shell for the Ga_{13}^- core, by analogy with CO ligands coordinating to precious metal clusters. With respect to the bonding situation, this demonstrates that $[Ga_{13}(GaR)_6]^-$ **4** does *not* consist of a metal atom core with a high positive charge (Ga_{19}^{5+}) that is surrounded by six negatively charged R^- units. Instead, it should be regarded as a ligand-covered Ga_{13}^- ion, which is an outstandingly stable cluster ion because of its closed shell configuration (jellium, 40 electrons, cf. Al_{13}^-, section 4.2). This interpretation is corroborated by laser desorption/ionization experiments on solid crystals containing $[Ga_{13}(GaR)_6]^-$, **4**,[49] where only Ga_n^- clusters were observed mass spectrometrically, with a dominant signal group that could be assigned to the preeminently stable Ga_{13}^-. Thus, all the GaR units were obviously lost during the aggressive laser vaporization process (Figure 4).
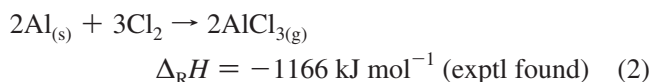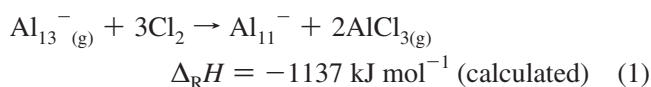
Very recently, we have successfully confirmed the stepwise fragmentation of the $Ga_{13}(GaR)_6$ cluster: The $Ga_7(GaR)_6$ cluster anion with identical ligands $[R = C(SiMe_3)_3)]$ exhibits the same fragmentation behavior:[50] $[Ga_7(GaR)_6]^- \rightarrow Ga_7^- + 6GaR$.

4.2. Relation to the Bulk Phase

The special electronic structure of Al_{13}^-, the lighter congener of Ga_{13}^-, has been discussed in many mass spectrometric and quantum chemical investigations.[51−54] Furthermore, there have been numerous investigations of the reactivity of Al_{13}^-: very prominent are two *Science* contributions detailing the reactions with HI and I_2 that give rise to some provocative statements about superatoms and a new periodic system of cluster species.[55,56] In this spirit, Al_{13}^- has been called a superhalide atom,[55,56] the high electron affinity (EA) of neutral Al_{13} of 3.6 eV being similar to those found for chlorine and fluorine atoms: Cl = 3.6 eV; F = 3.4 eV (the EA of Ga_{13} is calculated to be 3.4 eV[49]).

However, because Al_{13}^- exhibits a geometry of the central atom (icosahedrally surrounded by 12 aluminum atoms) not very different from the cuboctahedral geometry of the bulk metal itself, its chemical reactions have been investigated with the aim of determining whether Al_{13}^- may be a molecular model for the reactions of the bulk metal.[2] Such a model for any reaction occurring on a solid surface would be an asset, because metal surfaces cannot be realistically reproduced with respect to the topology of atoms at the atomic range. A priori, this idea of a molecular model for reactions on metal surfaces seems to be utopian since major differences between the reaction sequences of Cl_2 with Al_{13}^- and of Cl_2 with an Al surface are to be expected. When Cl_2 molecules come into contact with an Al surface, Al−Cl bonds are formed in an exothermic reaction. Simultaneously with the formation of many Al−Cl bonds, the temperature rises, and finally, at high temperatures, every additional Cl_2 contact leads to the formation of $AlCl_3$, which is then eliminated into the gas phase; that is, Al metal disappeared in a Cl_2 atmosphere, and $AlCl_3$, as Al_2Cl_6, sublimes to the cooler parts of the reaction vessel.[57] At lower Cl_2 pressures (e.g., under vacuum conditions), the heated Al metal reacts to form AlCl molecules, which are stable high-temperature species (see section 5.2).[58] Altogether, during the chlorination of Al metal, a variety of reactions proceeds on the metal surface, depending markedly on the reaction conditions. In contrast to these very complex reaction sequences, the situation after a single collision of a Cl_2 molecule with an Al_{13}^- cluster should be much clearer and easier to understand. But is this a realistic model system? Under UHV conditions, the first reaction step of Cl_2 and Al_{13}^- leads to a highly vibrationally excited or "hot" $Al_{13}Cl_2^-$ intermediate, which spontaneously ejects two AlCl molecules to form the smaller Al_{11}^- cluster: $Al_{13}Cl_2^-{}_{(g)} \rightarrow Al_{11}^-{}_{(g)} + 2AlCl_{(g)}$. Despite the principal differences between the chlorination of Al_{13}^- and of Al metal, that is, only a few reaction steps versus a complex reaction cascade, a surprising similarity emerges, at least with respect to the thermodynamics of the reactions (eqs 1 and 2[59]):

$$Al_{13}^-{}_{(g)} + 3Cl_2 \rightarrow Al_{11}^- + 2AlCl_{3(g)}$$
$$\Delta_R H = -1137 \text{ kJ mol}^{-1} \text{ (calculated)} \quad (1)$$

$$2Al_{(s)} + 3Cl_2 \rightarrow 2AlCl_{3(g)}$$
$$\Delta_R H = -1166 \text{ kJ mol}^{-1} \text{ (exptl found)} \quad (2)$$

Since this similarity of thermodynamic properties applies only to the Al_{13}^- cluster, the very special electronic structure of this cluster (jellium model),[60−64] as well as its highly symmetric arrangement (i.e., a double magic behavior) with a topological similarity to the bulk metal, is critical. In order to visualize the 40 electron jellium system for Al_{13}^- (13 × 3 + 1), the energy diagram for a Na_{40} cluster is presented in
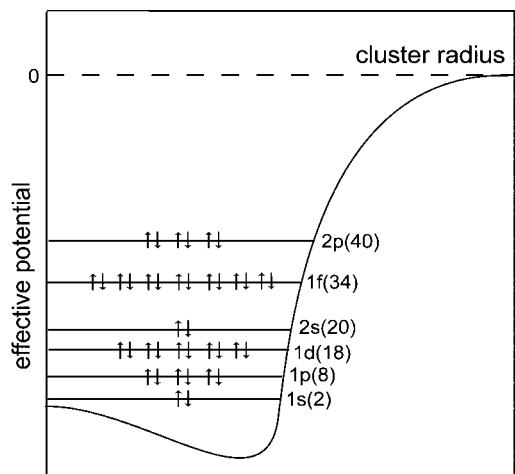
Figure 5. The jellium model for the 40 valence electrons of the Na$_{40}$ cluster exhibiting delocalized electron shells.
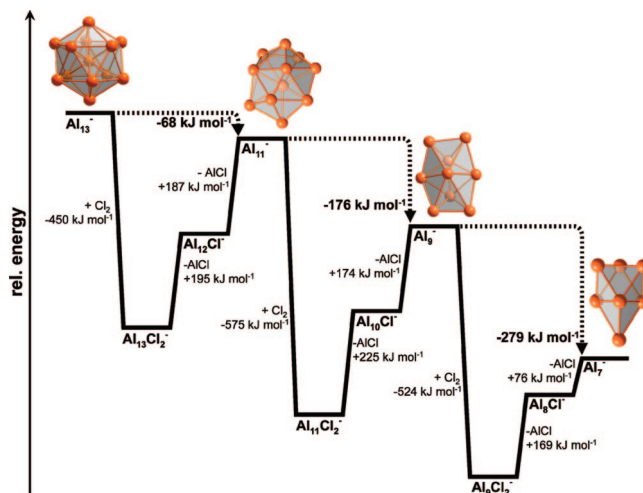

Figure 6. Schematic energy diagram for degradation of the Al$_{13}^-$ cluster in the presence of Cl$_2$; the energy values are given in kJ mol^{-1}.

Figure 5.[60–67] The high concentration of single Na$_x$ clusters (x = 8, 20, 34, 40, ...) under mass spectrometric conditions were the experimental basis for the introduction of the jellium model in cluster chemistry. Concerning the topology of the Al atoms in Al$_{13}^-$ clusters and in the bulk metal, a central Al atom is surrounded by 12 additional Al atoms, arranged icosahedrally in Al$_{13}^-$ and cuboctahedrally in the metal. However, the adoption of Al$_{13}^-$ as a model for Al metal in the reaction with Cl$_2$ and in other reactions to be described becomes more plausible if the energy needed to remove two Al atoms from an Al$_{13}^-$ cluster is compared with the corresponding energy change in the case of the bulk metal (eqs 3 and 4[59]):

$$Al_{13}^-{}_{(g)} \rightarrow Al_{11}^-{}_{(g)} + 2Al_{(g)}$$
$$\Delta_R H^\bullet (0\ K) = +698\ kJ\ mol^{-1}\ \text{(calculated)} \quad (3)$$

$$2Al_{(s)} \rightarrow 2Al_{(g)} \qquad \Delta_R H^\bullet (0\ K) = +654 \pm 8\ kJ\ mol^{-1}$$
$$\text{(exptl found)} \quad (4)$$
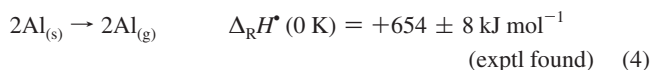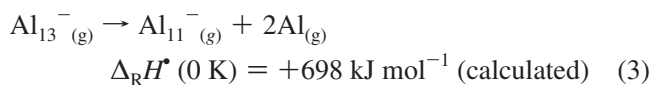
Thus, the energy needed for the removal of two Al atoms either from an Al$_{13}^-$ cluster or from bulk aluminum is almost identical, within the margins of error. Consequently, Al atoms are the energetically equivalent reference system, and therefore all reactions of Al$_{13}^-$ clusters and Al metal should be very similar with respect to their energy balance.[68] In the following reactions of Al$_{13}^-$, it becomes more evident that, besides this thermodynamic similarity to the bulk, there are plausible reasons for believing that similar primary steps are involved in reactions of Al$_{13}^-$ and in those on an Al surface. On these grounds, Al$_{13}^-$ emerges as a viable molecular model for the reaction kinetics of elementary reaction steps on an Al surface.

4.3. The Chlorination of the Al$_{13}^-$ Cluster and the Stepwise Formation of Its Intermediate Products, Al$_{11}^-$, Al$_9^-$, and Al$_7^-$ [2 68]

The primary reaction steps of Al$_{13}^-$ clusters in a Cl$_2$ atmosphere are described in the following. Upon exposure of Al$_{13}^-$ ions to a chlorine atmosphere of approximately 10^{-8} mbar, new signals, attributed mainly to Al$_{11}^-$, Al$_9^-$, and Al$_7^-$, were observed in the mass spectra after several tens of

seconds.[46,68,69] These new species arise in the following stepwise reaction sequence (eq 5):

$$Al_{13}^- \xrightarrow[-2AlCl]{Cl_2} Al_{11}^- \xrightarrow[-2AlCl]{Cl_2} Al_9^- \xrightarrow[-2AlCl]{Cl_2} Al_7^- \quad (5)$$
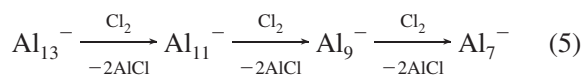
Based on these experiments and on the results of theoretical calculations, an understanding of the energetics of the stepwise elementary reactions occurring during the course of the reaction has been achieved (Figure 6). In the first step, oxidation of the Al$_{13}^-$ cluster surface proceeds to form the intermediate product [Al$_{13}$Cl$_2$]$^-$*. The resulting reaction energy of this step is around −450 kJ mol^{-1}, according to density functional calculations. This leads to vibrational and rotational excitation energy trapped in the [Al$_{13}$Cl$_2$]$^-$* cluster that cannot be removed by collisions at pressures around 10^{-8} mbar. This, in turn, results in fragmentation of [Al$_{13}$Cl$_2$]$^-$* into Al$_{12}$Cl$^-$ and AlCl in the next step after a lifetime of only several nanoseconds, as predicted by phase space theory.[69–71] In the next step, Al$_{12}$Cl$^-$* also fragments, ejecting AlCl once again and leaving Al$_{11}^-$. For this reaction channel, the lifetime of Al$_{12}$Cl$^-$* is estimated to be several tenths of a second. Because the rate constant for the reaction is k_L = 0.09 s^{-1} in the pressure range prevailing, an Al$_n^-$ cluster molecule collides with a chlorine molecule every 10 s on average, and these will react to form an Al$_{n-2}^-$ cluster within another 0.1 s, according to the lifetime estimates. So only the anionic Al cluster anions Al$_{13}^-$, Al$_{11}^-$, etc., were detected by their mass spectra.

The standard energy change of the first reaction (Al$_{13}^-$ → Al$_{11}^-$) is −68 kJ mol^{-1}. In principle, the corresponding reactions of Al$_{11}^-$ and Al$_9^-$ are taking place in the same way. However, their reaction energies, at −176 and −279 kJ mol^{-1}, respectively, are significantly more exothermic than that for the Al$_{13}^-$ → Al$_{11}^-$ process.[72] The reaction path presented here for the interaction of Al$_n^-$ cluster ions with Cl$_2$, resulting in the release of AlCl as the main product, is a plausible model for the corresponding reaction of bulk aluminum metal and chlorine. Moreover, the similarities between the bulk metal and Al$_{13}^-$ cluster for the removal of two Al atoms (698 and 654 kJ mol^{-1}) are reflected in the corresponding chlorination reactions (eqs 6a, 6b, 6c). The neutral Al$_{13}$, as well as the investigated anionic Al$_{13}^-$ cluster, can thus be considered as well-matched model compounds

for investigations of primary reactions on the surface of bulk aluminum.

$$Al_{13}^-{}_{(g)} + Cl_2 \rightarrow Al_{11}^-{}_{(g)} + 2AlCl_{(g)}$$
$$\Delta_R H^{\circ}{}_{(0\,K)} = -68 \text{ kJ mol}^{-1} \quad (6a)$$

$$2Al_{(s)} + Cl_2 \rightarrow 2AlCl_{(g)}$$
$$\Delta_R H^{\circ}{}_{(0\,K)} = -103 \pm 12 \text{ kJ mol}^{-1} \quad (6b)$$

$$Al_{13(g)} + Cl_2 \rightarrow Al_{11(g)} + 2AlCl_{(g)}$$
$$\Delta_R H^{\circ}{}_{(0\,K)} = -113 \text{ kJ mol}^{-1} \quad (6c)$$
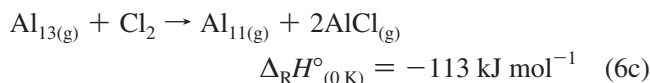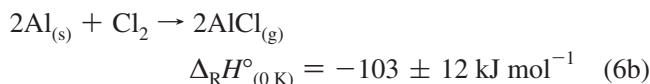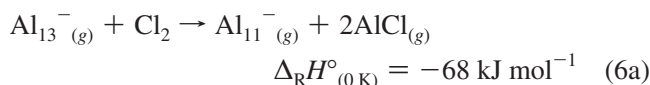
It follows that the chlorination of bulk aluminum metal must also proceed primarily by the addition of Cl_2 and the release of AlCl. The subsequent reaction in which AlCl is converted to $AlCl_3$ will take place with the release of a reaction energy that is several times higher (-534 kJ mol^{-1}). Consequently, the cumulative reactions (eqs 7a, 7b, 7c), which yield $AlCl_3$ as the final product, reflect the character of Al_{13}^- as a molecular model for the bulk metal:

$$Al_{13}^-{}_{(g)} + 3Cl_2 \rightarrow Al_{11}^-{}_{(g)} + 2AlCl_{3(g)}$$
$$\Delta_R H^{\circ}{}_{(0\,K)} = -1084 \text{ kJ mol}^{-1} \quad (7a)$$

$$2Al_{(s)} + 3Cl_2 \rightarrow 2AlCl_{3(g)}$$
$$\Delta_R H^{\circ}{}_{(0\,K)} = -1166 \pm 6 \text{ kJ mol}^{-1} \quad (7b)$$

$$Al_{13(g)} + 3Cl_2 \rightarrow Al_{11(g)} + 2AlCl_{3(g)}$$
$$\Delta_R H^{\circ}{}_{(0\,K)} = -1145 \text{ kJ mol}^{-1} \quad (7c)$$
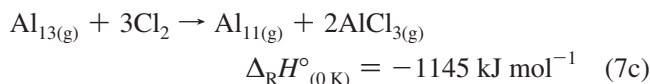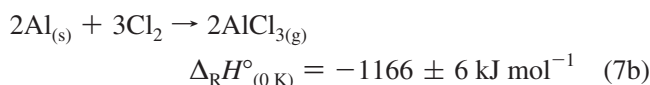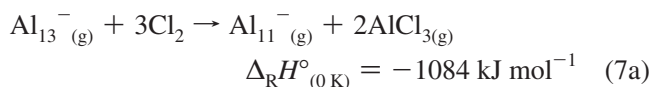
To sum up, the kinetics of the Al_n^- intermediates in the reaction sequence arising from the $Al_{13}^- + Cl_2$ reaction in an excess of chlorine can be explained in terms of association−elimination reactions, where the association reactions occur with a rate near the Langevin limit. Statistical rate theory calculations show that the experimentally observed degradation in double steps is likely to be due to a sequential elimination of two AlCl molecules from the highly excited associated clusters, for which average lifetimes have been calculated.[69] The primary steps of the chlorination of Al_n^- are fast; that is, they proceed before the next contact between the cluster anion and a chlorine molecule takes place. Furthermore, since the generated AlCl molecule will react fast and strongly exothermically with additional Cl_2 gas (excess) to $AlCl_3$ species as final products, these results represent a quantified kinetic model for the primary steps within the chlorination of metals, that is, of one of the oldest technical chemical processes.

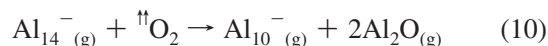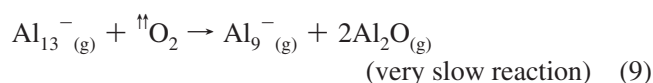## 4.4. Reactivity of the Al_{13}^- Cluster Anion with Triplet and Singlet Oxygen: The Role of Spin-Conservation[2,46]

When aluminum cluster anions Al_n^- (or cations) are exposed to normal (triplet) oxygen, those with an odd number of aluminum atoms react significantly more slowly than do those with an even number (see Figure 7).[46] This odd/even effect is further emphasized by studies of mass-selected clusters.

Thus, Al_{13}^- clusters, when exposed to O_2 ($10-8$ mbar), did not react even after 600 s; essentially no reaction products
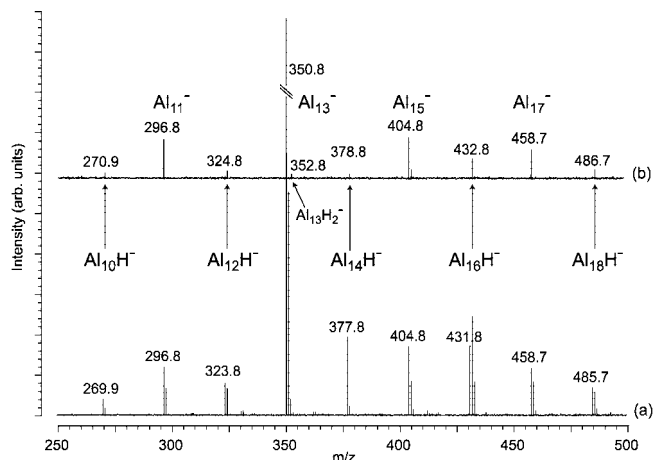
Figure 7. Typical FT-ICR mass spectrum after laser-desorption/ionization of LiAlH$_4$: (a) the distribution of aluminum cluster anions (Al_n^-) is displayed (directly after cluster generation); (b) in the presence of oxygen, all the Al_{even}^- anions are etched away.

were observed, and the initial Al_{13}^- signal remained strong (eq 9). On the other hand, mass-selected Al_{14}^- clusters were observed to react spontaneously under the same conditions to give Al_{10}^- and two Al_2O molecules (eq 10). Strikingly, then, the reaction of Al_{13}^- plus triplet oxygen (denoted hereafter by $^{tt}O_2$) is extremely slow.

$$Al_{13}^-{}_{(g)} + {}^{tt}O_2 \rightarrow Al_9^-{}_{(g)} + 2Al_2O_{(g)}$$
$$\text{(very slow reaction)} \quad (9)$$

$$Al_{14}^-{}_{(g)} + {}^{tt}O_2 \rightarrow Al_{10}^-{}_{(g)} + 2Al_2O_{(g)} \quad (10)$$

4.4.1. Spin Conversion

To elucidate this odd/even effect for Al_n^- clusters, the influence of spin conservation has been investigated, the influence of spin having been noted previously for reactions between O_2 and aluminum surfaces.[73−78] With its 40 valence electrons (closed shell), the spin multiplicity of the ground state of the Al_{13}^- cluster is a singlet (labeled as $^{lt}Al_{13}^-$). By contrast, $^{t}Al_{14}^-$ has a doublet ground state due to its one unpaired electron. During O_2 attack, an adduct is formed initially where $^{tt}O_2$ is associated on the cluster surface (denoted, for example, by $^{tt}[Al_{13}\cdot O_2]^-$). Therefore, eqs 9 and 10 can be dissected into the following primary steps (eqs 9a and 10a):

$$^{lt}Al_{13}^- + {}^{tt}O_2 \rightarrow {}^{tt}[Al_{13}\cdot O_2]^- \qquad -0.36 \text{ eV} \quad (9a)$$

$$^{t}Al_{14}^- + {}^{tt}O_2 \rightarrow {}^{t}[Al_{14}\cdot O_2]^- \qquad -2.76 \text{ eV} \quad (10a)$$
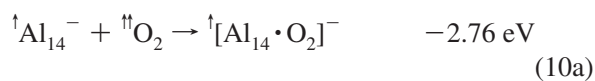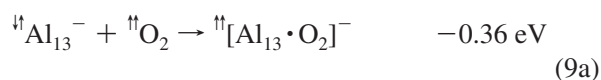
As a result of spin conservation restrictions,[79] $^{tt}[Al_{13}\cdot O_2]^-$ is formed in a triplet state and $^{t}[Al_{14}\cdot O_2]^-$ in a doublet state, so that the reactions are spin-allowed. Subsequently, any further reaction of these adducts, in which the oxygen molecule dissociates on the surface of the cluster, causing heating (reaction energy) and leading to fragmentation of the cluster, may be accompanied by a barrier and, if necessary, by a spin flip process (eqs 9b and 9c).

$$^{\uparrow\uparrow}[Al_{13} \cdot O_2]^- \rightarrow \rightarrow \ ^{\downarrow\uparrow}Al_{13}O_2^-$$

spin transition and formation of covalent Al−O bonds

$$(9b)$$

$$^{\uparrow\uparrow}[Al_{13} \cdot O_2]^- \rightarrow \ ^{\downarrow\uparrow}Al_9^- + 2Al_2O \qquad (9c)$$
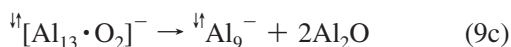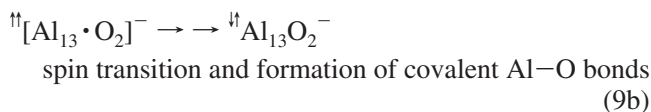
For $^{\uparrow\uparrow}[Al_{13} \cdot O_2]^-$, this barrier is well-defined: it is the crossing point of the triplet/singlet potential energy surface (PES), since the final fragments, Al_9^- and Al_2O, are both singlet species. Additionally, there must be a spin flip for $^{\uparrow\uparrow}[Al_{13} \cdot O_2]^-$, which is likely to have a low probability since the required spin−orbit coupling in the case of light metals like aluminum is expected to be small.[79] Thus, the direct formation of $^{\downarrow\uparrow}[Al_{13} \cdot O_2]^-$ (singlet state) from Al_{13}^- and $^{\uparrow\uparrow}O_2$ is spin-forbidden (eq 9d).

$$^{\downarrow\uparrow}Al_{13}^- + \ ^{\uparrow\uparrow}O_2 \qquad \cancel{\longrightarrow} \qquad ^{\downarrow\uparrow}[Al_{13} \cdot O_2]^- \qquad (9d)$$

In the case of Al_{14}^-, on the other hand, no such spin transition needs to occur since the $^{\uparrow}[Al_{14} \cdot O_2]^-$ initially formed can react without spin restrictions via $^{\uparrow}Al_{14}O_2^-$ to form the products $^{\uparrow}Al_{10}^-$ and Al_2O (eqs 10b and 10c):

$$^{\uparrow}[Al_{14} \cdot O_2]^- \rightarrow \rightarrow \ ^{\uparrow}Al_{14}O_2^-$$

formation of covalent Al−O bonds $\quad (10b)$

$$^{\uparrow}Al_{14}O_2^- \rightarrow \ ^{\uparrow}Al_{10}^- + 2Al_2O \qquad (10c)$$
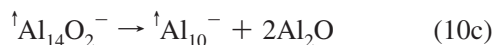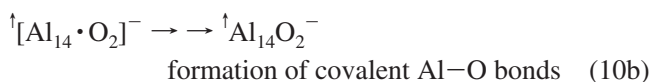
It is to be expected, therefore, that reactions of aluminum clusters with $^{\uparrow\uparrow}O_2$ should show diminished rates if the initially formed O_2 adduct is a triplet and the final products are singlets.

4.4.2. Reactions of Al_{13}^- with Singlet O_2

In order to substantiate this idea experimentally, the spin state of the aluminum-containing reactants is first manipulated by preparing aluminum hydride cluster anions, Al_nH^- (whereas Al_{13}^- exhibits a singlet ground state, HAl_{13}^- exhibits a doublet ground state),[46,80] and exposing them to $^{\uparrow\uparrow}O_2$. It was then found that all $Al_{odd}H^-$ react rapidly with $^{\uparrow\uparrow}O_2$, whereas $Al_{even}H^-$ proved to be inert. *Thus the reactivity pattern was dramatically inverted relative to the behavior of Al_n^-*; for example, $Al_{13}H^-$ reacted, even though Al_{13}^- (and $Al_{13}H_2^-$) were relatively unreactive, whereas the initial $Al_{14}H^-$ signal remained unchanged, while the Al_{14}^- signal decayed.[46,80]

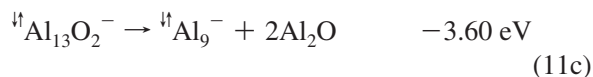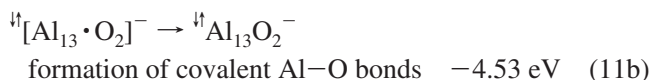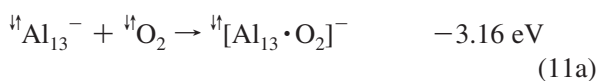Second, the spin of O_2 was changed by generating singlet oxygen ($^{\downarrow\uparrow}O_2$), and it was allowed to react with Al_{13}^- and other odd Al_n^- clusters. In the reaction of Al_{13}^- with $^{\downarrow\uparrow}O_2$, the primary product $^{\downarrow\uparrow}[Al_{13} \cdot O_2]^-$ in its singlet state is expected to be formed (eq 11a). In the course of further reactions going through $^{\downarrow\uparrow}Al_{13}O_2^-$ (where O atoms are covalently bound) to the products, Al_9^-, and two Al_2O molecules, all the reaction steps are spin-allowed (eqs 11b and 11c). In comparison with the reactions with $^{\uparrow\uparrow}O_2$, no spin transition is needed, and therefore no

$$^{\downarrow\uparrow}Al_{13}^- + \ ^{\downarrow\uparrow}O_2 \rightarrow \ ^{\downarrow\uparrow}[Al_{13} \cdot O_2]^- \qquad -3.16 \text{ eV}$$

$$(11a)$$

$$^{\downarrow\uparrow}[Al_{13} \cdot O_2]^- \rightarrow \ ^{\downarrow\uparrow}Al_{13}O_2^-$$

formation of covalent Al−O bonds $\quad -4.53$ eV $\quad$ (11b)

$$^{\downarrow\uparrow}Al_{13}O_2^- \rightarrow \ ^{\downarrow\uparrow}Al_9^- + 2Al_2O \qquad -3.60 \text{ eV}$$

$$(11c)$$

deceleration of the reaction is expected. This assumption was proven experimentally when Al_{13}^- was treated with a mixture of $^{\downarrow\uparrow}O_2$ and $^{\uparrow\uparrow}O_2$, leading to a significant acceleration of the reaction rate when compared with the reaction with pure $^{\uparrow\uparrow}O_2$.

It follows that all the experiments indicate spin conservation to have a significant impact on the reactivity of aluminum clusters and oxygen, the findings being supported by quantum chemical calculations and summarized in Figure 8. To model the odd/even effect, it is assumed that the overall reaction, where an Al_n^- cluster is degraded to a smaller fragment by oxygen, is a multistage process. In the initial step, O_2 interacts with the cluster to form an "adduct", which further dissociates into the products Al_{n-4}^- and $2Al_2O$.

Thus, in accordance with the experiments, the large exothermic energies calculated for the primary steps of all the spin-allowed processes is reflected in fast reactions (eqs 10, 11a−11c). By contrast, for the spin-forbidden reactions (e.g., eq 9), there is a 2-fold control of kinetics. First, starting from the ground state of the triplet primary product, the system must provide enough energy to reach the crossing point of the triplet/singlet PES, that is, surmount an energy barrier, and second, the spin flip, a very unlikely process for these clusters, has to proceed.[81] There is a lack of reliable methods to calculate the height of this barrier. However, for similar reactions in organic chemistry, a value of about 0.8 eV is indicated.[82,83] Therefore, spin-forbidden reactions are retarded for different reasons. Particularly stable systems such as Al_{13}^- do not release the required amount of energy upon educt formation (-0.36 eV), and therefore both factors (barrier + spin flip) are likely to be responsible for the slow reaction rate. By contrast, the spin-forbidden reaction of $^{\downarrow\uparrow}Al_{14}H^-$, like most less stable $Al_{even}H^-$ clusters, releases sufficient energy upon initial product formation (e.g., $^{\uparrow\uparrow}[HAl_{14}O_2]^-$, -1.43 eV) easily to overcome the energy
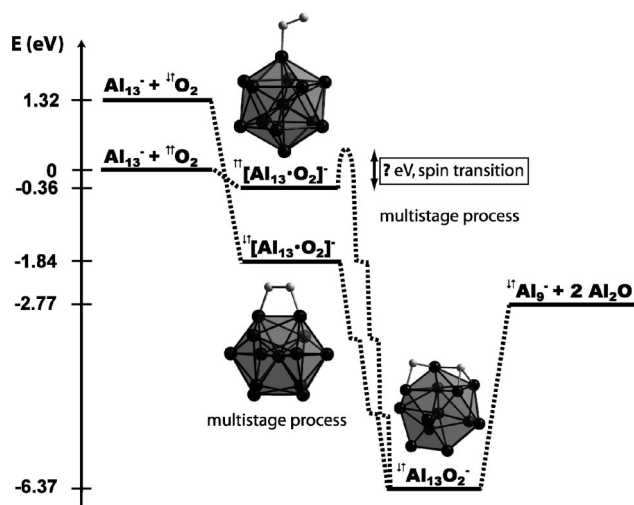
Figure 8. Energy diagram for the interaction of $^{\downarrow\uparrow}O_2$ and $^{\uparrow\uparrow}O_2$ on the Al_{13}^- cluster surface. The transition from $^{\uparrow\uparrow}[Al_{13} \cdot O_2]^-$ to $^{\downarrow\uparrow}Al_{13}O_2^-$ is assumed to be a multistage process, in which the spin state changes from triplet to singlet and the O_2 is bound side-on first and then the O−O bond is disrupted and new Al−O bonds are formed (μ^3). In addition, the further degradation to Al_9^- and two Al_2O molecules is displayed.

barrier where the unlikely transition between the two spin surfaces can occur; the kinetics are therefore entirely governed by the spin flip process.

This means that the observed inertness of Al_{13}^- clusters in a triplet O_2 atmosphere can be traced back to spin conservation restrictions. The results obtained via FT-ICR mass spectrometry may initiate further experiments in different areas[84] (environmental, biological, medical, material, or energy sciences), where reactions with O_2 are important and where a proper understanding of primary steps should not be underestimated.

5. Metalloid Al and Ga Clusters as Intermediates on the Way from the Salts to the Metals

The primary step of every metal cluster formation is the formation of a single, for example, AlAl bond. Snapshots on this way are presented first (section 5.1). Second, for the synthesis of many of the metalloid clusters discussed, the techniques of cryochemistry are essential, that is, trapping of a high-temperature species such as AlCl together with an excess of a suitable solvent in order to form a metastable solution of, say, AlCl (section 5.2). The metastable solution reacts on warming to give the thermodynamically stable products, metal (Al) and trihalide ($AlCl_3$), and during this process metalloid clusters $M_nX_{<n}$ with an increasing number of metal atoms are formed on the way to the bulk metal. Hence, with an average oxidation state between 0 and +1 for the metal atoms of the metalloid cluster compounds and in the light of the method of formation, these compounds can be viewed as intermediates on the way to the bulk metal. Therefore, size-dependent effects might be directly detectable. Apart from the investigation of these metalloid cluster compounds, studies of ligand-free "naked" metal clusters, detected in the gas phase under high-vacuum conditions, present the most common source of experimental information in the development of an understanding of how size affects the physical properties of metals from atoms via nanoparticles to the bulk phase. For the most part, however, no experimentally derived structural information is available for these gas-phase species, although quantum chemical calculations have provided an important supplement to such investigations, particularly in questions of topology.[65,85] In order to secure experimental details of the structure and to determine the physical properties of structurally known metal atom clusters, leading to structure/property relations, such clusters must be protected by ligands, leading to metalloid cluster compounds, which might then be made available in a crystalline form.

Thus, with the help of metalloid clusters as intermediates between the metal salt and the bulk metal, it should be possible to obtain insights into the elementary processes of dissolution and formation of metals. To clarify such fundamental issues, however, detailed information on many metalloid clusters with different numbers of "naked", non-ligand-bearing metal atoms in the cluster core is imperative. Additionally, physical data for nanostructured metalloid cluster compounds can be reliably interpreted only when a uniform and known arrangement of metal atoms in the cluster framework is present. It follows that crystalline compounds of metalloid clusters, where only one compound of known composition and structure is present, are the primary prerequisite for all investigations.

The next step in gaining a deeper understanding of nanostructured materials depends on being able to isolate the individual structurally determined cluster unit from the crystal lattice and then to determine the physical properties of the single clusters in question. This long-term objective has been partially achieved in the gas-phase investigations of the structurally characterized $Ga_{19}R_6^-$ cluster [R = C($SiMe_3$)$_3$], **4** (see sections 4.1 and 6.4).[48,49] Further investigations of isolated nanoscaled species, for example, with microscopic methods applied to Al and Ga clusters or with the help of quantum chemical calculations, are important tasks for the near future.

Besides these general aspects concerning structure and bonding of metalloid clusters, there will be presented two other subsections here: an unexpected alternative thermodynamical favored decomposition route for Al(I) and Ga(I) compounds (section 5.3) and the essential role of the metalloid cluster $Al_{50}Cp^*_{12}$, **2**, for the kinetic stability of $Al_4Cp^*_4$, **3** (section 5.4).

5.1. Snapshots during the Formation of AlAl σ Bonds[86,87]

The formation of metalloid clusters proceeds via the formation of an increasing number of metal to metal bonds. However, this primary process does not seem to be trivial, because the first molecular compound exhibiting an AlAl σ bond was found only 20 years ago.[88] In a very recent paper, we have now published two Al_2R_4 (R = PtBu$_2$) molecules as snapshots on the way to an AlAl σ bond.[86,87] In a first step, this process was investigated quantum chemically (as summarized in Figure 9).

Accordingly, highly energetic [AlR_2]$^\bullet$ species (R = PtBu$_2$) should dimerize under formation of a so far unknown biradical intermediate RAl†(μ-R$_2$)Al†R, **5** (C_i symmetry),[86] with a long Al···Al separation of ca. 3.5 Å and with both unpaired electrons residing in p-type orbitals (SOMOs) localized on both Al atoms. These triplet molecules **5** can formally undergo a spin flip procedure, followed by a disrotatory ring closure leading to closed-shell bicyclic molecules RAlR$_2$AlR, **6** (C_2 symmetry), as thermodynamically stable species (σ bond formation). This process is
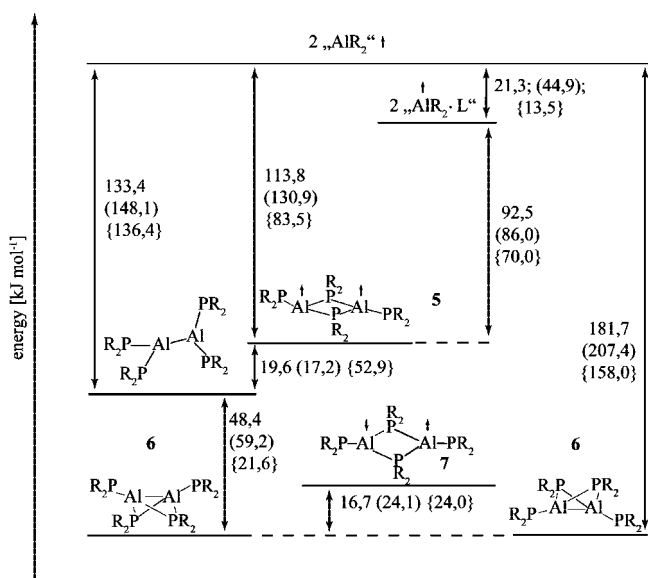
Figure 9. Relative energies (kJ mol^{-1}) for the [Al_2(PtBu$_2$)$_4$] isomers **5** and **6** and the transition state **7** with respect to the radical [Al(PtBu$_2$)$_2$]$^\bullet$ ("AlR$_2$$^\bullet$") and the Et$_2$O-stabilized radical {AlR$_2$†L} at the DFT/def2-TZVP//DFT/def2-TZVP† level of theory with DFT = BP86, (TPSS), and {B3LYP}.

Figure 10. Crystal structures of **5** and **6**. The experimental and calculated (in parentheses; BP86/def2-TZVP[†]) distances [Å] and angles [deg]: **5**, Al1−Al2 3.508 (3.462), Al1−P1 2.399 (2.391), Al1−P2 2.478 (2.450), Al2−P2 2.458 (2.439), Al1−P2−Al2 90.5 (90.2); **6**, Al1−Al2 2.587 (2.618), Al1−P1 2.370 (2.406), Al1−P2 2.422 (2.452), Al2−P2 2.362 (2.398), Al1−P2−Al2 65.4 (65.3).

Figure 11. Layer assembly of the biradical molecules in the crystal structure of [Al$_2$(PtBu$_2$)$_4$], **5**. Al blue, P yellow, C dark gray. The plane-to-plane distance of 8.915 Å corresponds to the length of the a axis in the unit cell.

Scheme 2. Intermediates in the Formation of 5 and 10 by Substitution Reactions (Cl → PtBu$_2$) and Al−Al Bond Formation via the Hypothetical Subhalide Al$_5$Cl$_7$·5L, 9′ (cf. Ga$_5$Cl$_7$·5Et$_2$O[92])
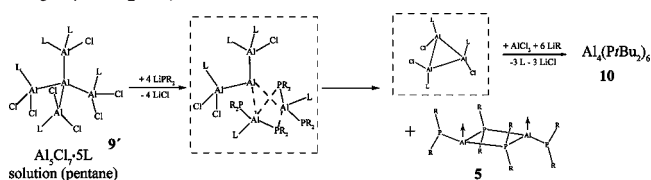

reminiscent of the ring inversion of bicyclo[1.1.0]butanes. The planar singlet transition state (TS) **7** (RAl^t(μ-R$_2$)Al^{i}R, C_i symmetry) with an imaginary frequency of 11i cm^{-1} has the two electrons in π orbitals. This TS lies 24 kJ mol^{-1} above the corresponding butterfly-shaped bicycle (**6**).

The synthesis of **5** and **6** proceeds via metastable AlCl solutions (see section 5.2) and their reactions with LiPtBu$_2$ under different conditions. The molecular structure within green crystals of [Al$_2$(PtBu)$_4$], **5**, and of yellow crystals of [Al$_2$(PtBu$_2$)$_4$], **6**, and the main structural parameters (experimental and computational) are presented in Figure 10.
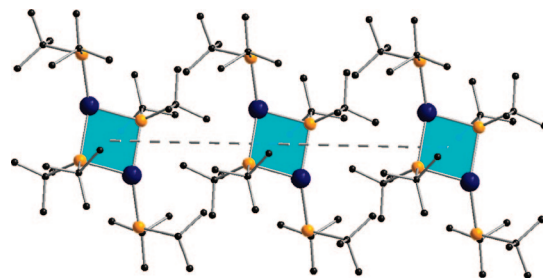
The most notable structural feature of **5** and **6** is the large variation in the observed Al···Al distances, ranging from 3.508 Å (3.462 Å calculated) in **5** to 2.587 Å (2.618 Å calculated) in **6**. We find a good agreement between the experimental X-ray and computed structural parameters.

The initial formulation of the formation of **5** and **6** from the radical intermediates [AlX$_2$]$^•$ and [AlR$_2$]$^•$ mentioned before represents only a formal description. Thus, we propose here a plausible reaction pathway considering known intermediates, which have previously been characterized by their crystal structure:

As a result of its generation process, the AlCl solution generally contains a certain percentage of AlCl$_3$.[58] Compound **5** is formed from AlCl and AlCl$_3$ in a donor-rich solution via Al$_2$Cl$_4$·2L, **8**,[89] and Al$_5$Br$_7$·5L, **9**,[90] already at low temperatures (−78 °C).

In solutions with low donor concentration and temperatures between −40 and −20 °C, Al$_2$Cl$_4$·2L is the predominant species,[91] which in turn can be trapped by the reactive PtBu$_2$ groups to finally yield the thermodynamically stable product **6**.

In compound **9**, as well as the known [Al$_5$Br$_8$·4L]$^-$ anion, the AlBr$_2$ entities are separated by 4.1 Å from each other (Al center to Al center). Consequently, the AlX$_2$ groups in these molecular units are arranged in an ideal topological fashion that allows for the stepwise substitution of halide units X by PR$_2$ groups (Scheme 2). The latter can partially act as bridging ligands, mediating a successive approach of

the Al atoms. These predefined subunits are ideally suited to finally produce **5**.

Parallel to this, compound Al$_4$R$_6$, **10**, is formed from the remaining Al$_3$Cl$_3$·3L units and AlCl$_3$ and LiR.[41] The formation of this cluster compound consisting of a distorted tetrahedral Al$_4$ framework with four terminal and two bridging ligands is indeed observed under these reaction conditions, nicely supporting the proposed reaction scheme for the formation of **5**.

The arrangement of the triplet molecules **5** in the crystal (cf. Figure 11) put further emphasis on the extraordinary bonding situation present in this species. It appears that the molecules' assembly in the crystal shows a distinct directional preference. We have recently described a similar, though yet not understood, stabilization of a radical species Al$_7$R$_6$ in the crystal (see section 7.1).[93,94] The sterically demanding PtBu substituents in **5** obviously prevent the intermolecular interaction tendency between Al$_2$(PR$_2$)$_4$ molecules and only permit a weakly interacting column structure (see Figure 11) and not the formation of dimers.

In contrast to very short-lived radical intermediates of organic reactions, numerous biradicaloids of heavy main group elements could be isolated in crystalline form in recent years, some of which formally represent intermediates in the σ bond formation process.[95,96] Pioneering work in this field was performed by Niecke and co-workers for P$_2$C$_2$R$_4$ ring compounds,[97] as well as Bertrand and co-workers with systematic investigations on B$_2$P$_2$R$_6$ species.[98] These structures are exemplified in Scheme 3, together with the biradicaloid molecules Sn$_2$N$_2$Cl$_2$(SiMe$_3$)$_2$[99] and Ge$_2$N$_2$(SiMe$_3$)$_2$Ar′$_2$.[100]

The presented results for the Al$_2$(PR$_2$)$_4$ compounds extend the area of intermediates of σ bond formation processes by contributing additional structurally characterized snapshots: For the first time, a particularly large distance between two metal centers was investigated in a biradical species, which, after several further steps, finally leads to a σ bond. This unprecedented discovery was only possible due to the particularly mild reaction conditions present in metastable AlX/AlR solutions. These show a complex disproportionation behavior, which is marked by several other intermediates that have already been characterized, finally forming the metal and AlX$_3$. Apparently, the ring system Al$_2$P$_4$ under study is particularly suited for such investigations because its Al−Al σ bond is weak but strong enough to compete with the bridging AlP bonds.

Scheme 3. Biradicaloid Four-Membered Ring Compounds Reported in the Literature (See Text)

5.2. Synthetic Aspects[58,101]

The equilibrium between the liquid metal and the gaseous mono- and trihalides of the metal is described, for the case of aluminum and chlorine, by the following equation:[58]

$$2Al_{(l)} + AlCl_{3(g)} \underset{10^{-2} \text{ mbar}}{\overset{1000\ °C}{\rightleftharpoons}} 3AlCl_{(g)} \qquad (12)$$

The conditions for gallium are almost the same, except that a comparable ratio of the partial pressures of mono- to trihalide is achieved at a reaction temperature about 100 K lower, that is, 900 °C. As a result of the increase in entropy, the equilibrium of the endothermic reaction shifts in favor of the gaseous monohalide with increasing temperature and decreasing total pressure.[102] The transport of aluminum in the presence of AlCl₃, as described by Klemm et al. and later by Schäfer et al., is also based on this reaction.[103,104] The partial-pressure behavior of the gaseous components is solely determined by the thermodynamic properties of the mono- and trihalides and the molten metal. This means that it does not matter which halogenation medium 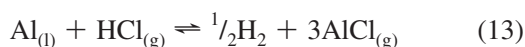is used in the preceding reaction. With respect to its easy handling and to ensure a continuous stream of gaseous AlX (X = Cl, Br, or I) during the reaction, a flow of the respective hydrogen halide gas (e.g., HCl) over the metal is normally used at a temperature of about 1000 °C (eq 13). Under these reaction conditions (ca. 10^{-1} mbar total pressure, 1000 °C), there is a more than 20-fold excess of AlCl over AlCl₃, so the yield of AlCl is more than 95%.

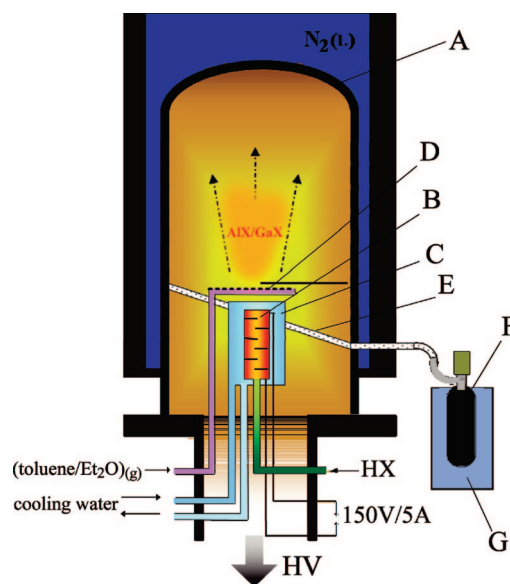$$Al_{(l)} + HCl_{(g)} \rightleftharpoons {}^{1}\!/_{2}H_2 + 3AlCl_{(g)} \qquad (13)$$

To investigate the reactivity of the molecular monohalides, many matrix-isolation experiments have been carried out, revealing that, in addition to dimerization, the aluminum and gallium monohalides enter into a number of other reactions.[105−108]

The positive results afforded by the matrix experiments with AlX molecules, started about 30 years ago, led to the adaptation of the technique to the preparative scale, in the so-called "preparative co-condensation" technique, where the monohalides are produced in gram amounts for synthetic purposes.[101] Although the experimental realization of this idea has been described many times,[7,58,109−111] it is appropriate briefly to describe the method here, because it forms the basis for much of the chemistry to follow. The required co-condensation apparatus is shown in Figure 12. Inside the co-condensation apparatus, at the center of a vacuum chamber of about 30 L capacity, there is located a high-temperature reactor containing molten aluminum in several graphite chambers heated to around 1000 °C. A flow of hydrogen halide gas is directed through these chambers, the flow being monitored by means of the pressure drop in a storage vessel.

In general, about 40 mmol of AlX are synthesized in two hours. After exiting the reactor, the gaseous AlX molecules condense, without undergoing further collisions, on the outer walls of the stainless steel vacuum vessel cooled to −196 °C. To prevent the aggregation of the AlX species, which disproportionate to form aluminum metal when warmed above −100 °C, an excess of a suitable solvent must be condensed with the monohalide molecules. Toluene is generally used, and to it a variable amount of a donor component is added (e.g., NEt₃, Et₂O, or THF). When the solid solvent mixture melts at about −100 °C, a deep red solution of the monohalide is usually obtained, and this can be stored at temperatures of −78 °C for several months. The solubilized metastable monohalide subsequently disproportionates according to the equation 3AlX → 2Al + AlCl₃ in the temperature range from −40 to +50 °C depending on the nature of the halide, the donor, and the donor concentration with respect to the monohalide. These metastable AlX solutions are the starting points for the chemistry described in the following sections. Metastable GaX solutions are prepared and manipulated in an analogous fashion.

Without any question, the preparation of metastable AlX/GaX solutions requires a high sophisticated technique. However, the high potential of these solutions for problems in fundamental chemistry (cf. chapter 1 and e.g. intermediates during formation and dissolution of metals) and for a novel area of metal-rich chemistry (e.g., for novel, often nanoscaled materials with unexpected properties) may justify these efforts.

Figure 12. Schematic representation of the co-condensation apparatus: A = stainless steel vessel (30 L); B = Al or Ga in the graphite cell with resistive heating; C = cooling shield; D = solvent input (toluene); E = drainage channel; F = Schlenk line; G = Dewar with dry ice (−78 °C); HX = hydrogen halide gas; HV = high vacuum.

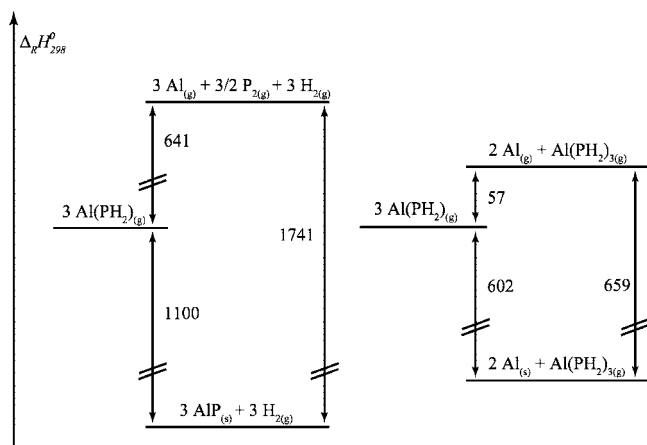## 5.3. An Unexpected Reaction of Al(I) Compounds Prevents the Formation of Metalloid Al Clusters[112]

As mentioned above, metalloid clusters are intermediates on the way from, for example, AlCl molecules to solid Al; that is, the back reaction of the synthesis for AlCl (eq 12′):
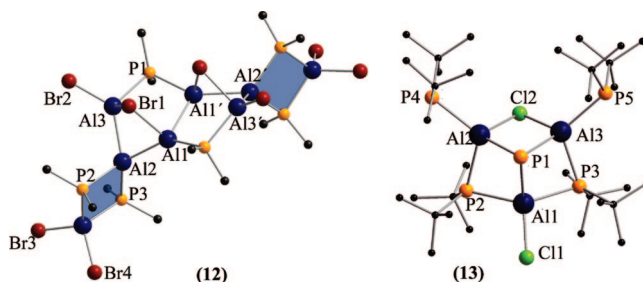
$$3AlCl_{(g)} \rightarrow 2Al_{(s)} + AlCl_{3(g)} \quad (12′)$$

This disproportionation reaction is strongly exothermic (-915 kJ mol^{-1}). However, especially for Al(I)/Ga(I) phosphanides and amides, an alternative reaction has to be taken into account since the formation of the salt-like materials (e.g., AlP or AlN) should be thermodynamically favored over the disproportionation reaction. In order to compare disproportionation with the formation of a salt with respect to their thermodynamic behavior in an orientating manner, we have examined both routes for the decomposition of the model molecule Al(PH$_2$). The results are visualized in Figure 13.[112]

As expected, the decomposition of Al(PH$_2$) to bulk AlP (according to the stoichiometry given in Figure 13) is strongly favored compared with the disproportionation reaction by 498 kJ (1100 kJ $-$ 602 kJ). For the similar decomposition of Ga(PH$_2$), GaP is also favored in comparison with the disproportionation, but a significantly smaller gain is calculated, 319 kJ (Supporting Information). For the decomposition of the amides Al(NH$_2$) and Ga(NH$_2$), moreover, the formation of the bulk nitrides AlN and GaN is also favored over disproportionation: Al 165 kJ; Ga 188 kJ (Supporting Information). On this basis, metalloid Al and Ga clusters carrying amide and phosphanide substituents might be expected to decompose finally to the bulk salts AlP/GaP and AlN/GaN. However, the existence of cluster species such as Al$_{57}$(AlNR$_2$)$_{20}$$^{2-}$, 1,[17] and Ga$_{64}$(GaNR$_2$)$_{20}$$^{3-/4-}$,[113-115] 11, with exclusively terminal bonding of the substituents demonstrates that there is a substantial kinetic barrier to the formation of bulk Al and, finally, bulk AlN and GaN. A similar kinetic barrier obviously exists for the phosphanide-substituted metalloid gallium clusters, although they display terminal as well as bridging [Ga$-$(PR$_2$)$-$Ga] bonding motifs. However, a different redox chemistry of the Al(I)PtBu$_2$ precursor is confirmed by the molecules Al$_8$Br$_8$(PtBu$_2$)$_6$, 12, and Al$_3$P(PtBu$_2$)$_4$Cl$_2$, 13, described recently (Figure 14).[112]

In the case of the compounds 12 and 13, which are formed from AlX subhalides and LiPtBu$_2$, the direct route leading ultimately to solid AlP is favored thermodynamically relative

Figure 14. The molecular structure of Al$_8$Br$_8$(PtBu$_2$)$_6$ (12) and Al$_3$P(PtBu$_2$)$_4$Cl$_2$ (13) in the crystal. CH$_3$ groups and H atoms of the PtBu$_2$ ligands are not shown for clarity.

Figure 15. An octahedral scheme like that in Figure 2 visualizes (a) the outstanding position of metalloid clusters (cf. Figure 2), (b) the disproportionation of, for example, Al(I) amides via metalloid clusters with an average oxidation number, n_{av}, between 0 and n_{salt}, and (c) the decomposition of Al(I) phosphanides to bulk AlP.

to the disproportionation path, that is, 12 and 13 represent kinetically stabilized intermediates on the way from Al(PR$_2$) to AlP. The building blocks in these intermediates with strong Al$-$(PR$_2$)$-$Al bridging bonds represent preorientated moieties of thermodynamically favored bulk AlP.

In order to visualize the results presented here for 12 and 13 in relation to general cluster chemistry (Figure 2), an additional point for oligomeric AlR/GaR clusters between naked and salt-like clusters is marked (Figure 15b). From this point, AlNR$_2$, GaNR$_2$, and GaPR$_2$ clusters disproportionate under mild conditions on the marked route via metalloid clusters to the bulk metal and, under drastic reaction conditions, finally to the thermodynamically favored bulk salts AlN, GaN, and GaP (Figure 15b). For Al(PR$_2$) clusters,

Figure 13. Calculated ΔH values for the two decomposition routes of Al(PH$_2$): to bulk AlP and H$_2$ (left); to bulk Al metal and Al(PH$_2$)$_3$ (right).

(14)

Figure 16. Molecular structure of Ga$_{16}$(PtBu$_2$)$_{10}$ (**14**) in the crystal. The central Ga$_4$-tetrahedron of "naked" Ga atoms is highlighted.

however, this reaction path is blocked, so only the marked route via salt-like clusters [AlP]$_n$ and R$_2$ and finally to bulk AlP is possible (Figure 15c).

The decomposition of Al(I) phosphanides represented in Figure 15c may offer an attractive route to nanoscaled AlP particles; for example, these particles should be generated if AlPR$_2$ species are heated in a high-boiling solvent. A more selective preparation can be expected, for example, for GaP, if one starts with defined metalloid Ga$_n$(PR$_2$)$_m$ clusters. An impressive example of this kind of reaction should start from a Ga$_{16}$(PtBu$_2$)$_{10}$, **14**, cluste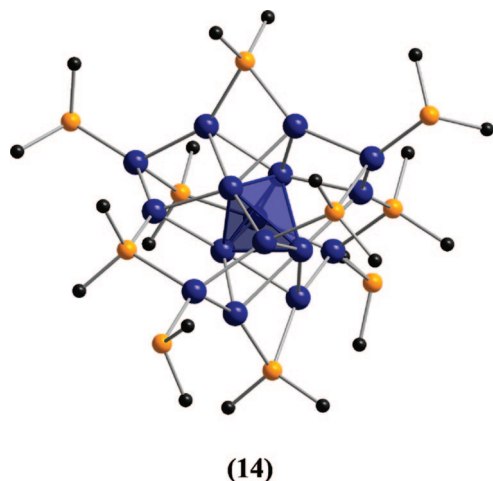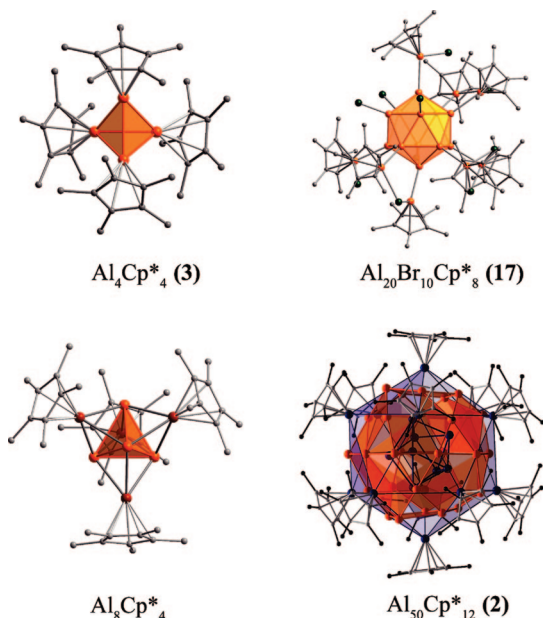r[116] (Figure 16), where a core of naked Ga atoms is surrounded by Ga(PR$_2$)$_2$ entities. If the Ga$_{16}$ cluster decomposes as visualized in Figure 15c, a dream of any nanochemist could come true: after cleavage of the P−C bonds, a defined nanoscaled Ga$_4$(GaP)$_n$ cluster should be formed in which a metallic core is protected in a well-defined way by a semiconducting GaP sheath. In the chemistry of metalloid gallium clusters, a first step toward a semiconducting coating has been observed when Se−C bonds are broken within SeR ligands during the formation of a Ga$_{24}$Se$_2$Br$_{18}$ (**15**) cluster containing Ga−Se−Ga bridging bonds (see section 7.2).[117] Thus, the ambition of generating a Ga$_n$(GaP)$_m$ nanoparticle or any other similar, well-defined GaP, GaN, AlSe, or AlTe nanoparticle starting from Al(I)/Ga(I) compounds with direct bonds from the metal to P, Se, or Te atoms could become reality in the near future. The experimental and theoretical results presented here may provide the motivation and the background for these efforts.

5.4. Formation Process of Al$_{50}$Cp*$_{12}$ as an Intermediate from Al$_4$Cp*$_4$ on the Way to Bulk Al[118]

The preparation of tetrahedral Al$_4$Cp*$_4$, **3**, as a textbook example for the first pure Al(I) organic compound[20] via metastable AlCl solution[58,101] initiated (a) a highlight article[119] and (b) its subsequent classical synthesis,[120] which was a starting point for a variety of applications in transition metal,[121−124] rare-earth,[125,126] and, finally, actinide chemistry.[127,128] However, the hindered disproportionation of **3** even above 100 °C has never been discussed, which is surprising because the unsubstituted analogue Al$_4$Cp$_4$, **16**, spontaneously decomposes to metallic aluminum and Al(III) species even when it is warmed to temperatures above −30 °C.[58,129]

Recently, we presented an answer:[118] metalloid clusters like the Al$_{50}$Cp*$_{12}$ cluster, **2**,[19] represent a barrier as intermediates on the way to the formation of metals (see

Al$_4$Cp*$_4$ (**3**)   Al$_{20}$Br$_{10}$Cp*$_8$ (**17**)

Al$_8$Cp*$_4$ Al$_{50}$Cp*$_{12}$ (**2**)

Figure 17. Experimentally determined molecular structures of **3**, Al$_{20}$Br$_{10}$Cp*$_8$ (**17**) and Al$_{38}$(AlCp*)$_{12}$ (**2**) and the calculated structure of Al$_8$Cp*$_4$ detected as a prominent species in mass spectrometric experiments during MALDI experiments on solid Al$_4$Cp*$_4$ (**3**).

Supporting Information); that is, clusters of this type may also be assigned as experimentally characterized nuclei for the crystallization of metals, which means that these investigations are of fundamental interest in the chemistry of any metastable organometallic compound, as well as in solid-state chemistry.

The following observations are the basis for this discussion:

1. When crystals of Al$_4$Cp*$_4$, **3** (Figure 17), are irradiated with a weak UV laser in the matrix-assisted laser desorption ionization (MALDI) chamber of an Fourier transform ion cyclotron resonance (FT-ICR) mass spectrometer, the metalloid cluster cation Al$_8$Cp*$_4$ (Figure 17) with a tetrahedral Al$_4$ core and four AlCp* units capping its faces is formed by a laser desorption process (LD).[130] During heating by the laser, monomeric AlCp* units are generated, which are added to **3**, and subsequently AlCp*$_3$ is eliminated (eq 14); that is, the classical disproportionation reaction of Al(I) compounds proceeds within this MALDI experiment:

$$Al_4Cp^*_4 \xrightarrow[-2AlCp^*_3]{+6AlCp^*} Al_8Cp^*_4 \qquad (14)$$

2. These mass spectrometric experiments initiated the thermal reactions at about 60 °C of Al$_4$Cp*$_4$ (**3**) with AlX (X = Cl, Br) in a gram scale under different conditions, where finally Al$_{20}$Cp*$_8$X$_{10}$,[131] **17**, and Al$_{50}$Cp*$_{12}$,[19] **2**, clusters result (Figure 17).

From these experimental observations and the easy disproportionation of Al$_4$Cp$_4$ (**16**), we developed the following hypothesis: There should be a barrier for the thermodynamically favored disproportionation reaction, which should be high in the case of Al$_4$Cp*$_4$, **3**, and low or even not present for Al$_4$Cp$_4$, **16**. With respect to energy and geometry, metalloid clusters seem to be the plausible species formed in the areas near the top of this barrier, since they have been proven to be intermediates between metastable Al(I) compounds and metallic aluminum several times.[6] In order to

Figure 18. Calculated energy diagram (kJ·mol^{-1}) of the monomerization of Al$_4$Cp*$_4$ (**3**) and Al$_4$Cp$_4$ (**16**) and of the disproportionation reaction of **3** and **16** via Al$_{50}$R$_{12}$ clusters to solid Al and AlR$_3$ molecules. The experimentally detected species are highlighted. The formation of Al$_4$Cp*$_8$/Al$_4$Cp$_8$, together with AlCp*$_3$/AlCp$_3$, corresponding to eq 14 is 941 kJ above the Al$_4$Cp*$_4$ and 84 kJ below the Al$_4$Cp$_4$ level.[132]

examine our hypothesis, we performed DFT calculations, which often have proven to be suitable for energetic and topological discussions in the field of metalloid and naked aluminum clusters.[1–3,6,7] In order to quantify the relation of the calculated gas phase species to the final formation of the bulk metal, the DFT results have been adjusted via the vaporization energy of Al to obtain a suitable thermodynamic ladder.[59] The results obtained are presented in Figure 18 for Al$_4$Cp*$_4$ (**3**) and Al$_4$Cp$_4$ (**16**). The following points are remarkable:

1. Both compounds (Al$_4$Cp*$_4$, **3**, and Al$_4$Cp$_4$, **16**) are metastable with respect to their disproportionation. However, the exothermic dissociation energy of **3** at 233 kJ/17.25 mol is dramatically smaller than that of **16** with 2441 kJ/17.25 mol.

2. There is a high barrier for the disproportionation of **3** via Al$_{50}$Cp*$_{12}$, **2**, clusters of about 1750 kJ, while there is almost no barrier via a similar Al$_{50}$Cp$_{12}$ cluster for the disproportionation of Al$_4$Cp$_4$, **16**; that is, in accordance with the observation, only **16** can decompose to metallic aluminum and Al(III) species spontaneously.

3. Since Al$_4$Cp*$_4$ **3** does not disproportionate during heating and dissociation to the monomers (+2004 kJ), the above-mentioned barrier via Al$_{50}$Cp*$_{12}$ can easily be reached via repeated addition of monomeric AlCp* to undissociated Al$_4$Cp*$_4$, **3**, and subsequent AlCp*$_3$ elimination (eq 14). Snapshots on this way are Al$_8$Cp*$_4$, Al$_{20}$Cp*$_8$X$_{10}$ (**17**), and Al$_{50}$Cp*$_{12}$ (**2**). However, the Al$_{50}$ cluster should not mark the final top of the barrier since its central Al$_8$ unit has not grown to the expected Al$_{13}$ core, which should be the typical core of any nucleus of the crystallization of metallic Al; that is, the top of the barrier may be a metalloid cluster a little bit larger than the Al$_{50}$Cp*$_{12}$ one (e.g., **1**, **22**).[3,7,17,133]

The conclusion of these experimentally based calculations casts a light on the decomposition of many known and so far unknown subvalent organometallic species. Though, in general, they are thermodynamically metastable, for special examples there is a chance to isolate crystalline compounds

if a barrier prevents the decomposition of these compounds. During the reaction path along this barrier, increasing metalloid clusters are growing, which may also be designated as snapshots of the nucleation during the crystallization of Al metal. This interpretation is confirmed for the hindered decomposition of Al$_4$Cp*$_4$ (**3**) (a) via its stability during heating for dissociation to monomeric units, (b) via its stability during the classical synthesis at about 100 °C, and finally (c) via the isolation of metalloid clusters like the Al$_{50}$Cp*$_{12}$ (**2**) one as snapshots during the decomposition of **3**.

To sum up, the hindered decomposition of Al$_4$Cp*$_4$, **3**, exhibiting Al–Al bonds of medium strength (∼30 kJ mol) and the spontaneous decomposition of Al$_4$Cp$_4$, **16**, have been outstanding lucky chances to start the investigation presented here. They cast a light on three fundamental questions: (a) what kind of low-valent metastable metallorganic compounds can be isolated; (b) what is the influence of metalloid clusters during the decomposition of organometallic compounds via a barrier; and (c) are metalloid clusters important snapshots for the nucleation during the crystallization of metals? Therefore, the results presented here demonstrating the essential contribution of metalloid clusters to many fields of chemistry may be the starting point for many theoretical papers since, for example, the number of subvalent organometallic compounds has considerably increased in the last two decades.

6. Selected Metalloid Al and Ga Clusters Exhibiting Their Outstanding Position

Since the great majority of metalloid clusters of group 13 exhibiting the general formulas M$_n$R$_m$ ($n > m$) are observed for the two elements Al and Ga, this section is divided into two parts.

Not discussed here are several Al and Ga clusters, which may not strictly be called metalloid, since they are on the borderline with normal valent or Wade-type clusters. They have more metal–metal bonds than metal–ligand bonds, but there are no "naked" metal atoms; as exemplified by the icosahedral Al$_{12}$R$_{12}$$^{2-}$ cluster [R = iBu], **18**,[134] and by some Ga$_6$R$_6$ clusters published recently.[135–137] On the other hand, there are "naked" Al and Ga atoms tetrahedrally coordinated only to other Al or Ga atoms carrying Al– and Ga–halide bonds, as in the neutral compound Ga$_5$Cl$_7$·5Et$_2$O [Ga(GaCl$_2$)$_3$GaCl], **19**, having an electron-precise bonding situation with formally one tetrahedrally surrounded by other Ga atoms, Ga^0, three Ga^{II}, and one Ga^I atom.[92] All these nonmetalloid clusters are not discussed here.

6.1. Metalloid Al$_n$R$_m$ Clusters

Formation of metalloid Al clusters starts with the generation of AlX monohalides at about 900–1000 °C and their trapping in, for example, a toluene/ether solvent mixture at low temperatures (see section 5.2). This metastable solution is then allowed to disproportionate (eq 12′) at a temperature between −40 and +50 °C, depending on the kind and concentration of the donor species (ether, amine, etc.) present. On the way to the bulk metal, which is

$$3AlX \rightarrow 2Al_{(s)} + AlX_3 \tag{12′}$$

deposited as a mirror on the walls of the reaction vessel at temperatures above about 70 °C, intermediates can be trapped

[Al7[N(SiMe3)2]6]− **20**

[Al12[N(SiMe3)2]8]− **21**
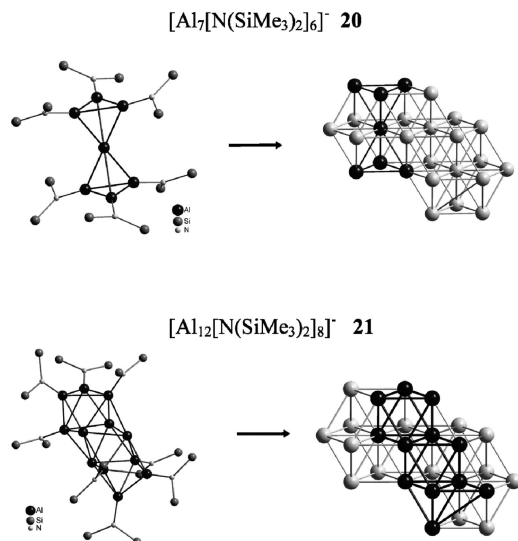
Figure 19. Molecular structures of [Al7R6]− (**20**) and [Al12R8]− (**21**) (R = N(SiMe3)2) and the topological relationship of **20** and **21** to the corresponding sections of the structure of solid elemental aluminum.

via simultaneous substitution of the halogen atoms by bulky univalent ligands (e.g., −N(SiMe3)2, −C(SiMe3)3, −Si-(SiMe3)3, −Cp*, or −PtBu2). The overall reaction cascade is therefore highly complex, depending on the rate of the disproportionation reaction in competition with the substitution reactions of the bulky ligands. During the "annealing" process at low temperatures, it seems plausible that the arrangement of the metal atoms will adopt more and more the arrangement of the bulk metal, because that is the end point of disproportionation. The N(SiMe3)2 group, which is linked by a two-center two-electron (2c−2e) bond to each aluminum atom, proves to be a particularly favorable species in this endeavor, since it became apparent that the substitution of the halogen atoms X in AlX (AlX + LiR → LiX + AlR) and the disproportionation of AlX (3AlX → 2Al + AlX3) occur in the same temperature range. Reactions in which substitution is favored tend to yield oligomeric AlR species (e.g., Al4Cp*4, **3**); when substitution is strongly hindered, though, disproportionation of the AlX species is dominant.

The size of the Al$_n$ cluster core is therefore determined by the reactivity of the AlX solution with respect to disproportionation. This intuitive prediction is indeed realized in the case of five Al$_n$R$_m$ clusters (R = N(SiMe3)2), which contain an increasing number of Al atoms. Thus, for a particular halide, the size of the resulting cluster can be increased by an increase in temperature. Starting from an AlCl solution, for example, the cluster size progresses from an Al7R6− cluster, **20** (Figure 19), at −7 °C[13] through an Al12R8− cluster, **21**, at room temperature[138] to an Al69R18^3− cluster, **22**, after warming briefly to +60 °C.[133] However, when a less reactive Al(I) iodine solution is used, a partially substituted Al14R6X6− cluster, **23** (Figure 20), is obtained at room temperature,[139] whereas after warming to +60 °C the Al77R20^2− cluster **1** forms.[17] In all these cases R is the N(SiMe3)2 ligand.

Another important factor having an impact on the arrangement of the metal atoms is, as expected, the electronic and steric influence of the ligand introduced during the substitution reaction. Consequently, ligands other than N(SiMe3)2 induce different topologies of the Al atoms in the resulting metalloid cluster, for example, Al50Cp*12, **2** (see section 5.4).

23
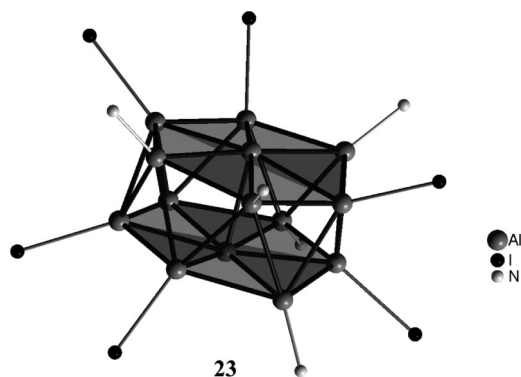
Figure 20. Molecular structure of [Al14[N(SiMe3)2]6I6]^2− (**23**).

A fuller understanding of this influence is only just beginning to dawn, although a growing number of Al and Ga metalloid clusters have been isolated in the past decade. This distinctive ligand−metal core interaction raises the question of whether it may be possible to generate new modifications of the elements, for example, a nonmetallic allotrope of aluminum with a topology similar to that of one of the boron structures, for example, the B12 moieties of α-boron. This possibility will be discussed in section 6.1.3 for the disproportionation of the Al22Cl20 (**24**) and Al22Br20 (**25**) subhalides, where the icosahedral Al12 moieties are already preformed.[140,141]

Most of the metalloid Al clusters are extremely sensitive to moisture and air and may even ignite spontaneously after only brief exposure to the atmosphere. It follows that handling of the compounds can be exceptionally difficult for physical measurements. This behavior contrasts dramatically with that of the metalloid noble metal clusters (e.g., ligand−shell bearing Au55 and Pd145 clusters[14,16,142]), some of which can be handled in aqueous solution and in contact with air. Such a difference comes as no surprise since it reflects the difference between noble and base metals (see section 8).

In the following, we will only present (a) a discussion on two outstanding Al7R6 clusters; (b) a discussion on the largest metalloid Al clusters, and (c) the relation of metalloid Al clusters to a hypothetical nonmetallic β-Al.

6.1.1. The Al7R6− Cluster: Should It Be Called a Metalloid Cluster or a Sandwich-Stabilized Al Atom?

The metalloid cluster anion Al7R6− [R = N(SiMe3)2], **20**[13] (Figure 19), is unique among metal atom clusters; no other example is known in which two tetrahedra of metal atoms are connected via a naked metal atom without additional bridging ligands. However, the bonding situation cannot be described satisfactorily for this compound, which may be a model for a single-atom contact.[143] With a different ligand, the neutral oxidized analogue, Al7R′6 [R′ = N(SiMe2Ph)2] (**20a**), has been prepared, thereby opening the possibility of gaining a deeper insight into the bonding situation inside these clusters.[94] Furthermore, the latest detailed investigations show the large influence of ligands with respect to the ground-state structure; for example, for an Al7(NH2)6− cluster like for a bare Al7 cluster a C_{3v} symmetric capped trigonal antiprism (see Figure 6) has been obtained.[144]

Comparing the distorted D_{3d} framework structures of **20** and **20a**, we note significant changes in bond length with the switch from the neutral to the anionic cluster: in the latter, the Al−Al distances within the Al3 moieties are short, while in the neutral compound all the Al−Al bonds are much more
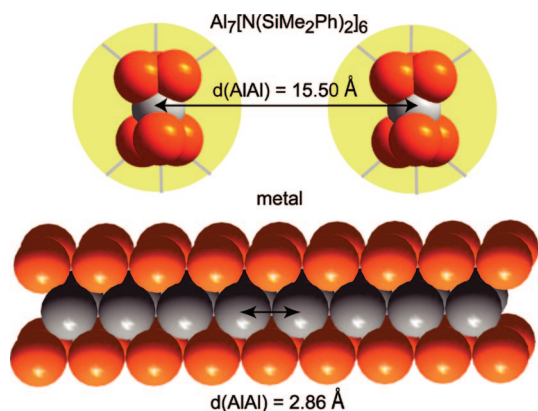
Figure 21. The Al_7R_6 cluster radical (**20a**) as a "tamed" AlR ligand-stabilized atom separated by 1.5 nm from the other Al_7R_6 radicals in the crystal. By comparison, the Al atoms in solid Al are separated by 0.29 nm.

nearly equal. Model calculations for $Al_7H_6^+$, Al_7H_6, and $Al_7H_6^-$ provide striking confirmation of this different behavior. In the cation, the centered Al atom exhibits short bonds to its six neighbors, while in the anion, as in the experimentally characterized $Al_7R_6^-$ cluster species **20**, short Al–Al bonds are calculated only for the terminal three-membered rings. The neutral model compound with its 12 very similar Al–Al bonds seems then to be the prototype of a metalloid cluster. These drastic changes in topology give a hint of the complex topological changes to be expected if electron transport proceeds through an Al_7-containing moiety having a single atom contact. The question then arises: may Al_7R_6, **20a**, also be called a stabilized or "tamed" Al atom. This situation is visualized in Figure 21 where the Al–Al distances in the metal (2.86 Å) are compared with the intercluster distances of 15.50 Å in the compound **20a**. There seem to be strong interactions between these "tamed" Al atoms because crystals of the compound could not be dissolved. The radical character of Al_7R_6, **20a**, in the solid state has been confirmed, however, via EPR measurements.[94] The EPR signal of a single crystal shows unusual behavior, suggesting directed interaction among the clusters in the solid. Such cluster···cluster interactions form the subject of section 7.1.

6.1.2. Al_{69} and Al_{77} Clusters[17,133]

The principle and significance of metalloid clusters in understanding the formation of metals are demonstrated by the two largest Al clusters, $Al_{69}R_{18}^{3-}$, **22**, and $Al_{77}R_{20}^{2-}$ (R = $N(SiMe_3)_2$), **1**, which have almost the same size with 69 and 77 Al atoms inside a shell of 18 and 20 $N(SiMe_3)_2$ groups, respectively.[17,133] In both cases, the Al atoms are arranged in "shells" (Figure 22), whereas a central Al atom
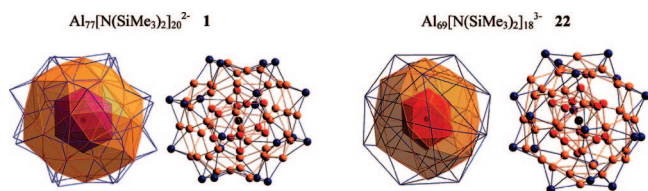
Figure 22. Arrangement of the Al atoms in the metalloid clusters (**1**) and (**22**) in a ball-and-stick and a shell-like representation with different colors for the different shells: (**1**) (1 + 12 + 44 + 20 Al atoms); (**22**) (1 + 12 + 38 + 18 Al atoms). The blue-colored outer shell Al atoms form 2c–2e bonds to 18 or 20 $N(SiMe_3)$ groups (omitted for clarity).

is surrounded by 12 nearest Al neighbors. Not only the coordination number of the Al atoms but also the mean Al–Al distance in a shell decreases from the center (average 2.78 Å) to the periphery (average 2.68 Å), indicating that the Al–Al bonds have become more localized and acquire a more molecular character from the inside to the outside of the cluster. Despite these similarities, the coordination spheres of the central Al atoms of both clusters are significantly different. The Al_{13} core of **22** can be described as a distorted D_{5h} structure (a geometry often described as decahedral),[145] whereas the central Al atom in the Al_{77} cluster **1** has been shown to have an icosahedral coordination sphere that is distorted in the direction of a cuboctahedron. In both clusters, the Al–Al distances from the center to the first Al_{12} shell and those within this shell are nearly identical.[4]

Both clusters differ in their geometry from noble metal clusters.[26,146] In the case of $[Au_{55}Cl_6(PR_3)_{12}]$,[142] for example, a cuboctahedral and icosahedral environment has been postulated for the central Au atom, although no experimental structural analysis of this cluster species is yet available. However, a larger Au_{102} cluster that *has* recently been structurally characterized is described in section 8.2 in the light of its unexpected structure.[16] For the Pd_{55} framework of "naked" Pd atoms in the center of the cluster $[Pd_{145}(CO)_{60}(PR_3)_{30}]$,[14] an almost undistorted icosahedral Pd_{13} unit is observed, with Pd–Pd distances between the central Pd atom and the first Pd_{12} shell (2.68 Å) about 5% shorter than those within the shell. Hence it appears that these large metalloid clusters (Al_{69}, Al_{77}, and Pd_{145}), for which structural data are available, exhibit significant differences in the core shells, both among the clusters themselves and with respect to the cuboctahedral arrangement of the corresponding bulk metals. In all cases, however, the distance of the 12 nearest neighbors to the central atom is shorter than that in the bulk metal, indicating that the bonding has shifted away from the predominantly delocalized situation in the metal in the direction of more localized molecular bonding. This interpretation is supported especially by the decreasing Al–Al distances on going from the center to the periphery of the Al_{69} and Al_{77} clusters. By contrast, the Pd–Pd distances develop in the opposite way. Thus, in a simple description, the Pd clusters represent small Pd particles surrounded by neutral CO ligands, while the Al clusters present a more complex situation involving highly mixed-valent bonding of a partially oxidized Al_n particle.

Interestingly, even small changes in the shells of the Al_{69} and Al_{77} clusters, which are probably too small to be observed with normal nanoscopic methods [e.g., atomic force microscopy (AFM)], lead to changes in the topology of the central metal framework that might be expected to affect the physical properties. These observations imply also that different surface reactions may lead to different topologies within the interior of the metal, down to the nanometer ranges. In order to understand the topology and the packing density of **22** and **1** with respect to metallic aluminum, the atomic volume of the "naked" Al atoms in **22** and **1** was calculated and compared with the volume of a hypothetical molecular Al_{55} section of the fcc Al metal lattice. For a better comparison, the same charge of −3 was assumed for the naked Al_{51} (**22a**, 1 + 12 + 38 Al atoms from **22**) and Al_{57} (**1a**, 1 + 12 + 44 Al atoms from **1**) species and for an Al_{55} species (1 + 12 + 42 Al atoms from α-Al). For **22a** and **1a**, the topologies within the experimentally determined structures of **22** and **1** and for Al_{55}^{3-} the coordinates of Al metal

were the basis for the single-point SCF calculations.[4,133] According to these calculations, the atomic volume decreases in the order **22a** (29.61 $Å^3$) > **1a** (29.51 $Å^3$) > Al_{55}^{3-} (29.21 $Å^3$). This indicates the driving force for the formation of the bulk metal and for Al_{55}^{3-} to be the energy gained by the most compact arrangement with the highest possible coordination number of 12, even if the distances are large (2.86 Å for Al_{55}^{3-}, as in the metal). By contrast, the hypothetical naked clusters **22a** and **1a** are less compact with shorter (more molecular) Al−Al contacts and lower coordination numbers. However, latest detailed calculations on the $Al_{77}R_{20}^{2-}$ cluster show that there is a large influence of the ligands on the ground-state structure of $Al_{77}R_{20}$ clusters: with the less sterical demanding NH_2 ligand a more compact fcc-like cluster results. This behavior is different from that of the larger metalloid Ga_{84} cluster (section 6.2.3).[144]

6.1.3. $Al_{22}X_{20}$ and $Al_{20}Cp*_8X_{10}$ Clusters and the Way to Hypothetical β-Aluminum

6.1.3.1. $Al_{22}X_{20}$.[140,141] The metalloid Al clusters discussed so far show that the favored arrangement of Al atoms involves close packing, as in the metal, with the observed distortions reflecting the adaptation of the cluster core to the $(AlR)_n$ "corset". Since the packing density comes even closer to that of the metal with increasing cluster size (see section 6.1.2), it is conceivable that an alternative pathway during the early stages of cluster formation could lead to a less compact modification of aluminum. Such a hypothesis is not so unlikely since the other group 13 elements, boron and gallium, also exist in several modifications. An experimental indication of a hypothetical nonmetallic β-aluminum modification is given by the results to be discussed below.

Directly after the condensation of AlX species (X = halogen), for example, in the presence of strong donors, the donor-stabilized $Al_4Br_4 \cdot 4NEt_3$, **26**, is obtained in which the bonding within the planar Al_4 moiety can be described by means of classical 2c−2e bonds.[147−149] With weaker donors, such as THF or tetrahydropyran (THP), and at a lower donor concentration, the clusters $Al_{22}Cl_{20} \cdot 12L$ (L = THF or THP), **24**, and $Al_{22}Br_{20} \cdot 12THF$, **25**,[140,141] can be obtained, representing the first examples of polyhedral aluminum subhalides, each with a unique cluster core (Figure 23). The icosahedral Al_{12} core in **24** and **25** is reminiscent of the polyhedral boron subhalides (such as B_4X_4, B_8X_8, B_9X_9, and $B_{12}X_{12}^{2-}$),[150−152] in which each halogen atom X is directly bonded to a boron atom of the polyhedral framework. In the Al_{22} halides **24** and **25**, however, 10 more Al atoms are directly bonded to
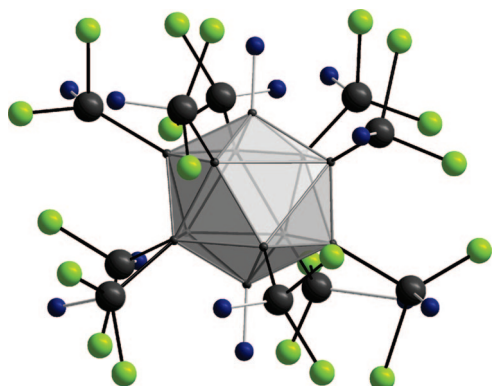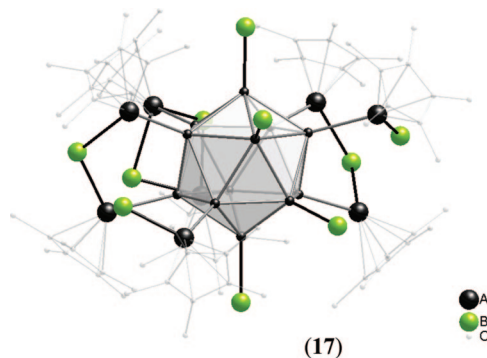
an Al atom of the icosahedral Al_{12} cluster core, presenting a unique configuration. Additionally, each of the outer 10 Al atoms is bonded to 2 bromine atoms and saturated by a donor molecule (THF or THP). The apex and base atoms in the Al_{12} icosahedron are not "naked": they are each coordinated by one donor molecule.

Despite the great sensitivity of the Al_{22} subhalides **24** and **25** to air and moisture, it was possible to secure solid-state ^{27}Al NMR spectra and XPS measurements, confirming the presence of three electronically different types of Al atoms, as expected from a structural point of view (one signal for AlX_2, one for the AlX_2-bound Al atoms of the central icosahedron, and one for the apex and base Al atoms of the central icosahedron).[140] The metal atom topology in **24** and **25** is surprising with no precedent in molecular chemistry. However, the α-boron structure, which consists of a network of molecular icosahedra connected by boron−boron bonds, has a similar topological motif. In order to check the possibility that **24** or **25** could be precursors to a nonmetallic Al modification with the structure of α-boron, ab initio calculations have been carried out. These reveal that, with an energy-consuming expansion of the closest packed Al atoms in elemental aluminum by about 30% (ca. 33 kJ mol^{-1}), a structure analogous to that of α-boron becomes energetically more stable than an expanded fcc lattice. Since contraction in the direction of the bulk metal actually takes place during disproportionation (see section 6.1.2),[140,141] the intermediate existence of a β-Al modification with a larger atom volume cannot be excluded. Such a modification might be accessed by a disproportionation of the $Al_{20}X_{20}$ compounds **24** and **25** (eq 15).

$$Al_{12}(AlCl_2)_{10} \rightarrow "Al_{12(s)}" + 5(Al_2X_4) \qquad (15)$$
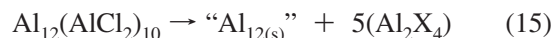
6.1.3.2. $Al_{20}Cp*_8X_{10}$.[131] Aside from the unique structures of **24** and **25** and the possibility of accessing a new modification of elemental aluminum, there remains open the question of how these compounds are formed from Al(I) halides. A clue to the mechanism is given via two partially substituted clusters, $Al_{20}Cp*_8X_{10}$ (X = Cl, Br), **17** (Figure 24), representing two molecular, partially substituted subhalides, which seem at first glance to be related to the gaseous anions $Al_{13}I_x^{56}$ and $Al_{14}I_x^{55}$ (x = 1−12) generated in mass-spectrometric experiments. In both sets of compounds, the halogen atoms form direct bonds to the Al atoms of an icosahedral Al_{12} cluster core. However, quantum chemical calculations on "naked" anionic clusters, for example, the $Al_{13}I_x^-$ anion, indicate that an additional Al atom is located in the center of an icosahedral Al_{12} moiety. The structure of **17** is furthermore closely related to those of the $Al_{22}X_{20}$

Figure 23. Molecular structure of $Al_{12}(AlX_2)_{10} \cdot 12L$ (**24** and **25**). The hydrocarbon framework of the L = THF and THP ligands has been omitted for clarity.

(17)

Figure 24. Molecular structure of $Al_{20}Cp*_8Br_{10}$ (**17**). The central icosahedron is emphasized by a polyhedral representation.

compounds (X = Cl or Br), e.g., $Al_{22}Br_{20}$, **25**[141] because their cluster frameworks exhibit icosahedral Al_{12} moieties. However, there is one major difference between the halide compounds **24** and **25** and the partially substituted compound **17** in that halogen atoms are directly bound to Al atoms of the central Al_{12} icosahedron in **17** (Figure 24).

Closer inspection of the molecular structure of **17** obtained by crystal structure analysis proves that this compound has an almost regular Al_{12} icosahedron in the center with an average Al−Al distance of 2.685 Å (Figure 24). This icosahedron includes four Al(I) atoms coordinated terminally by a halogen atom and eight Al(0) atoms that are coordinated exclusively by an exohedral Al atom. Each of the eight exohedral Al atoms bears a Cp* ligand, while two of them are additionally coordinated terminally by halogen atoms. Two pairs of the remaining six exohedral Al atoms are singly bridged and one pair is doubly bridged by halogen atoms. Thus, the Al_{12} icosahedron is surrounded by four halogen atoms, six Al(II)BrCp* units, and two Al(I)Cp* moieties. With this arrangement, there are available in principle 26 skeletal electrons for the central Al_{12} icosahedron ($4 \times 2\ e^-$ for bromine-bearing Al atoms + $6 \times 2\ e^-$ for Al(II)BrCp*-bearing Al atoms + $2 \times 3\ e^-$ for Al(I)Cp*-bearing Al atoms). In accordance with Wade's Rules,[29] this results in the bonding situation of a *closo* cluster ($2n + 4$; $n = 12$). The distances and bonding relationships in the Al_{12} icosahedron are therefore in accordance with those of the $Al_{12}R_{12}^{2-}$ anion, **18** [$r(Al-Al) = 2.69$ Å, R = iBu], and the $Al_{22}X_{20}$ species, **24** and **25** [$r(Al-Al) = 2.70$ Å]. Furthermore, the synthesis of **17** succeeds best if one starts with the specific halide [AlBr·NEt$_3$]$_4$ **26** for the reaction with the Al(I) compound Al$_4$Cp*$_4$, **3**. On the basis of the experimental findings and the results of quantum chemical calculations, a mechanism for the formation of compounds **17** and **25** can be postulated: Hence the dehalogenation of **26** to give **17** could also occur as a result of an excess of AlCp*. Such a dehalogenation was also observed during the formation of SiAl$_{14}$Cp*$_6$, **27**, from the tetrahedral Si-centered Si(AlCl$_2$)$_4$ species (see section 6.3). Nevertheless, the isolation of **17** makes the intermediacy of an $Al_{12}Br_{12}$ species also feasible during the disproportionation of AlBr.[131] $Al_{12}Br_{12}$ can then react further to give $Al_{22}Br_{20}$, **25**, or compound **17**, depending on the reaction conditions. Apart from the relevance of **17** to the understanding of the formation of an $Al_{22}X_{20}$ species, **24** or **25**, from an Al(I)X source, these results have broader significance: they add further weight to the assumption that there are at least two different ways to reach the bulk phase of aluminum. The first pathway leads via Al-centered clusters to metallic Al. A second reaction channel leads via Al_n clusters with an icosahedral Al_{12} center (but without a central Al atom as in **25**, for example) to the hypothetical, nonmetallic modification of Al (β-Al). Within this second pathway, compound **17** can be regarded as a "molecular dead end", that is, a snapshot of the complex reaction events of metastable AlX species on their way toward elemental aluminum via a hypothetical β-modification made possible only by ligand stabilization.

Therefore, the results on $Al_{22}X_{20}$, as well as those of some GaX compounds presented later on (see section 6.2.2) may support a fundamental principle that will influence our knowledge about the variation of properties and bonding of metallic phases under extreme pressure and temperature variations. Some recently published high-pressure experiments impressively show that metallic structures can change

in direction to charged clusters (salt-like structure) and to transparent semiconductive phases.[153−155] These investigations give strong evidence that a novel extended view of structure−property relations can be expected in the near future.

6.2. Metalloid Ga$_n$R$_m$ Clusters

By contrast with aluminum (cf. section 6.1.3), gallium provides many experimental hints to confirm the relation between the structure of a metalloid cluster compound and different modifications of the bulk element. On the borderline between real metals and semimetals or nonmetals, gallium is a singular case with its great variety of seven different modifications[6,8] (see Supporting Information). This "flexibility" of gallium atoms in achieving different connectivities is also reflected in the great variety of structural motifs displayed by metalloid Ga clusters. This unique characteristic of gallium was visualized in a cover image of *Dalton Transactions* (modified in Figure 25),[3] illustrating the different routes linking metastable gallium monohalides via disproportionation steps to metalloid clusters as intermediates on the way to the seven modifications of solid elemental gallium.

During the last decade, a great variety of metalloid Ga$_n$R$_m$ clusters have been synthesized,[8,9] containing nearly every number of Ga atoms up to 26 (e.g., for Ga$_{18}$, Ga$_{18}$(SitBu$_3$)$_8$ **28**,[156] [Ga$_{18}$(PtBu$_2$)$_{10}$]$^{3-}$ **29**;[157] for Ga$_{19}$, [Ga$_{19}$(C(SiMe$_3$)$_3$)$_6$]$^-$ **4**;[12] for Ga$_{22}$, Ga$_{22}$R$_8$ (R = Si(SiMe$_3$)$_3$) **30**,[158] [Ga$_{22}$Br$_{11}$R$_{10}$]$^{3-}$ (R = (Me$_3$Si)$_2$N) **31**,[159] [Ga$_{22}$Br$_{11}$R$_{10}$]$^{2-}$ (R = (Me$_3$Si)$_2$N) **32**,[159] Ga$_{22}$(PtBu$_2$)$_{12}$ **33**,[160] Ga$_{22}$R$_8$ (R = Ge(SiMe$_3$)$_3$;[161] SitBu$_3$[156]) **34**, [Ga$_{22}$R$_{10}$]$^{2-}$ (R = N(SiMe$_3$)$_2$) **35**;[162] for Ga$_{23}$, [Ga$_{23}$(N(SiMe$_3$)$_2$)$_{11}$] **36**;[163] for Ga$_{24}$, Ga$_{24}$Br$_{22}$ **37**,[164] Ga$_{24}$Se$_2$Br$_{18}$ **15**;[117] and for Ga$_{26}$, [Ga$_{26}$(Si(SiMe$_3$)$_3$)$_8$]$^{2-}$ **38**[165]). Furthermore, depending on the ligands involved, up to four different cluster arrangements are known for the same number of Ga atoms; for example, four distinct Ga$_{22}$ cluster types (**30** (**34**), **31** (**32**), **33**, **35**) are known. Among the many curiosities exhibited by the metalloid Ga clusters, we only want to discuss the following selected topics: section 6.2.1, Ga$_8$R$_6$, a metalloid cluster with a real metal-to-metal bonds; section 6.2.2, Ga subhalides and their relation to the modifications of Ga; and section 6.2.3, the largest Ga metalloid clusters, Ga$_{51}$R$_{14}$Br$_6$ and Ga$_{84}$R$_{20}$.

6.2.1. Ga$_8$R$_6$: A Metalloid Cluster with a Real Metal-to-Metal Bond[166]

The structure of the Ga$_8$R$_6$ cluster [R = C(SiMe$_3$)$_3$], **39**, is made singular by its prototypical central Ga−Ga bond (see Figure 26).[166] In order to understand this feature, it is helpful to go back to the first examples of metal−metal bonding. In the 1960s, the primary interest in simple cluster compounds such as [(CO)$_3$CpW−WCp(CO)$_3$], [(CO)$_5$Mn−Mn(CO)$_5$], and ClHg−HgCl lay in the bond between the metal atoms, since the complex bonding situation in the metals themselves is here reduced to a 2e−2c bond.[167,168] Since ligands such as halogen atoms or CO undergo strong interactions with the metal atoms and thus strongly influence the bond between the two metal atoms, however, such a bonding situation is fundamentally different from that in metals. Compounds of the type Y$_3$X−XY$_3$, where X and Y are metal atoms linked together in two XY$_3$ tetrahedral clusters, are therefore of particular significance. To date, however, there are only a few examples in which some of the metal atoms are replaced
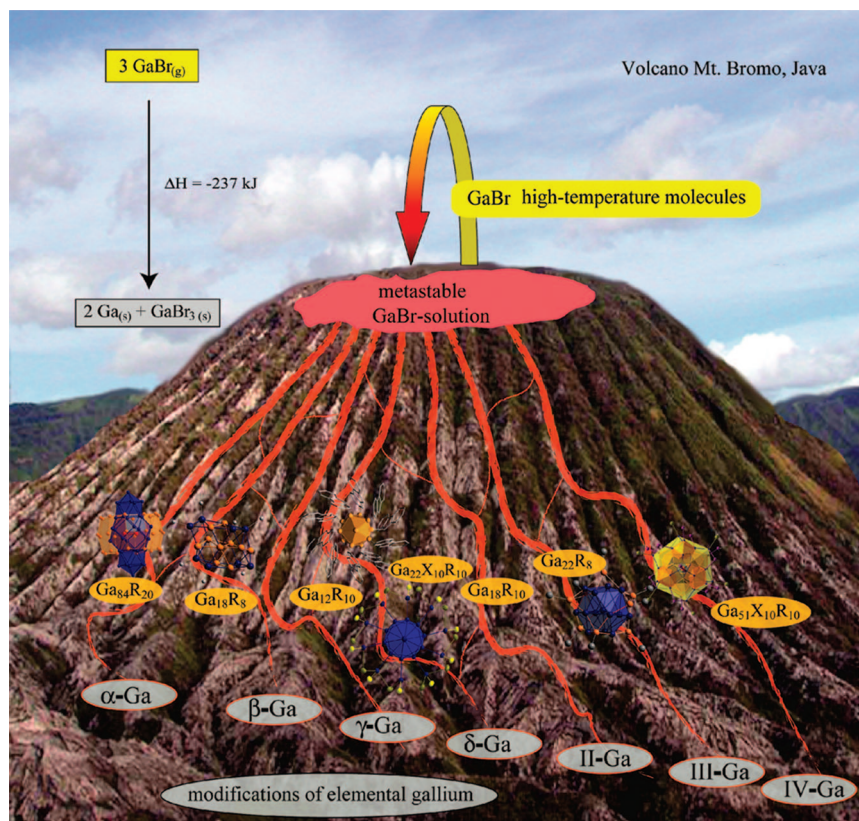
Figure 25. This cartoon with Mt. Bromo, East Java, Indonesia, illustrates in a simple manner the hypothetical routes to the formation of different modifications of bulk gallium via different metalloid gallium clusters affording snapshots of this highly complex process of self-organization initiated by the high temperature molecule GaX. Modified cover picture of *Dalton Transactions* 2005.

(39)
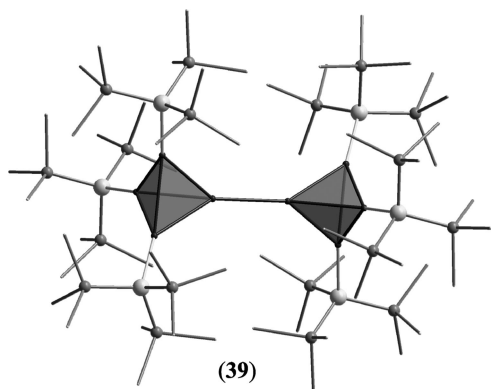
Figure 26. Molecular structure of $[Ga_8R_6]$ $[R = C(SiMe_3)_3]$ (**39**); the central Ga_8 unit is emphasized via a polyhedral representation.

by nonmetal atoms.[172,173] The metalloid cluster compound **39** provides the first example of a metal-to-metal bond constrained only by the interactions to other metal atoms, the eight metal atoms, M, in the form of two linked M_4 tetrahedra forming 13 metal−metal bonds but only 6 metal−ligand bonds. Consequently, the Ga_8R_6 cluster **39** can be regarded as a prototype[166] with a 2e−2c metal-to-metal bond unaccompanied by bridging atoms and with the metal atoms otherwise bonded to other metal atoms of the same type. The bond strength has been classified by theoretical calculations as lying between that of a classical 2e−2c bond and a 2e−3c bond.[110,174] As expected, the charges on the Ga atoms in **39** differ only slightly. The central Ga atoms bear a slightly negative partial charge (in contrast to the positive partial charges carried by the metal atoms engaged in the localized metal−metal bonds found in compounds such as

ClHg−HgCl), so that **39** contains metal−metal interactions similar in character to metallic metal−metal bonds. Hence, it is possible for the first time to compare a largely localized bond in a molecular unit with the delocalized bonding in metals. The Ga_8R_6 cluster could be said to represent the first model compound for a metal atom contact[143] in the form of a nanometal wire. Its characterization thus provides not only the stimulus, but also a yardstick for future theoretical and experimental investigations on the reaction between metal atom clusters, from their primary contact to their fusion to give larger clusters.

But is **39** really a metalloid cluster? We believe the answer to be "yes" for many reasons. First, the central Ga_2 unit reflects the motif of α-gallium. Second, the Ga−Ga distance in the Ga_2 unit at 2.61 Å is comparable to the Ga−Ga distances (2.60 Å) in the Ga_n wire in the center of the Ga_7 tubes of δ-gallium (see Supporting Information). Furthermore, the black color and the small HOMO−LUMO gap in **39** contrast with Wade-like species with a similar number of Ga atoms and testify to the metalloid character of this singular Ga cluster. Finally, we may view **39** as the gallium counterpart to the Al_7R_6 cluster **20**, which is the smallest truly metalloid cluster of aluminum. In **20**, only one metal atom connects two tetrahedral moieties, whereas in Ga_8R_6, by analogy with the structure of α-Ga, a Ga_2 moiety is the connecting unit.

6.2.2. Ga Subhalides and Their Relation to the Modifications of Ga

6.2.2.1. $Ga_{10}X_{10}$ and Ga_8X_8 Species.[175−177] The synthesis and especially the isolation of aluminum and gallium subhalides in pure crystalline form set a challenge, these
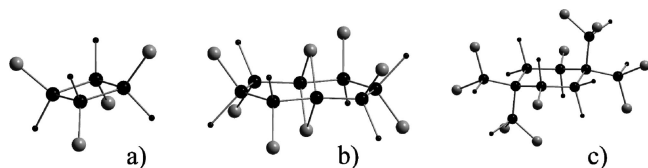
Figure 27. (a) $Al_4X_4 \cdot 4L$, **26**; (b) $Ga_8I_8 \cdot 6L$, **43**; (c) $Ga_{10}Br_{10} \cdot 10L$, **40**. Al, Ga (black); halogen (gray); directly bonded atoms of the donor molecules (small).

Scheme 4. Schematic Presentation of the Formation of $Ga_5X_7L_5$ Subhalides 36 via the Insertion Reaction of GaX Molecules into the Ga−X Bonds of GaX_3
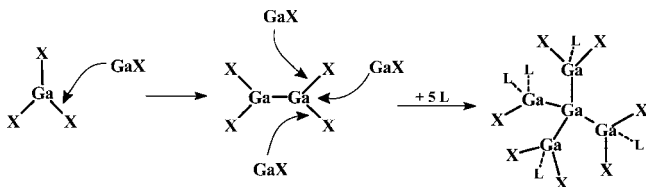
binary compounds being more difficult to handle than are ligand-stabilized clusters because there are fewer parameters that can be manipulated. However, the isolation of such subhalides, with or without ligand stabilization, is important for the direct insight it offers to the reaction pathways taken during the formation of metalloid cluster compounds via the facile disproportionation of the parent subhalides.

Planar metal moieties (Al_4 and Ga_8) are the remarkable structural features of the Al_4Br_4, Al_4I_4, and Ga_8I_8 compounds (Figure 27a,b). In contrast, the recently published $Ga_{10}Br_{10}$ molecule represented a highly mixed valent subhalide:[175] $Ga_4(GaBr)_2(GaBr_2)_4$ **40** (Figure 27c).

6.2.2.2. $Ga_{10}Br_{10}$.[175] With respect to the molecular formulas, the average oxidation state of the gallium atoms in $Ga_{10}Br_{10}L_{10}$ (L = 4-tBu-pyridine), **40**, is $+1$.[175] However, its structure, as shown in Figure 27, implies that it is really a mixed-valent subhalide composed of four gallium(0), four gallium(II), and two gallium(I) atoms. The arrangement of the gallium atoms might then be described as being similar to that found in elemental α-gallium. Furthermore, the structure of **40** and the conditions necessary for its synthesis allude to a plausible mechanism for its formation and subsequent reactions. Thus, it is formed by the reaction of two Ga_5Br_7 entities[178] (similar to $Ga_5Cl_7 \cdot 5Et_2O$, **19**[92]) with an excess of GaBrL with the elimination of $GaBr_3L$ (Scheme 4). The $GaBr_3L$ molecules generated will be further reduced by insertion of the excess of GaBrL, and Ga_5Br_7 is regenerated; an analogous mechanism has been described for the formation of the Al_5X_7 species **9**.[90,109] When THF is used as the donor, the 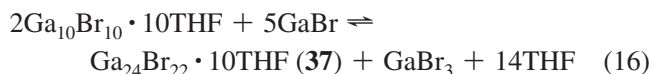reaction does not stop at **40** but proceeds via the formation of additional Ga−Ga bonds and further reduction of **40** by GaBr to the compound $Ga_{24}Br_{22}(THF)_{10}$, **37**, as represented formally by eq 16 (see above). According to DFT calculations, this reaction is exothermic by -560 kJ mol^{-1}. During the preparation of $Ga_{24}Br_{22}(THF)_{10}$, **37**, the volatile THF was

$$2Ga_{10}Br_{10} \cdot 10THF + 5GaBr \rightleftharpoons$$
$$Ga_{24}Br_{22} \cdot 10THF \text{ (37)} + GaBr_3 + 14THF \quad (16)$$

repeatedly removed by evacuation, so the equilibrium of eq 16 was shifted to the right to favor the formation of the polyhedral Ga_{24} subhalide **37**. During the synthesis of **40**, the less volatile donor 4-*tert*-butyl-pyridine was used instead of THF, and the reaction temperature was kept below −20

(42)
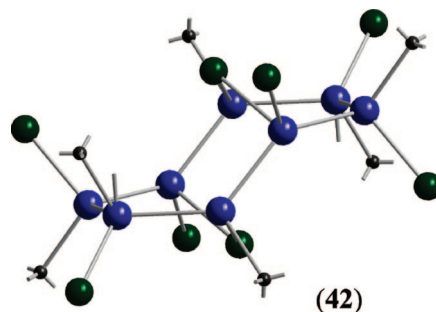
Figure 28. Molecular structure of $Ga_8Br_8 \cdot 6NEt_3$ (**42**) in the crystal. Only the directly bonded N-atoms of the NEt_3 donor molecules are shown.

°C. Consequently, **40** could be trapped as an intermediate during the formation of **37**.

The disproportionation of **40** to **37** and finally to gallium metal and $GaBr_3$ is a chain reaction, and thus $GaBr_3$ formed in each step reacts further with excess GaBr to form Ga_5Br_7 species, which are reintroduced into the reaction cascade. The formation of gallium metal by disproportionation is fairly restrained at temperatures below −20 °C (at this temperature, β-gallium and δ-gallium should form). It may well be that the activation energy for the transformation of the puckered Ga_6 ring structure of **40** into β-gallium (planar Ga_n layers) or δ-gallium (icosahedral fragments) is too high. The fragmentation of **40** with the simultaneous formation of gallium metal starts reluctantly even at −18 °C and proceeds rapidly and completely at a little above room temperature. In this temperature range, α-gallium and liquid gallium are the stable phases. Since the topology of the Ga_6 ring in **40** is very similar to the Ga_6 framework in α-gallium (see Supporting Information), it seems likely that the precipitation of α-gallium from **40** does not require a large activation energy. For the halides, kinetically simple insertion reactions (e.g., $4GaX + GaX_3 \rightarrow Ga_5X_7$) lead to their rapid disproportionation even at low temperatures, and consequently make extremely difficult the isolation of the subhalides. By contrast, further reactions are blocked if similar clusters are protected by bulky ligands; for example, the gallium(I) compound $[Ga_6(SiPh_2Me)_8]^{2-}$, **41**,[179] with a Ga_6 framework similar to that in β-gallium does not decompose to the metal even above room temperature.[175] The isolation of **40** as an intermediate during the disproportionation of a metastable GaX solution thus allows the first insight into this complex process of self-organization. During the process, metalloid clusters with an increasing number of "naked" Ga atoms in the core and GaX_2 entities in the periphery grow by association, redox, and elimination reactions and can be regarded as precursors to nuclei for the crystallization of the bulk metal.

6.2.2.3. Ga_8X_8.[176,177] In order to broaden the knowledge about Al and Ga monohalides, we frequently asked ourselves the following questions during the last years: (1) Are hypothetical Ga_4X_4 molecules (similar to Al_4X_4 species) precursor molecules for the formation of Ga_8X_8 species (see Ga_8I_8 in Figure 27)? (2) Is there a topological and energetic relation between the Ga_8 moiety in the Ga_8I_8 molecule and the structure of the low-temperature modifications of gallium (β-, γ-, δ-Ga)?[3,6,7] These questions have been answered in a recent contribution on the basis of the red-orange compound $Ga_8Br_8 \cdot 6NEt_3$, **42** (Figure 28).[176] Its ladder-like structure is significantly different from that of the isoelectronic $Ga_8(\mu_2\text{-}I)_2I_6 \cdot 6PEt_3$, **43**[177] (Figure 27b): its planar Ga_8-ring is only stabilized by an orthogonal transannular Ga_2I_2-ring system.

Scheme 5. DFT-Calculated Oligomerization and Disproportionation Energies of GaBr in the Presence of NEt₃[a]
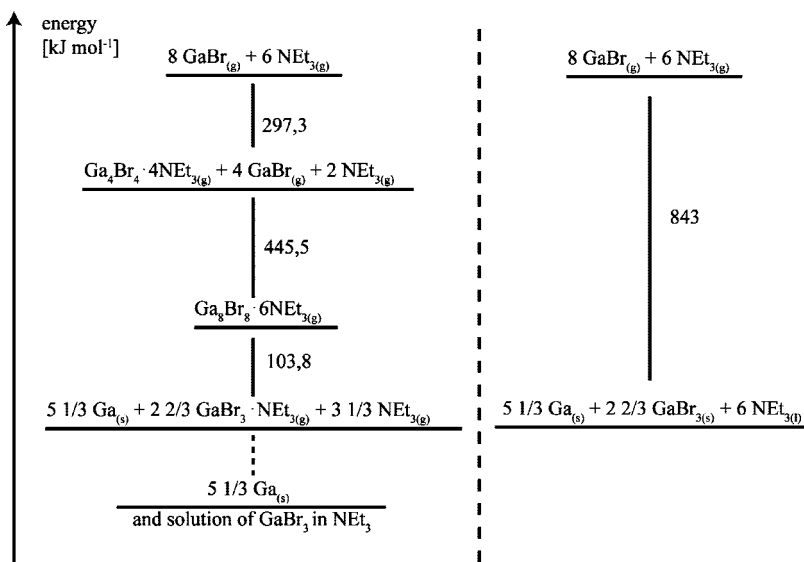
[a] The energy of the dashed reaction to the GaBr₃ solution in NEt₃ should not be significantly larger than the condensation energy of $3^{1}/_{3}$ NEt₃ (117 kJ). For comparison, the experimental ΔH°_{298} values for the disproportionation of eight GaBr molecules are included on the right side.
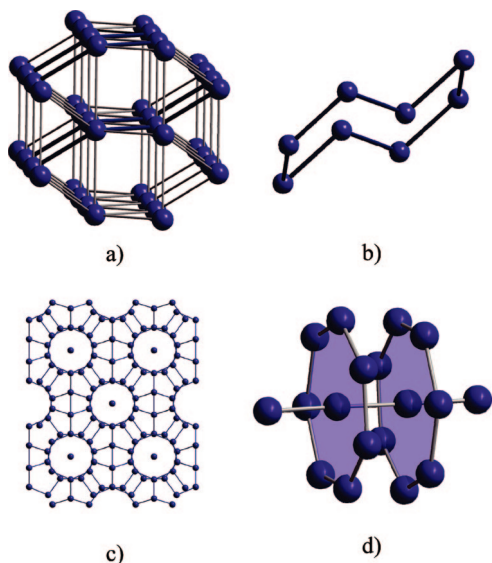
Figure 29. Fraction of the structures of the low-temperature modifications of β-Ga (a) and γ-Ga (c) (plane orthogonal to c-axis) and Ga_8 units of β-Ga (b) and Ga_8 units of γ-Ga (d) expanded to a Ga_{18} moiety.

Molecular $Ga_4Br_4 \cdot 4NEt_3$ detected mass spectrometrically[176] has been shown via DFT calculations to be an intermediate on the way to **42**. The energetic relation between the tetramerization and the octamerization of GaBr together with the disproportionation energy of **42** ($Ga_8Br_8 \cdot 6NEt_3$) to metallic Ga and NEt₃-stabilized $GaBr_3$ is visualized in Scheme 5.[176] The energetic similarity between **42** and its disproportionation products is in line with the experimental difficulties of the isolation and handling of Ga(I) halides, because elemental gallium often precipitates simultaneously.

Since the arrangement of the Ga-atoms in **42** is very similar to that of the low-temperature modifications of β-gallium (-16.3 °C)[180] (see Figure 29a,b and Supporting Information), it seems, in accordance with many of our former investigations, to be a plausible hypothesis to correlate the structure of **42** as an arrangement of gallium atoms in the direction of the formation of β-gallium.[6,7] Since γ-gallium

is formed at lower temperatures (-35.6 °C; see Figure 29c,d), the above-mentioned hypothesis can be expanded: **43** may represent a preorientated structure of γ-gallium.[181] This extended hypothesis is in line with the conditions under which **42** and **43** and, respectively, β- and γ-gallium are formed at different temperatures: **42** is formed at -25 °C analogous to β-Ga (less than -16.3 °C), and **43** is formed at -78 °C analogous to γ-Ga (less than -35 °C). In accordance with this hypothesis, based on the conditions of their formation, and the energetically preferred arrangement of the Ga atoms like in **43**,[176] the averaged Ga−Ga distances in **43** (see above) as well as in γ-gallium[182] are significantly shorter than those in **42** (see above) and β-Ga.[180,183] However, a comparison of the distances of β- and γ-gallium seems to be problematic, especially because there is a large variation of different coordination motifs.[182,183] Therefore, we have performed the following comparison, based on the volume of different moieties: For characteristic Ga_8 units (Ga_8-unit-containing fragments, see Figure 29b, d,with experimentally determined structure), the volume is calculated via DFT calculations. The following atomic volumes result: [volume/atom in Å³] Ga_8 in Ga_8Br_8 **42** 42.81; Ga_8 in Ga_8I_8 **43** 42.38; Ga_8 ($GaGa_7$) in γ-Ga 41.88 (40.79[176]); Ga_8 in β-Ga 42.54.

Our hypothesis with **42** and **43** as preorientated arrangements of Ga_8 entities within the low-temperature phases of β- and γ-gallium is supported by the missing observation of a gallium subhalide corresponding to the third low-temperature modification, δ-Ga (-19.4 °C).[180] The most remarkable feature of δ-gallium is the substructure of interpenetrating icosahedral Ga_{12} units. Therefore, it could be expected that via the addition of Ga_4X_4 molecules $Ga_{12}X_{12}$ species may be formed from Ga_8X_8 halides. However, this route postulated for Al subhalides ($Al_4 \rightarrow Al_8 \rightarrow Al_{12} \rightarrow Al_{22}$)[131] has to be excluded since $Ga_{12}X_{12}$ species prefer octahedral Ga_6 units (e.g., $Ga_6(GaX_2)_6$) instead of the icosahedral arrangement.[184] Therefore, preorientated Ga subhalides as intermediates on the way to δ-Ga have to be formed in a different manner as we recently have shown for the synthesis of the mixed valent $Ga_{10}Br_{10}$ (Figure 30)[175] and its coupling to a $Ga_{24}Br_{22}$ molecule (**39**).[164] This special and the complete relation
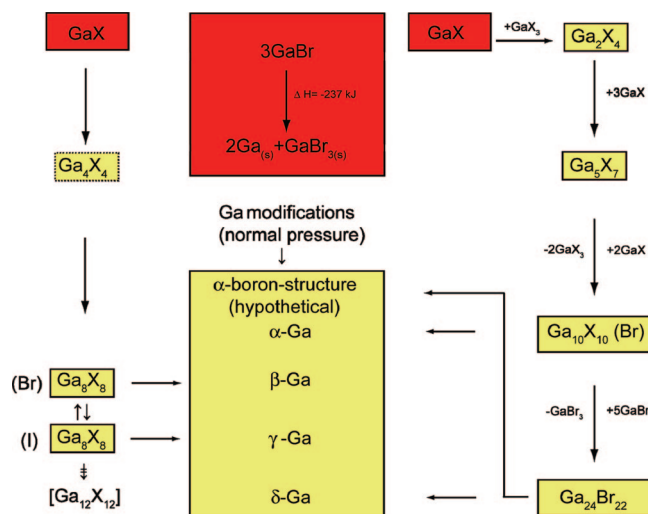
Figure 30. The formation of the different normal pressure modifications of gallium via disproportionation reactions of Ga(I) halides. Starting with monomeric GaBr, this process develops via association steps ($Ga_8X_8$) (left side) or via insertion steps into $GaBr_3$ molecules and subsequent addition of GaBr molecules ($Ga_{10}Br_{10}$, $Ga_{24}Br_{22}$) (right side).

between Ga subhalides and some modifications of Ga are summarized in Figure 30.

To sum up, the trend for the formation and structure of the bulk phases (β- and γ-fragments) very well corresponds to that of the Ga fragments within the molecules **42** and **43**.

6.2.2.4. Ga_{24} Subhalides with an Icosahedral Ga_{12} Core.[117,164] 6.2.2.4.1. $Ga_{24}X_{22}$ (37).[164] The aluminum subhalide clusters $Al_{22}X_{20} \cdot 12THF$, **24** and **25**, have been described as intermediates during the disproportionation of AlX to aluminum metal and the corresponding aluminum trihalide and as a step during the formation of a new modification of aluminum with a structure analogous to that of α-B.[140] The question naturally arises then whether a similar gallium subhalide can be formed. Such a possibility finds support from the metalloid clusters $[Ga_{22}Br_{11}R_{10}]^{3-}$, **31**, and $[Ga_{22}Br_{12}R_{10}]^{2-}$, **32**, which are partially substituted but also have an icosahedral Ga_{12} core without a central Ga atom. The compound that comes closest to $Al_{22}Br_{20} \cdot 12THF$, **25**, is $Ga_{24}Br_{22} \cdot 10THF$, **37**, which is synthesized from a donor-poor GaBr solution (toluene/THF) that is slowly warmed from $-78\ °C$ to room temperature over several days. During the synthesis, the THF concentration has to be kept low, so that eq 16 is displaced from a hypothetical metalloid cluster $Ga_{10}Br_{10} \cdot 10THF$, similar to **40**, so as to favor the formation of $Ga_{24}Br_{22} \cdot 10THF$, **37**.[164]

As shown in Figure 31, **37** consists of a molecule with a center of inversion, having a central, slightly distorted Ga_{12} icosahedron to which 12 other Ga atoms are linked by 2c–2e bonds. The Ga–Ga bond lengths of the central Ga_{12} icosahedron vary from 2.55 to 2.67 Å; the Ga–Ga bond distances from the Ga_{12} icosahedron to the terminal Ga atoms are significantly shorter (2.40 Å). This is to be expected since these Ga atoms are also bonded to Br atoms and so have a higher formal oxidation state, leading to a smaller covalent radius. Compared with the central Ga_{12} icosahedron, the external Ga_{12} icosahedron is strongly distorted as a result of the varied coordination of the Ga atoms: Two *para*-positioned Ga atoms are bonded to three Br atoms, one exclusively and the other two shared with neighboring Ga atoms. Each of the other external Ga atoms is bound to two Br atoms and one O atom from the THF molecule. The
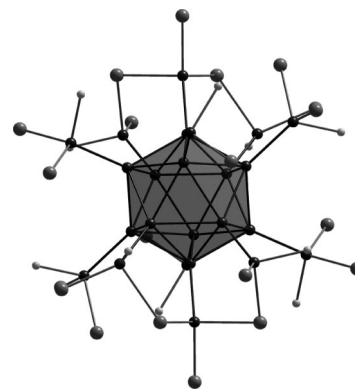
Figure 31. Molecular structure of $Ga_{24}Br_{22} \cdot 10THF$ (**39**) (of the THF molecules only the oxygen atoms directly bound to the gallium atom are shown).

average atomic volume calculated from the volume of the Ga_{24} core in **37** is about 3% smaller than the volume of an Al atom in the $Al_{22}X_{20}$ cluster **25**, a result consistent with the smaller atomic radius of Ga compared with Al. As in the earlier discussion of aluminum clusters, **37** might therefore be seen as an intermediate in the decomposition of the monohalide to an α-boron-type modification of gallium. Such a notion receives further support from theoretical calculations, as discussed in section 6.1.3.

6.2.2.4.2. $Ga_{24}Br_{18}Se_2$ (15).[117] Because the neutral binary metalloid cluster compounds $Al_{22}Br_{20} \cdot 12THF$, **25**, and $[Ga_{24}Br_{22}] \cdot 10THF$, **37**, occupy an exceptional position among metalloid Al and Ga clusters, further investigations are clearly indicated. In order to take advantage of the special features of **25** and **37**, substitution of some of the halogen atoms by other suitable functional ligands would allow the study of defined clusters and of their interactions with, for example, Au surfaces or other clusters. Substitution of halogen atoms by selenium seemed expedient because of the availability of suitable precursors, for example, $[Se(SiMe_3)_2]$, which allow the formation of neutral species (like **25** and **37**) without salt elimination or breaking of Ga–Ga bonds in the cluster framework. In fact, the reaction of a solution of $Se(SiMe_3)_2$ in THF with a metastable GaBr solution (toluene/THF) gives after several days the compound $Ga_{24}Br_{18}Se_2 \cdot 12THF$, **15**, in the form of yellow, air-sensitive rods in nearly quantitative yield.[117] Crystal structure analysis shows the central framework of the Ga_{24} cluster to be formed by an icosahedron of 12 Ga atoms (Figure 32). These "naked" Ga atoms feature only metal-to-metal bonds, so that **15** is unquestionably a metalloid cluster.[6,12] Each of the 12 inner Ga atoms is coordinated by a ligand-bearing Ga atom, leading to a second, though distorted outer Ga_{12} icosahedron (Figure 32c). Each of the inner Ga atoms is thus coordinated by six Ga atoms, and each of the outer Ga atoms is bound to two ligands as well as one THF molecule. Six of the outer Ga atoms bear two terminally bonded Br atoms, and the remaining six bear one terminally bonded Br atom and in total two 3-fold-capping Se atoms. Hence, the coordination number of all the outer Ga atoms is 4. The two Se atoms are at opposite ends of the cluster and form, together with the 18 Br atoms, a pentagondodecahedron (Figure 32d). The $Ga_{24}Se_2Br_{18}$ units are surrounded by an icosahedral shell formed by the 12 O atoms of the THF molecules (Figure 32e).

The shortest Ga–Ga distances are between the atoms of the inner and outer icosahedra (2.40 and 2.42 Å); those in the inner icosahedron vary between 2.57 and 2.67 Å. The
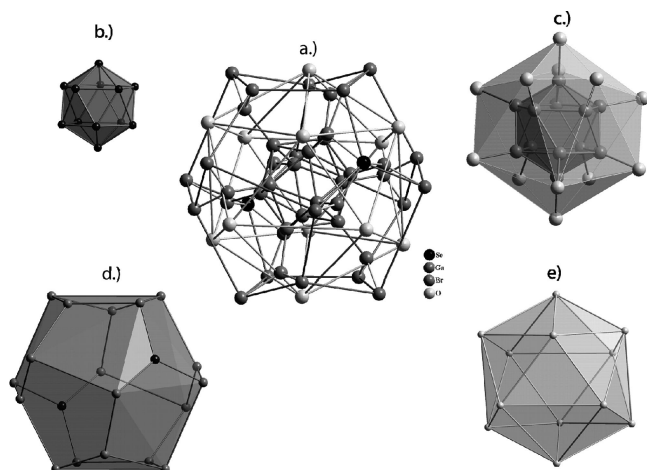
Figure 32. Molecular structure of $Ga_{24}Br_{18}Se_2 \cdot 12THF$ (**15**) inside the crystal: (a) complete $Ga_{24}Br_{18}Se_2O_{12}$ unit; (b) central Ga_{12} core; (c) Ga_{24} unit; (d) $Br_{18}Se_2$ pentagondodecahedron; (e) O_{12} icosahedron of the 12 THF molecules.

bonding situation is therefore similar to the one discussed for **25** and **31**.[140,141,164] Cluster **15** exhibits a nearly undistorted topology of icosahedral and dodecahedral moieties, as compared with the Ga_{24} cluster **37** and the Al_{22} cluster **25**. This finding is understandable because all three clusters contain a "shell" of 32 nonmetal atoms in addition to their metal atom framework[164] (**25**, 20 halogen atoms + 12 O atoms (THF); **37**, 22 Br atoms + 10 O atoms; **15**, 18 Br atoms + 2 Se atoms + 12 O atoms), but only for **15** does the number of shell atoms match that required by dual polyhedra (icosahedra and dodecahedra): 12 + 12 + 20 + 12 = 56. The arrangement of the individual $Ga_{24}Br_{18}Se_2 \cdot 12THF$ clusters in the crystal structure will be discussed elsewhere (section 7.2) since the Se···Se contacts show an unexpected relationship to solid selenium and an even closer one to crystalline GaSe.

6.2.3. The Largest Ga metalloid Clusters $Ga_{51}R_{14}Br_6$ and $Ga_{84}R_{20}$

6.2.3.1. $Ga_{51}R_{20}^{3-}$ (44).[185] The structures of the $PtBu_2$-substituted Ga clusters containing 12, 16, 18, and 22 Ga atoms (**45**, **14**, **29**, and **33**) have shown that, in contrast to the behavior of terminally bonded ligands such as $Si(SiMe_3)_3$ or $SitBu_3$, steric and electronic influences cause the phosphorus atoms in PR_2 ligands to form also bridging bonds, leading to an increased interaction with the Ga_n core, as emphasized in Scheme 6. This bridging ability has a constricting effect, causing the gallium core to become more compressed, as discussed for $[Ga_{16}(PtBu_2)_{10}]$, **14** (section 5.3; Figure 16). If larger Ga_n cores in metalloid clusters with surrounding $GaPR_2$ shells were to be available, it follows that centered structures with high coordination numbers for the central gallium atom, as in the fcc packing recently found in Ga-IV at high pressures, might be expected.[186,187] This speculation has been fulfilled in the anionic cluster $[Ga_{51}(PtBu_2)_{14}Br_6]^{3-}$, **44**, which is obtained, together with

Scheme 6. Bonding Principles in Metalloid $Ga_n(GaR)_m$ Clusters

$$nGa + mGaR \longrightarrow Ga_n(GaR)_m$$
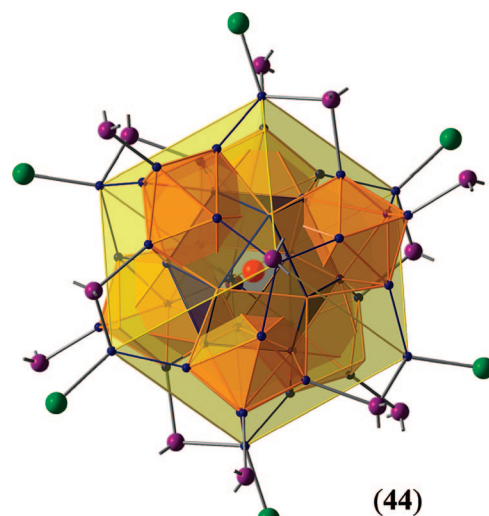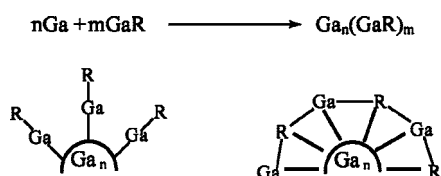
Figure 33. Molecular structure of $[Ga_{51}(PtBu_2)_{14}Br_6]^{3-}$ (**44**). For clarity, only the bonds to the α-carbon atoms are shown in the $PtBu_2$ groups.
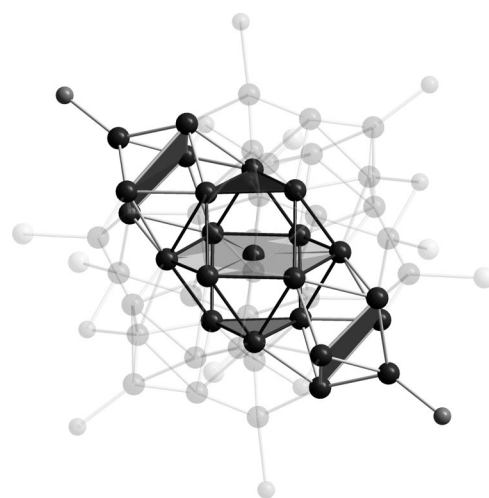
Figure 34. Arrangement of 51 Ga atoms inside $[Ga_{51}(PtBu_2)_{14}Br_6]^{3-}$ (**44**). The central cuboctahedral arrangement and two square antiprismatic Ga_8 arrangements are highlighted.

one $[Li_2Br(THF)_6]^+$ and two $[Li(THF)_4]^+$ ions, in the form of black crystals from the reaction of an annealed GaBr solution with a slight excess of $LiPtBu_2$.

The molecular structure of **44** deduced from crystal structure analysis reveals a metalloid cluster with 31 "naked" and 20 ligand-bearing Ga atoms (Figure 33). The central Ga atom (red, Figure 33) is surrounded by 12 more Ga atoms (blue) in an only slightly distorted cuboctahedral environment with an average Ga–Ga distance of 2.844 Å. The six slightly distorted square planes of this Ga_{12} cuboctahedron are capped with Ga_5 units (orange, Figure 33), with an average Ga–Ga distance of 2.68 Å, leading to square antiprismatic units containing a plane capped by a $GaPR_2$ unit. Two of the six Ga_5 moieties are depicted in Figure 34. Of the four Ga atoms in the distorted square formations, two form bonds to Br-bearing Ga atoms, one is bound to a Ga atom with a terminal $PtBu_2$ group, and the fourth binds directly to a bridging $PtBu_2$ group. The three Ga atoms that are directly bound to the six Ga_4 squares form a distorted Ga_8 cube, highlighted in yellow in Figure 33. Six of the eight Ga atoms in the cube form bonds to terminal Br atoms, while two are bonded to terminal $PtBu_2$ groups. Together with the six bridging $PtBu_2$ groups, this results in a pseudo-6-fold axis of rotation. The structure

of **44** is unique in cluster chemistry and merits some discussion and substantiation.

The central Ga_{13} unit (Figure 34) is very symmetrical and compact. Single-point DFT calculations based on the experimentally determined structural data result in a volume of 35.0 $Å^3$ $atom^{-1}$, which, as expected, lies between that of the fcc packing in the recently determined Ga-IV high-pressure modification (30.5 $Å^3$ $atom^{-1}$) and the volume calculated by extrapolation of this high-pressure version to normal pressure (38.5 $Å^3$ $atom^{-1}$) (cf. Figure 40 above).[185] Additionally, the Ga–Ga distances in **44** steadily decrease with decreasing coordination number from the interior to the exterior; the increasing covalent component of these bonds also becomes clear on moving outward from the center. The Ga_5 units on the square surfaces of the cuboctahedron form square Ga_8 antiprisms. The topology of these Ga_8 units on the one hand and the almost perfect cuboctahedral arrangement around the central Ga atom on the other hand resemble the different bonding patterns in modifications of solid elemental gallium. Hence, it is clear that both nonmetalloid and metalloid bonding types are present in **44**, as exemplified by the Ga_8 unit and Ga core, respectively. The arrangement of the $[Ga_{51}(PtBu_2)_{14}Br_6]^{3-}$ cluster anions (roughly 2 nm in diameter) in the crystals is slightly distorted cubic closed packed, with all of the tetrahedral holes filled by $[Li(THF)_4]^+$ ions and all of the octahedral holes by $[Li_2Br(THF)_6]^+$ ions. The result is similar to the Li_3Bi structure typical for $C_{60}M_3$ fullerides, but the diameter of the cluster anion $[Ga_{51}(PtBu_2)_{14}Br_6]^{3-}$ is about three times that of the fulleride ion C_{60}^{3-}. In the light of the behavior of the $Ga_{84}R_{20}^{4-}$ cluster, **11**[113] (metallic conductivity, superconductivity; see section 7.3), similar investigations should surely be performed on **44**. Since **44** could be present as both a 3– and 4– anion in the same crystal,[115] such cluster doping is a challenge inviting conductivity measurements.

6.2.3.2. $Ga_{84}R_{20}^{4-}$ (11): The Largest Metalloid Cluster and Comparisons with Metalloid Clusters of the Noble Metals.[113] Under reaction conditions similar to those used for the synthesis of the $[Al_{77}R_{20}]^{2-}$ cluster, **1**[17] (section 6.1.2), the Ga_{84} cluster $[Ga_{84}\{N(SiMe_3)_2\}_{20}]^{4-}$, **11**,[113] is obtained from the reaction of a metastable GaBr solution (toluene/THF) with $LiN(SiMe_3)_2$. The molecular structure of the anion **11** is illustrated in a fashion similar to that of **1** in Figure 35. At the center is a Ga_2 unit, a feature unique in this field of chemistry and resembling the Ga_2 dumbbell unit of α-gallium. The Ga_2 unit is surrounded by a Ga_{32} shell in the form of a football with icosahedral caps. The icosahedral caps resemble the structure of δ-gallium or of the clusters $[Ga_{22}R_{10}X_{11/12}]^{n-}$, **31** and **32**. The apex and base atoms of the Ga_{32} unit, which are naked, are oriented toward each other in the crystal in an unusual fashion. The Ga_2Ga_{32} unit is surrounded by a meandering belt of 30 Ga atoms that are also naked. Finally, the entire Ga_{64} framework is protected by 20 GaR groups [R = $N(SiMe_3)_2$].

The high pseudosymmetry of the cluster molecule **11**, clearly shown in Figure 36, resembles the approximate 5- and 10-fold symmetry of quasicrystals, pointing to molecular bonding of the type found in the fullerenes. An affinity to the recently published cadmium/gallium phases can also be perceived.[188] On the other hand, the spherical layered construction (Figure 35) is wholly in character with metalloid clusters such as $[Al_{77}R_{20}]^{2-}$, **1**, so that the bonding in **11** can be described as intermediate between the two extremes. In addition to crystals containing only $Ga_{84}R_{20}^{4-}$ species **11**
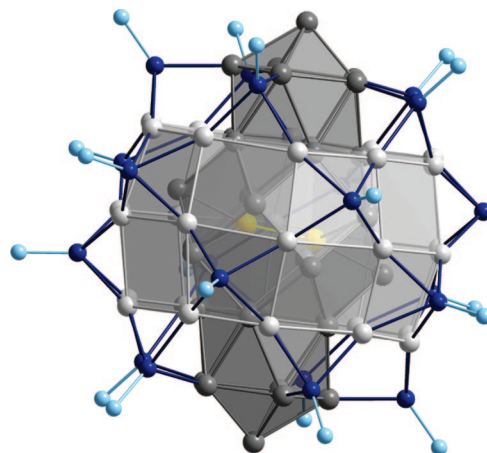
Figure 35. Molecular structure of the anion $[Ga_{84}R_{20}]^{4-}$ [R = $N(SiMe_3)_2$] (**11**); only the N atoms (light blue) directly bonded to the Ga atoms are shown. There are 2 (yellow) + 32 (dark gray) + 30 (light gray) = 64 "naked" and 20 ligand-bearing (blue) Ga atoms.
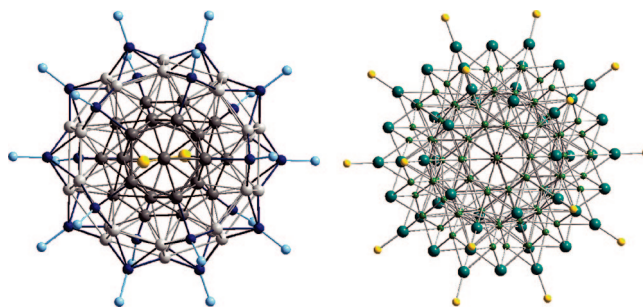
Figure 36. Projection of the metalloid Ga_{84} cluster (**11**, left) and $PtPd_{164}(CO)_{72}(PPh_3)_{20}$ (right) to show the similar arrangement of metal atoms with respect to the 5-/10-fold axis. In both clusters, 20 Ga–N or 20 Pd–P units represent the outer sphere. In $PtPd_{164}(CO)_{72}(PPh_3)_{20}$, however, there are 72 additional CO ligands to connect the different cluster shells [Pt/Pd_{12}/Pd_{30}/Pd_{12}/$(CO)_{12}$/Pd_{60}/Pd_{30}/Pd_{20}/$\{PPh_3\}_{20}$].

(denoted by Ga_{84}^{4-}),[113] another charge state of the Ga_{84} unit can be obtained in crystalline form, namely, the $Ga_{84}R_{20}^{3-}$ cluster species **11'** (denoted by Ga_{84}^{3-})[1,115] exhibiting a slightly different arrangement in the ionic lattice. With respect to the number of "naked", non-ligand-bearing metal atoms, the Ga_{84} clusters **11** and **11'** are the largest of this type as yet to be structurally characterized.[113] With their 64 naked Ga atoms, they are even larger than a very recently published $PtPd_{164}$ cluster[189] or a Au_{102} cluster.[16] In the Au_{102} cluster, only 39 "naked" Au atoms build up the cluster core (see section 8), and there are only 43 such atoms in the $Pt@Pd_{42}$ core of the $PtPd_{164}$ cluster (Figure 36; see section 6.3). In both cases, therefore, the ligands are not only a protecting shell for the cluster core, but also the glue between the inner and outer metal shells of these metalloid cluster compounds.[16,189] Yet there are obvious structural similarities between the Ga_{84} and $PtPd_{164}$ clusters, for example, the 10-fold/5-fold symmetry and the very similar arrangement of the 20 outer ligands (see Figure 36). Nevertheless, the Ga_{84} cluster units show several special structural peculiarities.

First, the cluster center (which is also the inversion center of the cluster) houses a Ga_2 dumbbell with a very short Ga–Ga distance of 2.34 Å. This is not much larger than in the so-called Ga–Ga triple bond[6,190] and only slightly shorter than, for example, the Ga–Ga distance in $Ga_2I_6^{2-}$ units.[191] Second, the 42 (84/2) crystallographically different Ga atoms

(differing in coordination number and distances) are, in principle, also chemically different. In other words, this cluster represents a molecule with the highest degree of mixed valency. This special bonding feature is valid, although to a lesser degree, for nearly all the other metalloid clusters discussed so far. A direct experimental proof of this special highly mixed-valent bonding will be presented in section 7.3. There is a fundamental difference here from the precious metal atom clusters such as Pd_{145}[14] and $PtPd_{164}$,[189] whose synthesis and structure show that all the metal atoms retain their zero-valent character. Thus, there is no suggestion of mixed valency with the precious metal clusters, whereas the situation is quite different with any metalloid Al or Ga cluster, and especially with the Ga_{84} cluster. Recently, detailed theoretical investigations on the influence of the ligands on a $Ga_{84}R_{20}^{4-}$ cluster have been performed:[144] In contrast to the $Al_{77}R_{20}^{2-}$ cluster (section 6.1.2), even with smaller ligands like NH_2 the experimentally determined structure of the core of 84 Ga in **11** represents the ground-state structure for this hypothetical cluster $Ga_{84}(NH_2)_{20}^{4-}$. Thus, this structure is mostly determined by the special electronic structure of the Ga atoms and their tendency to form clusters as intermediates on the way to the bulk metal.

Another peculiarity of the Ga_{84} cluster compound is the finding that crystals containing the Ga_{84}^{4-} units show a metallic luster suggestive of special physical properties, for example, electrical conductivity. Further consideration of this feature is deferred, however, to section 7.3.

6.3. Si-Substituted Metalloid Al Clusters

6.3.1. $SiAl_{14}R_{12}$[192,193]

To prepare Al cluster compounds that incorporate Si atoms and may thus be important for nanoscale physics, a suitable source of Si atoms must be found. Some 10 years ago, the following experiments were performed. A metastable AlCl solution in toluene/Et_2O (section 6.1.3) was caused to react with $SiCp*_2$ or $SiCl_4/AlCp*$ (as a Si atom source). This was found to give a unique cluster species, $SiAl_{14}Cp*_6$ (**27**), that bears six Cp* ligands protecting the compound from disproportionation with the formation of elemental Al or a Si/Al alloy (Figure 37).[192] The structure of the $SiAl_{14}$ core represents a section of body-centered packing where a Si atom resides at the center of an Al_8 cube and each of the six faces of the cube is capped by an additional AlCp* moiety.
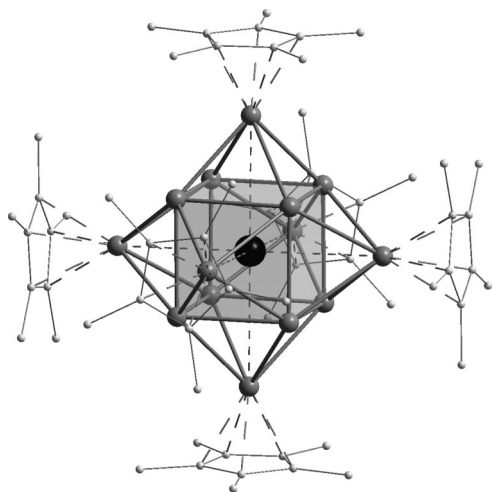
Figure 37. Molecular structure of the metalloid Al cluster $SiAl_{14}Cp*_6$ (**27**).

Table 1. Comparison of Experimentally Determined Average Bond Lengths (Å) in the Metalloid Cluster Compounds $SiAl_{14}Cp*_6$ (27) and $SiAl_{14}R'_6$ (27a [R' = N(SiMe₃)Dipp; Dipp = C_6H_3-2,6-iPr_2; Al_L = Ligand-Bound Al Atom])

distance	**27**	**27a**
Si_{center}—Al_{cube}	2.502	2.493
Al_{cube}—Al_{cube}	2.889	2.878
Al_{cube}—Al_L	2.813	2.749

This cluster compound was investigated by mass spectrometry, X-ray diffraction, ^{27}Al NMR spectroscopy, and ab initio calculations. Hence, $SiAl_{14}Cp*_6$, **27**, came to be the first example of a metalloid cluster to suggest the validity of the jellium model (40 electrons as in Al_{13}^-) for a species that is stable at room temperature. However, the solid contains minor amounts of molecules with additional Cl atoms bonded to the Al atoms at the corners of the cube, and the presence of Cl-containing molecules in the crystal can be rationalized on the basis of the suggested reaction path. Although theoretical and experimental results strongly support the structure shown in Figure 37, X-ray investigations do not allow its rigorous assignment.

Accordingly, another $Si@Al_{14}R'_6$ compound **27a** was synthesized, now with the R' = N(SiMe₃)Dipp (Dipp = C_6H_3-2,6-iPr_2).[193] In this case, there was no contamination of the crystal by Cl-containing molecules. The bond lengths of both $SiAl_{14}$ clusters are collected in Table 1. With the structural data of the new $SiAl_{14}$ compound **27a** and additional FT mass spectrometric measurements using the MALDI technique, it was concluded that about one-third of the $SiAl_{14}Cp*_6$ clusters **27** in the original crystal lattice are replaced by $Si_2Al_{13}ClCp*_6$. The second Si atom occupies one corner of the central Al_8 cube and is directly bonded to one Cl atom. The difficulties of determining the correct composition and structure of the nanoscaled $SiAl_{14}R_6$ clusters thus revealed provide strong arguments for extreme caution in the interpretation of structural results for any nanoscaled species based, for example, on STM/AFM measurements. The potential dangers will become more apparent with the next cluster, $SiAl_{56}R_{12}$ species, **46**.

6.3.2. $SiAl_{56}R'_{12}$[194]

At present, $Si@Al_{56}R'_{12}$ [R' = N(SiMe₃)Dipp], **46**, represents the largest structurally characterized Si-centered Al cluster.[194,195] Its molecular structure is shown in Figure 38. Compared with the $Pt@Pd_{164-x}$[189] and Au_{102} clusters[16] recently described, $Si@Al_{56}R'_{12}$, **46**, actually contains the largest neutral, nanoscaled "metal ball" to be structurally characterized, that is, if only the "naked" and not the ligand-
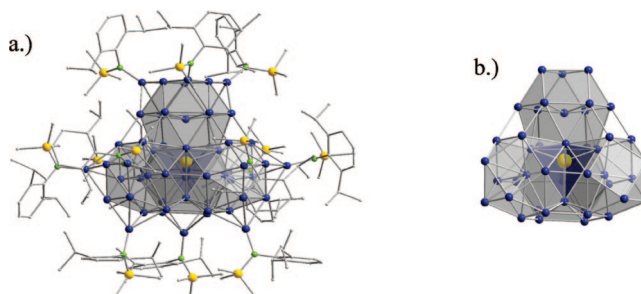
Figure 38. (a) Molecular structure of $Si@Al_{56}R'_{12}$ [R' = N(SiMe₃)Dipp; Dipp = C_6H_3-2,6-iPr_2] (**46**) omitting the hydrogen atoms. (b) Structure of the "naked" $SiAl_{44}$ core in (**46**) built up from four Al_{12} cuboctahedra.

bound metal atoms are considered. Whereas **46** contains 45 such atoms, $Pt@Pd_{164-x}$ has only 43, and the Au_{102} cluster only 39 in the cluster core (section 6.2.3, Figure 36, and section 8).[15,16,189,196] With respect to the synthesis, the formation of the Si-centered metalloid cluster **46** from the reaction of a metastable AlX solution with the Si-containing ligand $N(Dipp)SiMe_3^-$ may come as something of a surprise. However, the preparation of $Si@Al_{14}R'_6$, **27a**, has already established that $N(SiMe_3)Dipp^-$ can serve as a Si source for the formation of Si-centered Al clusters.[193] Obviously, the very slow decomposition of the ligand $N(Dipp)SiMe_3^-$ and the slow release of reactive Si-containing species are absolute requirements for the formation of **46** and its growth around the central Si atom.

In its structure, **46** exhibits a shell-like arrangement in the cluster core dominated by the structure-determining Si center, which might be described as follows. The central Si atom is tetrahedrally surrounded by four Al atoms at a distance of 2.43 Å. The four triangular planes of this Al_4 tetrahedron are the basic triangular planes of four Al_{12} cuboctahedra, resulting in an $SiAl_{44}$ framework of "naked" atoms for the cluster core (Figure 38b). Twelve ligand-bearing Al atoms forming another cuboctahedron are then located on the three rectangular planes of each of the four central Al_{12} cuboctahedra of the $SiAl_{44}$ core. It is to be noted that the Si atom is situated at a tetrahedral site, so that there is no substitution of Al by Si as found, for example, in the SiGa clusters observed in mass spectrometric experiments ($SiGa_{12}$, $SiGa_{22}$, etc.)[197] or in zeolites (SiOAl compounds). This result is in accordance with the Al/Si phase diagram where Si-poor mixed crystals are observed only in a range with less than 2% Si.[198] For this mixed crystal phase, however, no structural information has been reported until now. The concentration of silicon in compound **46** is very similar to that in the mixed crystal phase, so that the experimentally determined structure of **46** might be seen to model microcrystalline areas of the mixed crystal phase in the Al/Si phase diagram. The structure-determining role of the central Si atom in **46** is significant in showing how a small amount of "impurity" can result in drastic effects on the structure of nanoscaled particles. Such impurities are detectable, if at all, only by single-crystal structure analysis; by contrast, STM or AFM measurements would fail to detect such details, and **46** might well have been misinterpreted as an Al_{55}^- or as the aforementioned $Al_{50}Cp^*_{12}$, **2**, cluster compound (Figure 17). The present results serve therefore as a warning as regards both the preparation and the identification of nanoscaled species. How only one more electron and proton in the central atom can determine the structure of a large number of surrounding metal atoms and hence the properties of the assembly signals none-the-less a major challenge for future research. But on the evidence of **46**, even small changes in a synthetic protocol can lead to new materials with completely different properties.

A further interesting aspect of the $SiAl_{44}$ core of **46** is its isoelectronic situation to Al_{45}^- ions, which recently has been discussed to be a superconducting cluster.[199] However, the global minimum structure calculated for an Al_{45} cluster is completely different from the experimentally observed $SiAl_{44}$ core of **46**.[200]

6.4. Metalloid Clusters and the Jellium Model

Up to now, the discussion of the bonding situation has focused first of all on similarities to the different structures

of elemental gallium. We will now review the role of the number of valence electrons inside a metalloid cluster compound. Consideration of the metalloid clusters $Ga_{22}R_{10}^{2-}$ (**35**), $Ga_{23}R_{11}$ (**36**), and $Ga_{22}R_8$ (**30**, **34**) will demonstrate for the first time that the number of valence electrons plays a central role in determining the stability of a metalloid cluster. With reference to the jellium model, the structural data of some similar metalloid clusters then offer a new aspect to the understanding of these intermediates on the way from isolated metal atoms or GaX species (the disproportionation $3GaX \rightarrow 2Ga + GaX_3$) to the bulk metal. However, the results show the virtual impossibility of predicting new clusters or hypothetical modifications of the solid metal; the seemingly simple process of metal formation is actually beset by great complexity, reflecting the multitude of reaction channels[3] and the abundance of energetically similar structures open to the products. Simple rules of electron-counting or models suitable for all atoms in the periodic table are tools too crude adequately to compass the interrelations discussed. Furthermore, in contrast to the well investigated chemistry of boron cages, quantum-chemically based model calculations for metalloid Al and Ga clusters seem at present to be far too imprecise to admit much detailed understanding of these complex intercorrelations.[85,201]

The simple concept of the jellium model (see Figure 5) has been extensively applied to the unusually stable Al_{13}^- cluster and its reactions under mass spectrometric conditions (see section 4.2). With 40 valence electrons, Al_{13}^- is a special jellium case, and with its topology of a centered icosahedron, it resembles an atom like Ar in its highly symmetric shell structure.[189,202] The highly symmetrical naked Ga_{23}^- cluster with its 70 valence electrons is another jellium case, and this cluster too is observed in high concentration in mass spectrometric experiments.[49] The connection between the naked Al_{13}^- or Ga_{13}^- cluster and metalloid clusters has also emerged from mass spectrometric experiments (see section 4.1). Thus, the structurally characterized $Ga_{13}(GaR)_6^-$ cluster **4** can be transferred intact into the gas phase where it has been degraded via collision-induced dissociation.[48] In this way, the weakest bonds of the ion cluster can be broken step by step, leading finally to Ga_{13}^- with its stable shell of 40 valence electrons (eq 17). This investigation is a key experiment because it sheds light on

$$Ga_{13}(GaR)_6^- \rightarrow Ga_{13}(GaR)_5^- + GaR... \rightarrow Ga_{13}^- + 6GaR \quad [R = C(SiMe_3)_3] \quad (17)$$
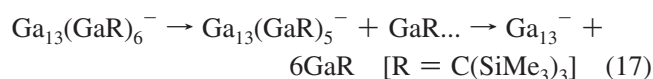
the bonding of every metalloid cluster: There is a core of a naked Ga_{13}^- cluster surrounded by GaR moieties, that is, by oxidized Ga^+R^- species. However, $Ga_{13}(GaR)_6^-$, **4**, is a very special case, demonstrating this concept to optimum effect, since the resulting product, Ga_{13}^-, happens to be an energetically preferred cluster. Perhaps this is why the cluster ion **4** is one of the very rare cases in which a crystalline metalloid compound can be taken into solution, for example, in THF, being self-sufficient as a $(GaR)_6$-stabilized closed shell Ga_{13}^- cluster. Nearly all the other metalloid cluster compounds are insoluble in organic solvents, suggesting that they are stabilized via special secondary interactions to be discussed in more detail in section 7.

A further example of the stabilizing power of a closed shell jellium-like situation is the $Ga_{23}[N(SiMe_3)_2]_{11}$ cluster, **36**, which consists of a central Ga_{12} moiety of naked Ga atoms (Figure 39) surrounded by 11 GaR ligands.[163] Thus,
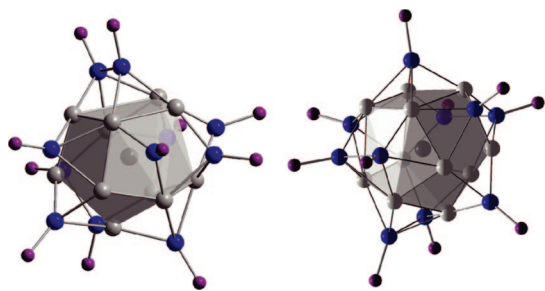
Figure 39. Molecular structures of (right) $[Ga_{22}R_{10}]^{2-}$ (**35**) and (left) the $Ga_{23}R_{11}$ cluster [R = $N(SiMe_3)_2$] (**36**); $SiMe_3$ groups are omitted for clarity.

the overall valence electron number is 58 (12 × 3 + 11 × 2). Obviously the electron number represents a jellium case and therefore a stable electron configuration can be expected, a view supported by another Ga cluster containing the same kind of $N(SiMe_3)_2$ ligands, $Ga_{22}[N(SiMe_3)_2]_{10}{}^{2-}$, **39**, Figure 39.[162] In this dianionic cluster, there is a similar core of 1 + 11 naked Ga atoms, which is surrounded by 10 GaR moieties. In order to achieve stabilization via the jellium case, two further electrons are added to make the overall number of valence electrons up to 58, as with **36**. These metalloid clusters, like the naked $Al_{13}{}^-$ and $Ga_{13}{}^-$ species, may also be viewed as stabilized superatoms. The cluster $Ga_{22}R_8$ [R = $Si(SiMe_3)_3$], **30**, is another possessing 58 valence electrons contributing to its stability. However, metal clusters may be expected to behave according to the jellium model only if they are indeed spherically symmetrical. If a minor distortion of the atomic torso by the ligand shell leaves the electronic shell structure virtually unchanged, the simple model is likely to remain fundamentally valid. This hypothesis can be checked with the aid of **30** (**34**), **35**, and **36**. Because all three compounds have 58 valence electrons but different surroundings (8 ligands in **30** (**34**), 10 and 11 in **35** and **36**, respectively), **30** (**34**) shows a higher density in its Ga_{14} core, the average atomic volume being only 34.6 Å^3 (Figure 40). Decreasing the number of ligands from 11 in **36** to 8 in **30** (**34**) without changing the total number of electrons results in an 8% contraction of the volume of the Ga_{12} unit (Figure 40).

This change is expected, according to the studies of Häussermann,[140,203] to require only a small energy gain of some kJ mol^{-1}, indicating that a filled jellium shell will tolerate even such volume changes. Increasing the number of ligands obviously distends the clusters, causing them merely to be "inflated", while the electronic stabilization stays essentially the same. This suggests a certain analogy to isoelectronic ions or atoms. Just as there is a 5% reduction in volume with the switch from S^{2-} to Cl^- ions because of the greater core attraction, the jellium-like clusters can show a volume change depending on the ligands. They resemble closely in their behavior atoms with a constant electron number, and can indeed be termed "superatoms", although it is the ligand shell and not core attraction that accounts for the changes of volume.

6.5. Metalloid Clusters and Wade's Rules

While the jellium model seems suitable for describing the naked $Al_{13}{}^-$ cluster, it fails, for example, with the first icosahedral *closo*-cluster $Al_{12}R_{12}{}^{2-}$ (R = *i*Bu), **18**,[134] which represents, by contrast, an ideal example for the application of Wade's rules.[29] For a few larger cluster compounds of

Al, Ga, In, and Tl (e.g., $Ga_{19}\{C(SiMe_3)_3\}_6$, **4**; $Ga_{22}\{Si-(SiMe_3)_3\}_8$, **30**; and $Ga_{26}\{Si(SiMe_3)\}_8{}^{2-}$, **38**), attempts have been made to establish a correlation between the bonding electrons and the structure, following the example set by the successful application of Wade's rules to boranes.[204−206]

7. Interactions between Metalloid Cluster Species within the Crystal

Individual Al and Ga clusters discussed in detail in the preceding sections are really an exception, because only very few of them are stable in solution or even in the gas phase (e.g., $Ga_{19}R_6{}^-$, **4**).[12,48,49] The overwhelming majority of metalloid clusters prepared in the past decade are trapped in an ionic lattice or in a lattice stabilized by special cluster···cluster interactions. Depending on the functionalization of a cluster (by charge or by ligand), different one-, two-, or three-dimensional arrangements of these nanoscaled clusters are obtained. This issue is a matter central to nanoscience, the properties of different cluster arrangements depending on cluster···cluster interactions. In this section, we consider three examples of different metalloid clusters: (1) Al_7R_6, **20a**;[94] (2) $Ga_{24}Se_2Br_{18}$, **15**;[117] and (3) the ionic compound containing $Ga_{84}R_{20}{}^{4-/3-}$ anions, **11/11′**.[113,115]

7.1. The Three-Dimensional Arrangement of Al_7R_6 Clusters, 20a, in the Lattice

In the crystal lattice of Al_7R_6 [R = $N(SiMe_2Ph)_2$], **20a**,[94] each cluster has a coordination sphere of 8 + 6, and the distances between the centers of the clusters vary between 14 and 26 Å (see Supporting Information). However, there is a preferred direction in the crystal along the *c*-axis, because the 3-fold axis of the cluster molecules is arranged in this direction. Anisotropy of the EPR spectrum stemming from this special arrangement of the clusters could be confirmed by rotating the sample.[93,94]

In order to elucidate the origin of the interactions between the clusters, we consider first of all the lattice stabilization in comparison with the situation within the compound containing the anionic $Al_7R_6{}^-$ cluster species **20**. Model calculations[94] show that the anion $Al_7R_6{}^-$ is about 170 kJ mol^{-1} more stable than the neutral isolated cluster. Furthermore, calculations of the lattice energy of the compound containing the anionic cluster suggest a stabilization of 284 kJ mol^{-1}, so crystals containing the $Al_7R_6{}^-$ species are about 450 kJ mol^{-1} more stable than the gaseous neutral Al_7R_6 cluster, **20a**. Nevertheless, this neutral cluster forms crystals that could not be dissolved again without decomposition. Very special cluster···cluster interactions must therefore be responsible for the formation of this crystal lattice. To elucidate whether the interactions are magnetic in nature, ongoing SQUID measurements are in progress.[207] Furthermore, special EPR techniques are being employed in current investigations to find out whether dynamic behavior within the electrical charge distribution is responsible. The unpaired spin density is concentrated at low temperatures mainly at the central atom but becomes more delocalized over all the Al atoms of the cluster at temperatures above 30 K, thus hinting at this possibility.[207,208] Additionally, collision experiments with the isolated $Al_7R_6{}^-$ cluster, **20**, in the gas phase with mass spectrometric analysis show that the "weakest point" in this cluster is just the center, so that the cluster dissociates in the first step to $Al_4R_3{}^-$ and Al_3R_3.[209] Thus, a nonsymmetrical electron distribution may occur during
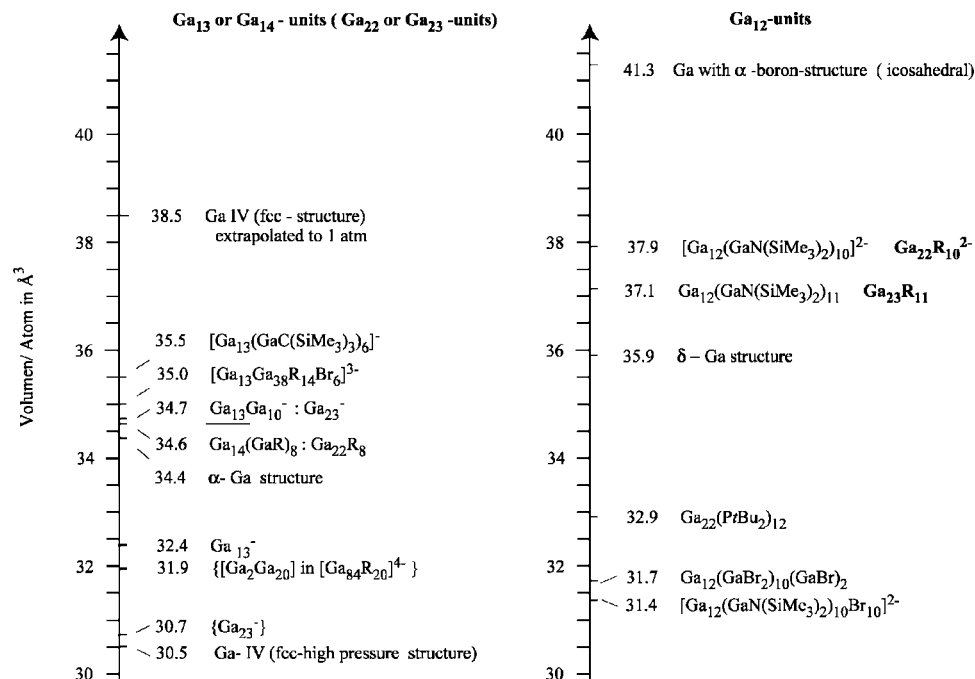
Figure 40. Average atomic volumes of one atom of central Ga_{12} and Ga_{13}/Ga_{14} moieties in metalloid clusters, naked Ga_n clusters, and solid elemental Ga modifications [$Å^3$].

vibrations of the cluster molecule in the lattice. Plainly, the origin of what are obviously strong interactions between the $Al_7R_6^{\bullet}$ radicals, **20a**, in the lattice is still an open question, and theoretical investigations, as well as the EPR measurements, are under way in an attempt to shed more light on this phenomenon.[207] Nevertheless, our first example shows that electronic or magnetic interactions between metalloid clusters can have energies in the order of the lattice energies of salts, leading to insoluble crystalline products.

7.2. $Ga_{24}Br_{18}Se_2$ (15), a Highly Symmetrical Metalloid Cluster and Its One-Dimensional Arrangement in the Crystal: A Model for the Photoconductivity of Crystalline GaSe?

In sections 6.1.3 and 6.2.2, we met two subhalides, $Al_{22}Br_{20} \cdot 12THF$, **25**,[141] and $Ga_{24}Br_{22} \cdot 10THF$, **37**,[164] which comprise a central M_{12} icosahedral core of naked M atoms and MX_2 or MX moieties in the outer shell. These structural features suggest that **25** and **37** could be interpreted as possible intermediates along the route to hypothetical nonmetallic modifications of elemental aluminum and gallium (similar to α-boron).[140] A similar Se-functionalized cluster, $Ga_{24}Br_{18}Se_2 \cdot 12THF$ (**15**), is obtained by the reaction of GaBr with $Se(SiMe_3)_2$ and can be isolated in the form of yellow crystals (eq 18).[117] Compound **15**

$$GaBr \text{ (toluene/THF)} + Se(SiMe_3)_2 \xrightarrow{\Delta} Ga_{24}Se_2Br_{18} \cdot$$

$$12THF(\textbf{15}) + BrSiMe_3 \quad (18)$$
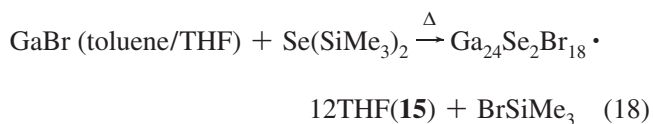
(Figure 32) exhibits a topology of nearly undistorted icosahedral and dodecahedral moieties as compared with the clusters $Ga_{24}Br_{22}L_{10}$, **37** (Figure 31), and $Al_{22}Br_{20}L_{12}$, **25** (Figure 23). The coordination of the individual, roughly spherical clusters **15** leads to an almost perfect dense packing with distances for 10 of the 12 nearest cluster molecules that vary only between 16.1 and 15.8 Å. Only the distance to
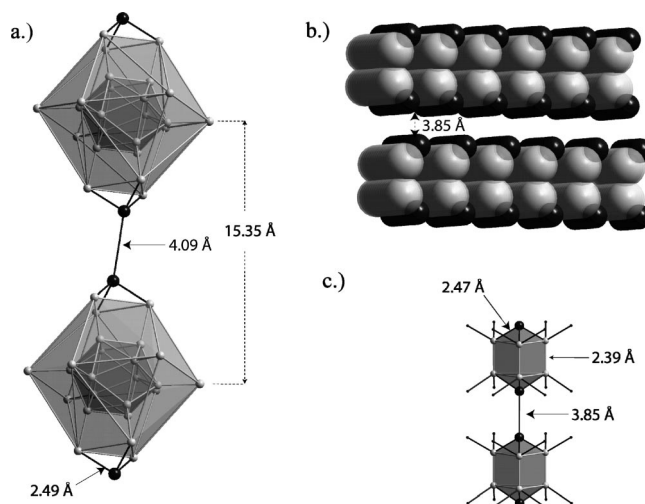
Figure 41. (a) Coordination of the Se and Ga atoms in the $Ga_{24}Br_{18}Se_2$ clusters along the b-axis of the crystal of **15**. (b) The lattice structure of solid GaSe (Se = dark). (c) Coordination sphere of the Ga and Se atoms in GaSe.

the two remaining clusters is shortened to 15.3 Å by Se•••Se contacts measuring 4.09 Å parallel to the crystallographic b-axis. The resulting linkage, also shown in Figure 41, can be compared with the much shorter one-dimensional linkage of Pt atoms (2.88 Å) found in "Krogmann's" salts (e.g., salts of the $[Pt(CN)_4]^{2-}$ anion).[57,210] It seems feasible therefore to regard $Ga_{24}Br_{18}Se_2 \cdot 12THF$ as "a chain of Ga_{24} superatoms".

Closer scrutiny of the Se•••Se interactions was provided by DFT calculations involving the model compound $Ga_{24}Br_{18}$-$Se_2 \cdot 12H_2O$ and the corresponding dimeric species. The calculated dimerization energy, the Se•••Se distances, and the HOMO−LUMO gap exhibit some similarities to, as well as some differences from, the situation in Se_6 molecules and also in gray selenium.[117] In order to elucidate possible similarities to the situation in "Krogmann's" salts, the cations and anions of all the model compounds have been investigated as products of a possible electron transfer. Again, there

are some similarities but also considerable differences, so solid gallium selenide (GaSe) might offer a better analogy.

The layer structure of gallium selenide with double layers of Ga atoms has very short Ga−Ga distances (2.39 Å compared with 2.32 Å for a so-called Ga−Ga triple bond)[190] and short Ga−Se bonds above and below each layer (Figure 41). Between these layers, there are weak Se···Se interlayer contacts measuring 3.85 Å. The local $Ga_3Se···SeGa_3$ contacts thus resemble very closely the topology between individual clusters of $Ga_{24}Br_{18}Se_2$ **15** along the *b*-axis (Figure 41). In addition to this obvious analogy of the Se···Se linked chains in **15** with the Se···Se linked Ga_2 layers in solid GaSe, the relation of **15** to solid GaSe is also apparent in the absorption spectra of the two compounds.[117] The special stabilization of crystalline $Ga_{24}Br_{18}Se_2$ **15** is obviously caused by these unusual Se···Se contacts. As a simple one-dimensional model compound, **15** could thus lead to a better understanding of the photoconductivity of solid GaSe.[117] Moreover, it could help to enhance the understanding of conduction phenomena as in, for example, the superconductivity in a string of nanoscaled metalloid particles with a defined topology, a topic now to be discussed in the special case of Ga_{84} clusters.

7.3. The $Ga_{84}R_8^{4-}$ Anion, Its Arrangement in the Crystalline State, And Electrical and Superconducting Transport

In our opinion, this section may well contain the most important message of the whole review, since it presents details of the largest known metalloid cluster, its unusual arrangement in the crystal, and what we believe to be the first detailed physical investigations of a nanoscaled metalloid cluster compound, including the first observation of superconducting behavior in such an assembly. On the basis of the topology of the individual clusters, calculations assessing the stabilization of the clusters in the lattice have been carried out; these have incorporated some orientating calculations on the possible electron transport via Ga_{84}^{3-} anions and the corresponding donor-stabilized Li^+ cations. Lastly, we describe the initial investigations of the electrical conductivity, and, subsequently, the structure−property relations with respect to the superconducting behavior.

7.3.1. Stabilization of the $Ga_{84}R_{20}^{4-}$ Cluster 11 in an Ionic Lattice

7.3.1.1. The Energetic Relation to Elemental Gallium.[114] With the aid of quantum chemical calculations, it can be shown that the two neutral metalloid aluminum clusters $Al_{22}X_{20}L_{12}$, **24** and **25**, and $Al_{50}Cp^*_{12}$, **2**, are metastable with respect to disproportionation into solid aluminum and the corresponding oxidized species. Cluster **24/25** is ca. 150 kJ mol^{-1} higher in energy with respect to aluminum and aluminum trichloride, and the Al_{50} compound **2** is ca. 1600 kJ mol^{-1} higher in energy with respect to elemental aluminum and AlCp* (see Supporting Information).[19] Since both these compounds are neutral species, the influence of the lattice energy must additionally be taken into account in considering the stability of the anionic Ga_{84} cluster compound **11**.[114] The important question is whether **11**, as a "salt-like" compound, is energetically situated above or below the energy level of solid or liquid elemental gallium as a reference point. Two energy terms have to be compared: (a) the vaporization energy of solid or liquid gallium to release
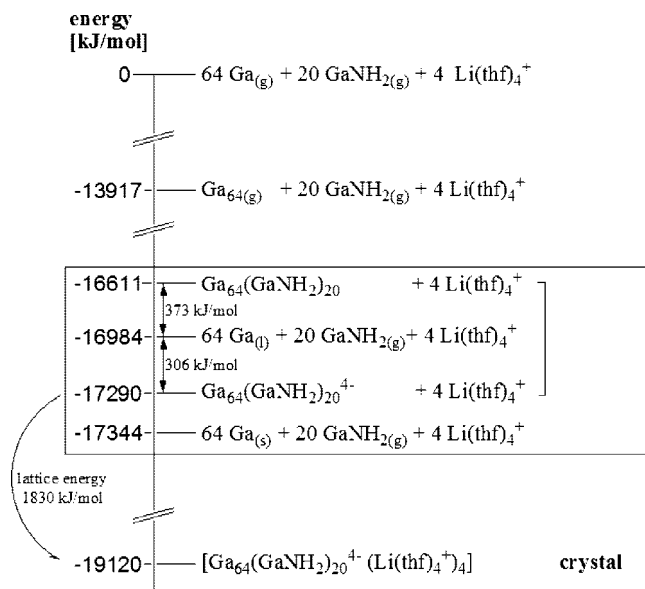
Figure 42. Energetic relation between 64 Ga atoms, 20 $GaNH_2$ molecules, and 4 THF-stabilized Li^+ cations and the crystal containing $[Ga_{84}(GaNH_2)_{20}]^{4-}4[Li(THF)_4]^+$. The diagram is based on (1) the experimentally determined crystal structure (in order to obtain the lattice energy), (2) the experimentally determined vaporization energy of elemental Ga, and (3) DFT calculations.

64 Ga atoms (this being the number of "naked" Ga atoms in the $Ga_{84}R_{20}^{4-}$ cluster, **11**, which are stabilized by 20 GaR moieties) and (b) the formation of a Ga_{64} cluster starting from 64 Ga atoms, the stabilization of this naked cluster with the help of 20 GaR moieties, and the subsequent reduction to the tetra-anion. Finally, the energy of lattice formation from the tetra-anion and Li^+ cations has to be estimated.[114]

A simplified DFT model calculation, where the $N(SiMe_3)_2$ group of the $[Ga_{84}\{N(SiMe_3)_2\}_{20}]^{4-}$ anion, **11**, was substituted by the NH_2 group, leads to the energy diagram presented in Figure 42. In comparing the results of the calculations and to quantify the influence of reduction of the neutral $Ga_{64}(GaNH_2)_{20}$ species to the tetra-anion, the highest and lowest energies of the gaseous products, as represented in Figure 42, are separated by the experimentally determined vaporization energy of liquid or solid gallium to form Ga atoms.

(1) maximum energy: $64Ga_g + 20Ga(NH_2) +$
                                      $4Li(THF)_4^+$

(2) minimum engergy: $64Ga_{l/s} + 20Ga(NH_2) +$
                                      $4Li(THF)_4^+$

Based on the experimentally determined structural data for the Ga_{84} cluster compound, a lattice energy of ca. 1830 kJ mol^{-1} is obtained for the model compound via the Kapustinskii equation[211] and via the empirical correlation described by Jenkins and Liebman.[114,212,213] According to these model calculations, liquid gallium is only ca. 370 kJ mol^{-1} lower in energy than the neutral cluster, and the tetra-anionic cluster is already 306 kJ mol^{-1} lower in energy compared with liquid gallium. Hence, the isolated cluster species are energetically comparable with liquid or solid gallium, and it follows that the lattice energy of the Ga_{84} cluster compound is responsible for stabilizing the individual cluster molecules in a crystalline solid. Above room tem-

perature, then, the Ga_{84} cluster compound may be regarded as a perfect arrangement of Ga metal spheres within a solid dielectric matrix.
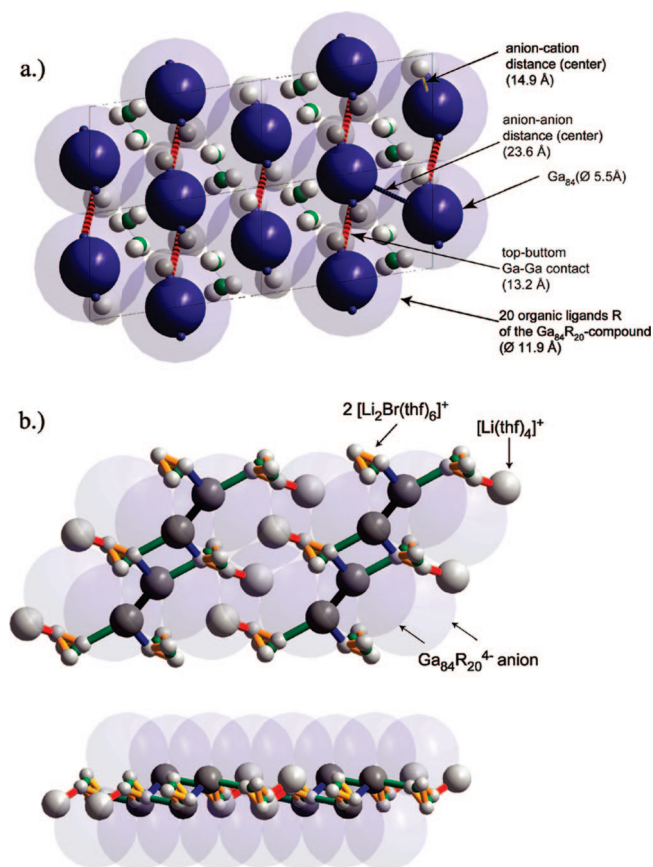
7.3.1.2. Model Calculations Concerning the Charge Transfer between the Anionic Clusters Themselves and between the Anions and Cations of the Ga_{84} Compound.[114]

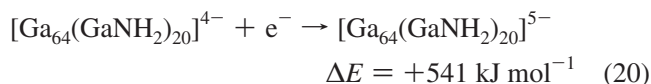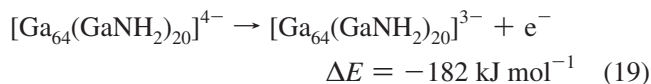We consider now the results of DFT calculations concerning the stability of the model cluster $[Ga_{64}(GaNH_2)_{20}]$ with different negative charges in order to investigate whether charge transfer might proceed in the crystal either via the anionic cluster molecules themselves or from the anions to the Li^+ cations.[114] These very rough model calculations throw some light on the conduction phenomena, in the absence of reliable DFT or other calculations designed to simulate the band structure in a system such as that presented by the solid Ga_{84} cluster compound.[214,215]

Figure 43a illustrates the large separations between the cluster anions, which are structure-determining in securing the nearly closest packing. By contrast, the distances between the Ga_{84}^{n-} anions and the solvated Li^+ cations in the tetrahedral and octahedral holes are significantly shorter. Furthermore, the distances between the solvated Li^+ cations,

a.)

anion-cation distance (center) (14.9 Å)

anion-anion distance (center) (23.6 Å)

Ga_{84}(Ø 5.5Å)

top-buttom Ga-Ga contact (13.2 Å)

20 organic ligands R of the $Ga_{84}R_{20}$-compound (Ø 11.9 Å)

b.)

2 $[Li_2Br(thf)_6]^+$

$[Li(thf)_4]^+$

$Ga_{84}R_{20}^{4-}$ anion

Figure 43. (a) Crystal lattice of the Ga_{84}^{4-} compound (**11**) displaying some of the distances between the structure-determining cluster anions. As examples, two distances are marked, one anion···anion and one anion···cation contact, each with respect to the centers, as well as the shortest Ga···Ga distance between the top and bottom of two Ga_{84} clusters. (b) The cations within the lattice of the Ga_{84}^{4-} compound: (top) perpendicular to the Ga_{84}^{4-} layers, a projection of the different cations $[Li(THF)_4]^+ \cdots [Li_2Br(THF)_6]^+$, where red = 8.9 Å, blue = 10.3 Å, green = 12.3 Å, the distances between two $[Li(THF)_4]^+$ cations measure 13.5 Å (black); the Li···Li contacts between two Li_2Br^+ cations in the same octahedral hole (yellow) measure only 7.2 Å; (bottom) the cation···cation contacts between two layers of the big anion clusters.

between 8.9 and 13.5 Å, are significantly shorter than those between the anions (Figure 43b). Because electron transfer proceeding only via the anions is likely to be difficult in view of the large separations, the following energy terms were estimated by DFT methods.[114] For isolated, infinitely separated Ga_{84} anions, the following energies were calculated for the oxidation and reduction processes:

$$[Ga_{64}(GaNH_2)_{20}]^{4-} \rightarrow [Ga_{64}(GaNH_2)_{20}]^{3-} + e^-$$
$$\Delta E = -182 \text{ kJ mol}^{-1} \quad (19)$$

$$[Ga_{64}(GaNH_2)_{20}]^{4-} + e^- \rightarrow [Ga_{64}(GaNH_2)_{20}]^{5-}$$
$$\Delta E = +541 \text{ kJ mol}^{-1} \quad (20)$$

These show that disproportionation of the isolated Ga_{84}^{4-} anion to the Ga_{84}^{3-} and Ga_{84}^{5-} anions requires an energy input of ca. 360 kJ mol^{-1}. This value corresponds to the Hubbard parameter U, that is, the intermolecular Coulomb repulsion between two electrons in a Ga_{84} cluster.[114] By contrast, the disproportionation process for two Ga_{84}^{4-} anions separated by 2.3 nm is endothermic to the extent of only 300 kJ mol^{-1} (Figure 44). This value corresponds to a Hubbard parameter U' corrected by the Madelung potential.[114]

In order to compare this endothermic process with the energy change associated with the reaction of Li^+ cations with Ga_{84}^{4-} to give neutral Li atoms and Ga_{84}^{3-}, DFT calculations were performed for $[Li(THF)_4]^+$ and also for $[Li(THF)_4]^{\pm 0}$, showing that the reduction process is exoergic to the extent of 196 kJ mol^{-1}.[216,217] This energy change is significantly smaller than that for the reduction of "naked" Li^+ cations to Li atoms, namely, 526 kJ mol^{-1}. For the charge transfer from an anion $[Ga_{64}(GaNH_2)_{20}]^{4-}$ to a $Li(THF)_4^+$ cation (eq 21), there is a release of energy amounting to about 378 kJ mol^{-1} (196 kJ mol^{-1} for the reduction of $Li(THF)_4^+$ and 182 kJ mol^{-1} for the oxidation of the $Ga_{64}(GaNH_2)_{20}^{4-}$ to the trianion). Oxidation of a Ga_{84}^{4-} to a

$$[Ga_{64}(GaNH_2)_{20}^{4-} + 4Li(THF)_4^+] \rightarrow$$
$$[Ga_{64}(GaNH_2)_{20}^{3-} + 3Li(THF)_4^+ + Li(TFH)_4^{\pm 0}] \quad (21)$$
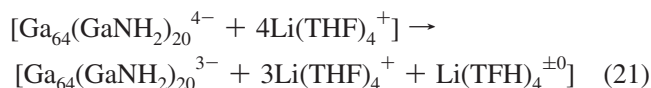
Ga_{84}^{3-} anion with simultaneous neutralization of a $Li(THF)_4^+$ cation results in a reduced lattice energy (estimated to be about 1100 kJ mol^{-1}), so the overall energy change associated with the reaction 21, as it occurs in the crystal, is $1828 - 378 - 1100 = +350$ kJ mol^{-1}. This is nearly the same as the energy input needed for the disproportionation of the anions (300 kJ mol^{-1}). The energy change of $+350$ kJ mol^{-1} associated with eq 21 corresponds to the Δ parameter introduced by Zaanen, Sawatzky, and Allen.[218,219] However, besides the results presented so far and in contrast to earlier calculations,[215] very recent results have been published on the electronic situation of the Ga_{84} cluster exhibiting that the DOS near the Fermi level is mostly contributed by Ga atoms.[144] However, there is an important and interesting difference in the DOS around the Fermi level between the $[Al_{77}\{N(SiMe_3)_2\}_{20}]^{2-}$ cluster, **1**, and the $[Ga_{84}\{N(SiMe_3)_2\}_{20}]^{4-}$ cluster, **11**: the Fermi level of the $[Ga_{84}\{N(SiMe_3)_2\}_{20}]^{4-}$ cluster, **11**, locates at a peak of the DOS, and the $[Ga_{84}\{N(SiMe_3)_2\}_{20}]^{4-}$ cluster has a much larger DOS at the Fermi level than the $[Al_{77}\{N(SiMe_3)_2\}_{20}]^{2-}$ cluster, which might be responsible for the superconductivity observed in the crystalline ordered compound containing $[Ga_{84}\{N(SiMe_3)_2\}_{20}]^{4-}$ clusters.[144,220]
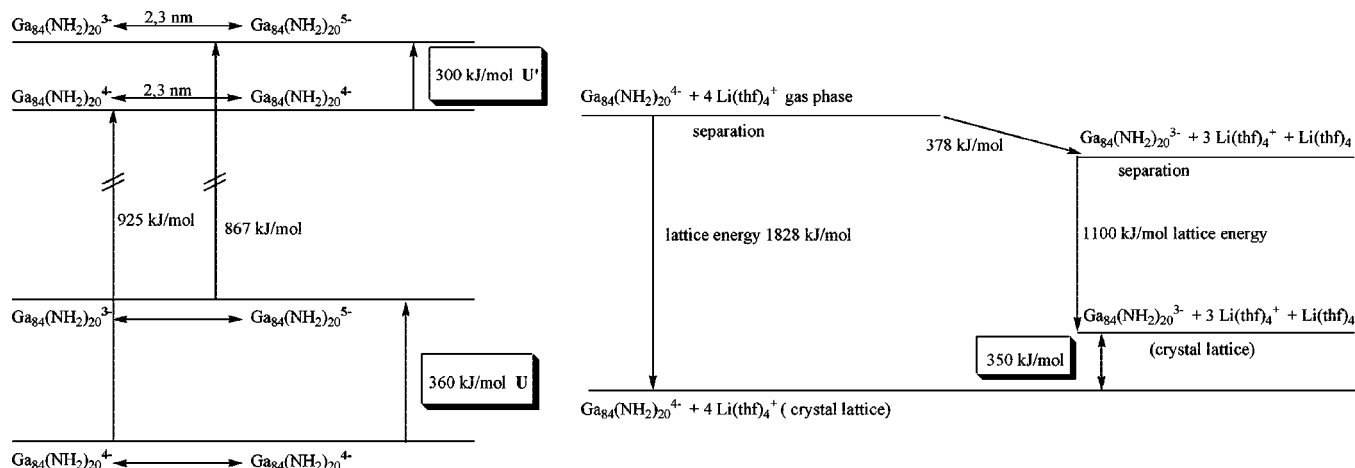
Figure 44. Energy diagram deduced via DFT calculations to determine the Hubbard potential U and the Madelung-corrected value U' (left). If the reduction of Li^+ to Li is considered in the electron transport, the Δ parameter (see text) is estimated to be ca. $+350$ kJ mol^{-1} (right).

7.3.2. Experimental Evidence for the Electrical and Superconducting Behavior

To find out whether the unusual topology of the Ga_{84} cluster in the lattice and the metallic luster of the crystals have consequences for electric charge transfer, orientation experiments have been performed. These involve (1) four-point conductivity measurements on single crystals down to 1.5 K,[221] (2) conductivity measurements in a glovebox at temperatures ranging from 244 to 345 K,[221] and (3) ^{71}Ga NMR measurements on the solid.[222] The orienting measurements give unambiguous evidence of unusual electronic transfer phenomena, pointing to electronic conduction and superconductivity below 7 K; the latter was found, however, only within a limited volume fraction of the crystals. More sophisticated measurements were therefore necessary, as described in the following paragraphs.[114,223−225]

7.3.2.1. Electrical Conductivity of the $Ga_{84}R_{20}$ Compound via ^{71}Ga NMR Investigations.[114,223,225] For a $Ga_{84}{}^{4-}$ sample containing a nearly perfect ordering of all the cluster anions, as well as all the toluene solvent molecules included in the crystal, a ^{71}Ga NMR spectrum measured at 175 K (Figure 45)[114,223,225] showed two different resonances. One is weak (relative intensity 14%) and occurs near $\nu_0 = 122$ MHz (in the region characteristic of molecular Ga^{III} compounds, corresponding to a shift of around 0 ppm, cf. Ga^{3+} in H_2O). The other, which is strong (relative intensity 86%), exhibits fine structure and occurs in the region where liquid gallium exhibits its low-field signal, at ca. $+4100$ ppm. This so-called Knight shift is the hallmark of metallic conductivity.[226,227] Hence, the main part of the sample behaves like a typical metal. Furthermore, this interpretation of the signal at $+4100$ ppm is supported by temperature-dependent T_1 relaxation measurements, showing that the Korringa relation essential for metallic behavior is fulfilled, that is, $T_1^{-1} \approx aT$, where $a = K_s/S$, S being the Korringa constant and K_s the Knight shift.[222,223] Since $K_s = \delta\nu/\nu_0$ is proportional to the density of states at the Fermi level, all the NMR results demonstrate convincingly that the major fraction of the sample behaves like a metal (c = conducting). The signal at about 0 ppm of the nonconducting fraction (nc) exhibits, as expected, a significantly slower relaxation rate reflecting only the quadrupolar character of the Ga nuclei.[222]

Although the T_1 and K_s values are identical for all the measured samples, the fraction of the conducting (c) to the nonconducting (nc) phase varies markedly from sample to sample. This behavior can be traced back to the fact that different samples exhibit different deficiencies in the toluene molecules that stabilize the crystal lattice (cf. Figure 46), leading in turn to slightly different interactions and arrangements between the Ga_{84} cluster moieties. These findings suggest that the nc fraction originates basically in the outer region of the crystallites, extending inward to a varying extent and leaving a core of the conducting fraction in the interior of the crystallites (upper part of Figure 46). In order to confirm this interpretation, calculations have been carried out on the model compound containing the anion $Ga_{84}(NH_2)_{20}{}^{4-}$.[114] The pattern of the calculated ^{71}Ga NMR spectrum of a single molecular cluster, included in Figure 45, corresponds pleasingly well to the region where the nc fraction is observed. Thus, the center of the calculated resonance occurs at $\delta = 100$ ppm, and the calculated splitting approximates closely that of the measured spectrum of the c fraction. No sharp signal was observed in the $\delta = 0$ ppm region since every cluster belonging to the nc fraction is exposed to a different environment. The ^{71}Ga NMR investigations leave little doubt that the Ga_{84} cluster consists of many different Ga atoms with respect to their electronic surroundings (Figure 45);[114] in other words, this cluster represents a highly mixed valence system. Raising the temperature to 210 K caused the different resonances to coalesce to just two single sharp lines; on the NMR time scale, there appear then to be only $Ga_{84}(GaR)_{20}$ moieties, which behave like "superatoms" consisting of only two types of Ga nuclei. Model calculations suggest that the rotation of the central Ga_2 dumbbell in a cage of 20 Ga atoms (Figures 35 and 36) is responsible for the magnetic equivalence of all the other Ga atoms.[114]

However, one important question concerning the electrical conductivity remains. The experiments described so far indicate unequivocally that all the Ga atoms of the Ga_{84} cluster **11** are involved in the electrical transport mechanism. Since the distances between the $Ga_{84}{}^{4-/3-}$ anions are large, however, a mechanism that proceeds via the Li^+ cations cannot be excluded (see the aforementioned calculations concerning the lattice energy and the influence of $Ga_{84}{}^{3-}$ anions). Accordingly, ^{7}Li as well as ^{1}H NMR investigations need to be performed to assess whether the cations or other molecular entities (e.g., the THF molecules and the $N(SiMe_3)_2$ ligands) are involved in this mechanism.
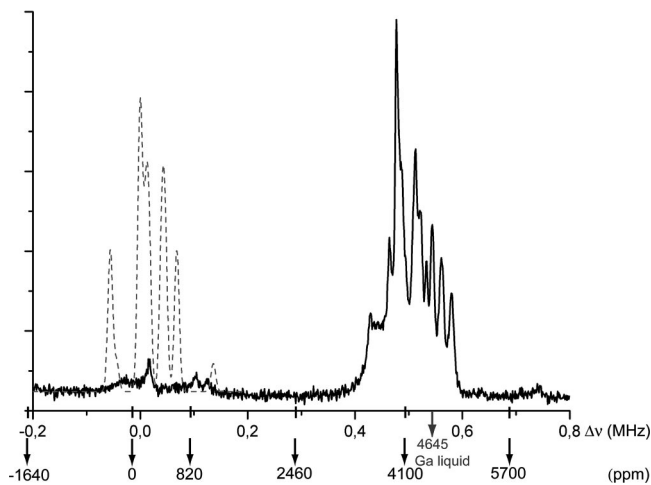
Figure 45. ^{71}Ga NMR spectrum of the solid Ga_{84}^{4-} cluster compound (**11**) containing mainly the conducting phase (c). The dashed spectrum represents the calculated ^{71}Ga NMR spectrum of a single model cluster anion $Ga_{84}(NH_2)_{20}^{4-}$ in the region where the nonconducting (nc) Ga_{84}^{4-} phase exhibits a weak resonance.
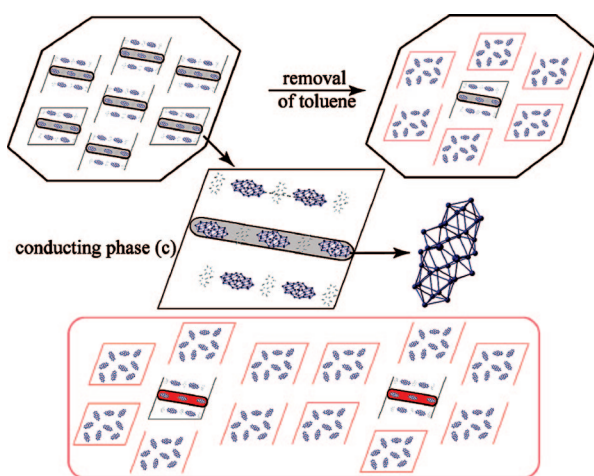
Figure 46. Conducting (c) phase (gray) within the crystallites with a perfect arrangement of Ga_{84} clusters in **11**, destruction of the perfect order by removal of toluene molecules (upper part), and superconductivity via intergrain Josephson coupling between the remaining c phases of different crystallites (lower part in red border).

7.3.2.2. Experimental Evidence of the Superconducting Behavior of the Ga_{84} Cluster Compound.[223−225]

Although the Ga_{84}^{4-} cluster compound constitutes the first example of superconductivity to be found in this class of metal cluster material, the preliminary measurements leave many questions unanswered, because only a small fraction of the sample exhibited superconducting behavior.[221] However, after some years of intensive ^{71}Ga NMR, muon spin resonance (μSR), and magnetization studies,[228] the picture is becoming clearer.[114,223−225] The ^{71}Ga NMR measurements have shown that there are two phases: a nonconducting (nc) and a conducting (c) phase. Cooling the sample below 7 K causes only the c fraction to become superconducting, as evidenced by the NMR, μSR, and magnetization measurements.[222−225] By contrast with the situation regarding the electrical conductivity, however, the superconducting properties of the Ga_{84} compound depend strongly on the nc content. Although the conducting fraction in all samples undergoes a superconductivity transition at about the same temperature, $T_c \approx 7$ K, irrespective of the nc/c ratio, the upper critical field, B_{c2} (i.e., the magnetic field needed completely to

Table 2. Superconducting Transition Temperatures and Critical Fields (Extrapolated to $T = 0$) for the "High T_c" and "Low T_c" Phases in Two Samples of the Ga_{84} Compound 11 Containing, Respectively, 12% and 90% of the Conducting Phase (c)

sample	T_{c1} (K)	T_{c2} (K)	$B_{c1}^{high}(0)$ (mT)	$B_{c1}^{low}(0)$ (mT)	$B_{c2}(0)$ (T)
12% (c)	7.4(2)	6.1(2)	≤ 10	~ 35	5.0(5)
90% (c)	8.0(1)	6.0(2)	85(5)	70(5)	0.26(1)

suppress the superconducting state) appears to vary drastically from about 0.25 to 5 T for samples with a c content ranging from 90% to 10%. B_{c2} values even as large as 13 T have been reported during four-point conductivity measurements of single crystals, where the nc fraction must therefore be well in excess of 90%.[221] These observations, in combination with constant T_c values, are well-known in the field of superconducting alloys and of "dirty" superconductors, for instance, superconducting materials with a certain amount of nonmagnetic impurities.[229] Theory and experiment agree therefore that, under such conditions, the value of B_{c2} is inversely proportional to the electronic mean free path l associated with the concentration of impurities. In view of the marked effect of the toluene molecules on the conductivity, the observed variation of B_{c2} can be attributed to a varying degree of lattice defects and local orientated disorder of neighboring cluster molecules in the conducting phase.

All NMR, μSR, and especially recent magnetization measurements show that the Ga_{84} compound exhibits superconductivity of type II,[230] that is, unlike bulk α-gallium, which is an archetypical type I superconductor with $T_c = 1.1$ K and a critical field as small as $B_c \approx 6 \times 10^{-3}$ T. In type II superconductors, the thermodynamic critical field is replaced by a lower and upper critical field, B_{c1} and B_{c2}, respectively. The corresponding values for samples of the Ga_{84} compound containing about 12% and 90% of the c fraction are presented in Table 2. We conclude therefore that superconductivity is in fact established in two steps, corresponding to slightly different transition temperatures, namely, $T_{c1} \approx 7.4-8$ K, and $T_{c2} \approx 5.8-6.2$ K.[225] The results lead via the Landau−Ginzburg theory to the following penetration depth λ and coherence length ξ: $\lambda(0) \approx 70$ nm; $\xi(0) \approx 35$ nm.[225,229] Even in the case of a decrease of the mean free path caused in "dirty" superconductors (12% c), the effective coherence length is reduced to only 8 nm,[231] that is, much larger than the dimension of a single Ga_{84} cluster.

All the results relating to the superconductivity of the Ga_{84} compound are visualized in Figure 46 and can be summarized as follows. At the first transition, T_{c1}, individual grains (i.e., the polycrystals) become superconducting, whereas at the second transition, T_{c2}, the intergrain Josephson couplings become effective, and superconductivity is established throughout the whole volume of the powder sample.[232] This scenario also accounts for the fact that the NMR and μSR experiments fail to show any sign of the second transition, since both techniques are microscopic probes that sense primarily the intragrain superconducting properties. Further support comes from the behavior of all the samples investigated for which the field dependence of T_{c2} is roughly the same, with similar values of $T_{c2}(0)$ and $B_{c1}(0)$: by contrast, the field-dependence of T_{c1} varies drastically from sample to sample, in parallel with the marked variation of the upper critical field.

The basis of all the unexpected results described here is found in failings of the idealized perfect arrangement of the nanoscopic Ga_{84} clusters in the crystal. This theoretically predicted condition for superconductivity in a chain of

identical cluster molecules[233] is a requirement that can hardly be realized by means of physical fabrication methods.[234] On the one hand, the results presented here tend to shatter some of the illusions of nanoscience; on the other hand, they present an immensely stimulating challenge for fundamental work in the future, and especially in the field of synthetic chemistry, if the most perfect arrangement of molecules or atoms in a single crystal is to be realized.

8. Metalloid Clusters of Ge and Au

The outstanding position of metalloid clusters as intermediates between salts and salt-like clusters and metals and metallic clusters and of the metalloid clusters of Ga/Al as path-making examples for this cluster type is evident by the small number of such cluster species containing other elements. Here we would like to mention only a few examples: some Ge_nR_m clusters and a comparison of the recently investigated $Au_{102}R_{44}$ cluster with the Ga/Al clusters discussed above.

8.1. Metalloid Ge Clusters

For some years now, especially A. Schnepf has shown via trapping of metastable Ge(I) and Sn(I) species that this method is a suitable route for obtaining metalloid Ge_nR_m ($n > m$) clusters. Besides a small number of Ge/Sn clusters presented by other authors (Ge_6R_2,[235] $Ge_{10}R_6I^+$,[236] $Sn_{15}R_6$[237] and Sn_{17}[238]),[239] A. Schnepf has started to systematically investigate the field of Ge_nR_m clusters. He has studied the following:

1. The influence of ligands R/R′ on the cluster core by two Ge_8R_6/Ge_8R_6′ species[243,244]
2. Synthesis and bonding of a Ge_9R_3 cluster via fragmentation experiments in the gas phase exhibiting completely different behavior than that of the $Ga_{19}R_6$ **4** cluster[48,245−247] (see section 4.1)
3. The high potential of the Ge_9R_3 cluster for further reactions in direction to nanochemistry[248]
4. A $Ge_{10}SiR_7$ cluster exhibiting the topology of the Ge atoms in direction to α-germanium[249]
5. $Ge_{10}R_8$[250] and $Sn_{10}R_6$[251] species, which give a hint to a molecular model for a phase transition between α- and β-Sn.
6. The $Ge_{14}R_5$ cluster (Figure 47) pointing to the $Ge(cF)_{136}$ modification of Ge[252,253] giving also a hint in direction of fullerene-like structures possibly typical also for the heavy group 14 elements.[254]
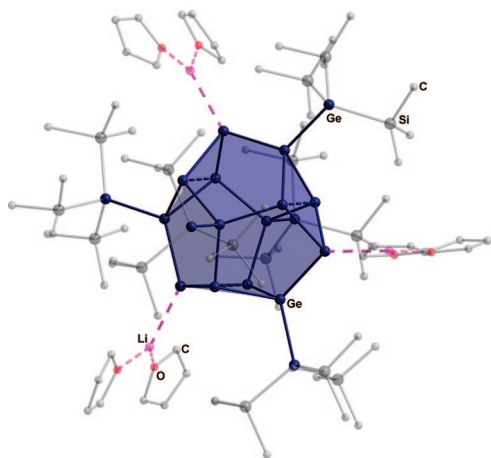
8.2. The Metalloid $Au_{102}R_{44}$ Cluster (R = *p*-MBA = *p*-Mercaptobenzoic Acid = *p*-S-C₆H₄COOH)

8.2.1. General Remarks

After the structure determination of a Au_{39} cluster, [(Ph₃P)₁₄-$Au_{39}Cl_6$]Cl₂, nearly 20 years ago[255] and after a large number of applications of the famous Au_{55} cluster[256,257] in the field of nanosciences during the last two decades,[258] the structure determination of a giant $Au_{102}R_{44}$ cluster was a sensation.[16,259] The consequences of this result, especially of the ligand-stabilized outer Au shell by, for example, reactions of these gold atoms with sulfur-containing molecules, have convincingly been described by R. Whetten.[15] However, as far as we know, a comparison of this result and of the giant Pd clusters[14,264] with the metalloid Al/Ga clusters discussed here has never been performed, though, for example, the $Al_{77}R_{20}$ cluster had been described[17] 10 years before the $Au_{102}R_{44}$ cluster[16] and though A. Cotton had already mentioned the $Al_{77}R_{20}$, **1**, cluster in the introduction to a three-volume handbook of cluster chemistry.[18] Therefore we are working on a detailed comparison;[265] here we would like to present a condensed discussion comparing the structure of the $Au_{102}R_{44}$ cluster. Some remarks about the background concerning the preparation methods of metalloid Au and Al/Ga clusters are given in the Supporting Information.

8.2.2. Structure of the Metalloid $Au_{102}R_{44}$ Cluster

The structure of $Au_{102}R_{44}$ has been described by the authors of the original paper[16] via a Marks polyhedron surrounded by additional Au shells (Figure 48).

The authors described the outer shell as influenced by special interactions of the thiol ligands called "staple effect".[196,262,263] We here present a different picture that may be valid for all metalloid clusters.

On the basis of the spherical jellium model, we have recently interpreted the electronic stabilization of three metalloid gallium clusters (**35**, **36**, and **30/34**) containing 58 valence electrons (see section 6.4). In contrast, though the $Au_{102}R_{44}$ cluster is also stabilized via 58 valence electrons,[15] it contains not a central atom but a Au_7 moiety that is surrounded by 32 Au atoms. This arrangement of the first and second shell is presented in Figure 49. A similar geometric situation is observed for the $Al_{50}Cp*_{12}$, **2**, cluster where an Al_8 unit is surrounded by a shell of 30 Al atoms.

Figure 47. Molecular structure of $Ge_{14}[Ge(SiMe_3)_3]_5Li_3(THF)_6$ in the crystal.
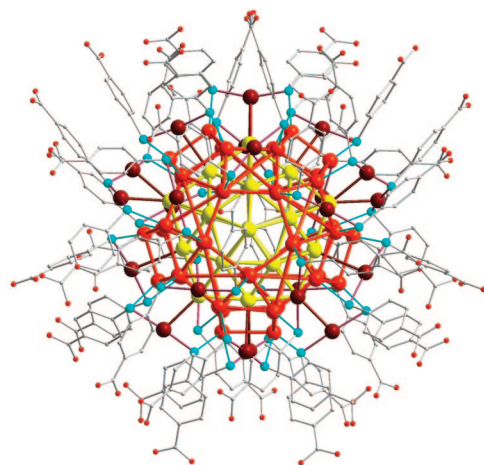
Figure 48. The molecular structure of the metalloid $Au_{102}R_{44}$ (R = *p*-MBA) cluster in the crystal. View along the 5-fold axis of the central Au_7/Au_{32} unit.
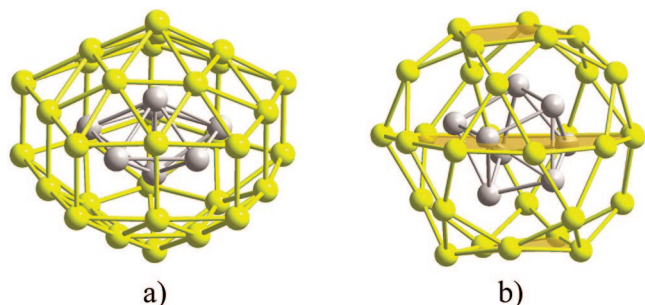
Figure 49. The central shell motifs of (a) the $Au_{102}R_{44}$ cluster (Au_7/Au_{32}) and (b) the $Al_{50}Cp*_{12}$ cluster **2** (Al_8/Al_{30}).
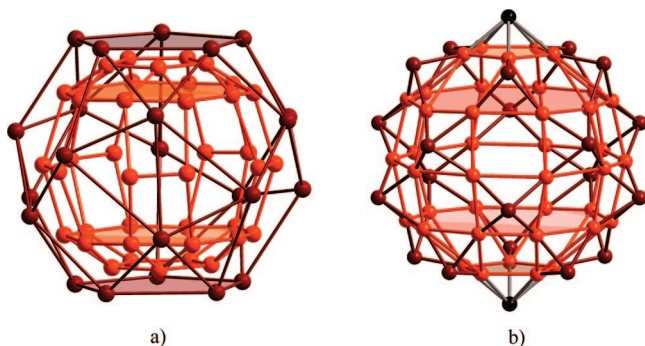
Figure 50. The third and the fourth (outer) shell of (a) the $Au_{102}R_{44}$ cluster (40/23) and (b) the $Ga_{84}R_{20}$ cluster, **11** (40 + 2/20).

Scheme 7. Chain-like Structure of Solid AuCl
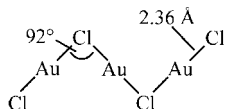
For both clusters, there are observed noncentered structures but structures containing M_7 and M_8 entities, which are unknown for both bulk metals. Thus, it was concluded for **2** that the special arrangement of the ligands in the outer sphere is responsible for the unusual structure in the center.[19]

The third and the fourth shells of the $Au_{102}R_{44}$ cluster containing 40 and 23 Au atoms are shown in Figure 50a.

There is a similar shell-like situation with 40 + 2 and 20 Ga atoms in the $Ga_{84}R_{20}$ cluster **11** (Figure 50b). However, while the 20 outer Ga atoms of **11** as well as the 20 outer Al atoms in the $Al_{77}R_{20}$ cluster, **1**, only form one strong GaR/AlR bond each (see section 4.1), there is a more complex behavior within the Au_{102} cluster: Every $R-S^-$ ligand moiety as an isoelectronic entity to Cl^- forms two bonds to Au atoms. This behavior is typical for Au^+ species and convincingly evident within the chain-like solid-state structure of AuCl (Scheme 7).[57]

Therefore, the 44 RS^- ligands form altogether 88 Au–S contacts: 46 in the Au_{23} shell (38 + 8) based on 19 S–Au–S (2 internal AuS bonds each) and two S–Au–S–Au–S (four internal AuS bonds each) moieties, and 42 contacts in the Au_{40} shell (38 + 4) based on two terminal Au–S bonds of each of the SAuS and SAuSAuS moieties (Scheme 8). This description corresponds to 23 Au^+ ions in the fourth shell and in the third shell to 38/2 Au atoms with an oxidation number of +0.5 and to two Au atoms with an oxidation number of +1. Thus, altogether there are 23 + 19 + 2 = 44 positive charges compensating the negative charge of 44 RS ligands.

Therefore, in a first approach the $Au_{102}R_{44}$ cluster can be described by a core of 39 naked Au atoms that is surrounded by a $Au_{63}S_{44}$ double shell containing 63 Au atoms with an

Scheme 8. Schematic Presentation of the AuS_2 and Au_2S_3 Moieties with Their Two or Four Internal AuS bonds in the Fourth Shell and Two Terminal S Contacts to the (Au) Atoms of the Third Shell
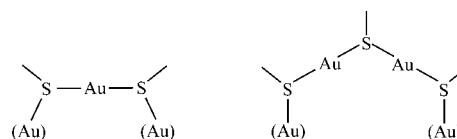
average oxidation number of +0.7. However, like in all Al/Ga metalloid clusters, every atom in this cluster (also in the center) is more or less different (electronically and topologically) from that of the bulk Au metal and Au^+ ions in, for example, AuX compounds; that is, we have a highly mixed valent situation with an average oxidation number of the 102 Au atoms of 0.42. *Therefore, there is no principal but only a gradual difference between the metalloid $Au_{102}R_{44}$ cluster and e.g. the $Ga_{84}R_{20}$ cluster **11** with its electronically and topologically 42 different Ga atoms (see below and section 7.3).*

To sum up, none of the recent papers describing metalloid clusters of Au has mentioned the principle of metalloid clusters on the basis of the large number of Al/Ga clusters although they have been known for about 13 years. Therefore, the common principles valid for all metalloid clusters presented here should open our eyes for this singular outstanding type of cluster with its highly mixed valent situation for the metal atoms and with the intermediate character of these clusters between the bulk metals and the salts causing the unexpected properties of the $Ga_{84}R_{20}$ cluster, **11**, discussed in section 7.3.

## 9. Summary and Outlook

Metalloid clusters are by no means restricted to the chemistry of the elements Al and Ga; the preparation, structure, and bonding of such species may be expected to provide for the sustainable development of similar chemistry for all metals, especially of the base ones. Two features in particular stand out in this account.

(1) Metalloid clusters represent snapshots during the formation and dissolution of metals, giving insights into highly complex processes that are not well understood, at least on an atomic scale. Consequently, they may be viewed as intermediates during reactions, which belong to some of the oldest technical chemical processes known to humankind.

(2) Because of their complex electronic properties, being highly mixed valence individual species, and because of the easy transfer of electrons to and from individual metalloid clusters, electron transport phenomena among perfectly arranged metalloid clusters, for example, in an ionic lattice, can be studied for the first time via normal electrical or superconducting processes (see section 7.3).

With reference to Figure 2, the intermediate character of metalloid clusters is also visualized in Figure 51. The classical inorganic chemistry of solid metals and solid salts, representing the starting and ending points in the formation and dissolution of metals, suggests processes 1 that can be divided via a Born–Haber-type cyclic process into the reactions 1a, 1b, and 1c as displayed in Figure 51. During reaction 1a, the metal is vaporized to deliver naked metal atom clusters, M_n; during reaction 1b, the M_n clusters are completely oxidized to the metal salt clusters, for example, $[MX]_n$ (X = halogen); and finally, these $[MX]_n$ clusters are allowed to form the bulk phase of the salt, that is, solid MX. During these processes, only classical
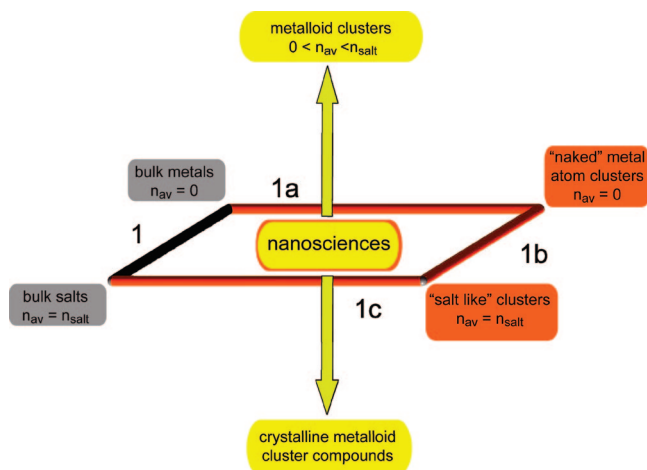
Figure 51. The central position of metalloid clusters between classical inorganic chemistry (bulk metal and metal salts) and modern inorganic/physical chemistry (naked metal atom clusters and "salt-like" clusters), and their pre-eminence for structure/property relations in nanoscience.

disaggregation, oxidation, or aggregation steps are involved. Nearly all the research on clusters in nanoscience is based on sophisticated structural and spectroscopic investigations concerning either naked metal atom clusters M_n or salt-like clusters $[MX]_n$. Accordingly, nanoscience can be visualized as occupying the center of the square in Figure 51. Of the three steps 1a, 1b, and 1c, step 1b is by far the most complex, because the average oxidation number of the cluster changes within a complex reaction cascade, and only a very rough knowledge of this process is yet open to us. One of the final goals would be to monitor this process directly, for example, via a special spectroscopic method. Only for the special case of the reactions of the Al_{13}^- anions with Cl_2, HCl, and O_2 has such a process been investigated step by step (see section 4). Hence the primary reaction steps between isolated Al_{13}^- anions and isolated oxidizing molecules (Cl_2, HCl, or O_2) have been detected for the first time via FT mass spectrometry. Furthermore, it can be argued that Al_{13}^- is a very suitable molecular model for the bulk metal (see section 4.2), that is, with respect to the arrangement, as well as the binding, of the Al atoms. Further insight into the complex reaction cascade of step 1b may thus be gained via mass spectrometric methods.

What, however, is the position of metalloid clusters within Figure 51? They can be found between $M_{(solid)}$ and $MX_{(solid)}$ and also between M_n and $[MX]_n$ clusters, and therefore a third dimension should be added to the 1/1a/1b/1c square to represent the molecular area of isolated metalloid clusters above, and the solid state area of perfectly arranged metalloid clusters in a solid crystal below, the center of the square. In order to accommodate also the many investigations of salt-like clusters as crystalline materials and of metal atom clusters of precious metals in Figure 51, however, the solid state area of nanoscience is divided into two parts, as in Figure 2, with the crystalline metalloid clusters on the right, and the crystalline naked metal atom clusters, for example, Au_x species[15,266] and salt-like clusters,[22,23] on the left.

With respect to their physical properties (e.g., conductivity and superconductivity), the metalloid clusters, once perfectly arranged within a crystal, offer exciting prospects. In principle, they belong to the field of metal-rich, nonstoichiometric compounds where unusual properties are to be expected, as with the cesium suboxides,[25,267] for example. By contrast with typical solid compounds exhibiting nonstoichiometry, however, the

nanoscaled metalloid clusters are molecular species, often called superatoms, where features such as transport phenomena can be investigated at a molecular level. The electronic situation within metalloid clusters is therefore more complex than in the initial simple picture of small metal particles surrounded by a protecting shell of ligands.

To sum up, the outstanding position of metalloid clusters, both the isolated species and those perfectly arranged within a crystal, is revealed by Figure 51 and more generally by Figure 2 (where the clusters occupy the top and bottom positions of the schematic octahedron). The clusters are outstanding with respect to their structural and electronic complexity, and to their potential as models for solving fundamental problems, such as (1) the process of forming metals from salts and (2) the description of bonding, so as to link the topology of atomic assemblies with their electronic properties. The bonding of metalloid clusters has been shown to be too complex to admit the description by any single rule valid for all metal atom clusters. Accordingly, our review has been restricted mainly to a topological description of the clusters and to drawing on the relation to the solid elements themselves. On the basis of the many experimental hints provided by metalloid gallium clusters, this approach seems to offer a first rough but plausible interpretation that acknowledges the singularity of solid elemental gallium, with its seven different modifications. Gallium atoms both in the element and in the clusters adopt different coordination and electronic spheres, depending on the pressure and temperature in the case of the element and on the ligand shell in the case of the metalloid clusters. Thus, gallium can form more localized bonds (e.g., in the Ga_2 moiety) or delocalized bonding in the metallic fcc high-pressure modification or Ga clusters with a central Ga atom coordinated cuboctahedrally.

The synthesis of metalloid clusters has already opened our eyes to much that is new and significant and promises still more for the future. Plainly there is much still to be learned. The high reactivity of the clusters isolated to date, combined with the experimental difficulties of making them reproducibly in the first place, has been a major obstacle to progress.[268-271] Nevertheless, it has been one of the goals of this review to show that experimental difficulties overcome form an essential first step to innovation and better understanding in chemistry at large and in nanoscaled materials in particular.

11. Supporting Information Available

Modifications of gallium, thermodynamic relationship between the disproportionation and the decomposition (GaN, AlN) of metalloid Al^-/Ga clusters, energetic relation between the $Al_{50}Cp^*_{12}$ cluster (**2**), the naked Al_{38} cluster, and bulk Al, the molecular structure of $Al_7R'_6$ (**20a**) and its orientation in the crystal, and remarks on the synthesis of the $Au_{102}R_{44}$ cluster. This material is available free of charge via the Internet at http://pubs.acs.org.

12. Appendix

Table 3. Table of All Cluster Compounds Discussed

M_nR_m	R/L/X	compd no.	ref	M_nR_m	R/L	compd no.	ref
$Al_{77}R_{20}^{2-}$	$N(Me_3Si)_2$	**1**	17	$Al_{14}I_6R_6^{2-}$	$N(Me_3Si)_2$	**23**	139
$Al_{50}R_{12}$	Cp*	**2**	19	$Al_{22}Cl_{20}L_{10}$	thf, thp	**24**	140
Al_4R_4	Cp*	**3**	20	$Al_{22}Br_{20}L_{12}$	thf	**25**	141
$[Ga_{19}R_6]^-$	$C(SiMe_3)_3$	**4**	12	$Al_4Br_4L_4$	Net_3	**26**	147, 148
$RAl^\dagger(\mu R)_2Al^\dagger R$	$PtBu_2$	**5**	87	$SiAl_{14}R_6$	Cp*	**27**	192
Al_2R_4	$PtBu_2$	**6**	87	$SiAl_{14}R_6$	$NSiMe_3Dipp$	**27a**	193
$RAl^\dagger(\mu R)_2Al^\dagger R$	$PtBu_2$	**7**	87	$Ga_{18}R_8$	$SitBu_3$	**28**	156
$Al_2X_4\cdot2L$	Br	**8**	89	$[Ga_{18}R_{10}]^{3-}$	$PtBu_2$	**29**	157
$Al_5Br_7L_5$	THF	**9**	90	$Ga_{22}R_8$	$Si(SiMe_3)_3$	**30**	158
Al_4R_6	$PtBu_2$	**10**	41	$[Ga_{22}Br_{11}R_{10}]^{3-}$	$N(Me_3Si)_2$	**31**	159
$[Ga_{84}R_{20}]^{4-}$	$N(Me_3Si)_2$	**11**	113	$[Ga_{22}Br_{12}R_{10}]^{2-}$	$N(Me_3Si)_2$	**32**	159
$[Ga_{84}R_{20}]^{3-}$	$N(Me_3Si)_2$	**11′**	115	$Ga_{22}R_8$	$Ge(SiMe_3)_3$	**34**	161
$Al_8Br_8R_6$	$PtBu_2$	**12**	112		$SitBu_3$		156
$Al_3P(R)_4Cl_2$	$PtBu_2$	**13**	112	$[Ga_{22}R_{10}]^{2-}$	$N(Me_3Si)_2$	**35**	162
$Ga_{16}R_{10}$	$PtBu_2$	**14**	116	$Ga_{23}R_{11}$	$N(Me_3Si)_2$	**36**	163
$Ga_{24}Br_{18}Se_2L_{12}$	THF	**15**	117	$Ga_2Br_{22}L_{10}$	thf	**37**	164
Al_4Cp_4		**16**	58	$[Ga_{26}R_8]^{2-}$	$Si(SiMe_3)_3$	**38**	165
$Al_{20}X_{10}R_8$	Cp*; Cl, Br	**17**	131	$[Ga_8R_6]$	$C(SiMe_3)_3$	**39**	166
$[Al_{12}R_{12}]^{2-}$	iBu	**18**	134	$Ga_{10}Br_{10}L_{10}$	$4-tBu$-py	**40**	175
$Ga_5X_7L_5$	Et_2O; Cl, Br	**19**	92, 178	$Ga_6R_8^{2-}$	$SiPh_2Me$	**41**	179
$[Al_7R_6]^-$	$N(Me_3Si)_2$	**20**	13	$Ga_8Br_8L_6$		**42**	176
$[Al_7R_6]^\bullet$	$N(Me_2PhSi)_2$	**20a**	94	$Ga_8I_8L_6$	PEt_3	**43**	177
$[Al_{12}R_8]^-$	$N(Me_3Si)_2$	**21**	138	$[Ga_{51}R_{14}]^{3-}$	$PtBu_2$	**44**	185
$Al_{69}R_{18}^{3-}$	$N(Me_3Si)_2$	**22**	133	$Ga_{12}Br_2R_6R'_2$	$R = PtBu_2$	**45**	272
				$SiAl_{56}R_{12}$	$NAr*SiMe_3$	**46**	194

13. References

(1) Schnöckel, H. *Dalton Trans.* **2008**, 4344.
(2) Burgert, R.; Schnöckel, H. *Chem. Commun.* **2008**, *18*, 2075.
(3) Schnöckel, H. *Dalton Trans.* **2005**, 3131.
(4) Schnöckel, H.; Köhnlein, H. *Polyhedron* **2002**, *21*, 489.
(5) Schnöckel, H.; Schnepf, A. *ACS Symp. Ser.* **2002**, *822*, 154.
(6) Schnepf, A.; Schnöckel, H. *Angew. Chem., Int. Ed.* **2002**, *41*, 3532.
(7) Schnöckel, H.; Schnepf, A. *Adv. Organomet. Chem.* **2001**, *47*, 235.
(8) Linti; G. Schnöckel; H. Uhl; W. Wiberg; N. In *Molecular Clusters of the Main Group Elements*; Driess, M., Nöth, H., Eds.; Wiley-VCH: Weinheim, Germany, 2004; p 126.
(9) Schnepf, A.; Schnöckel, H. In *Chemistry of the Group 13 Metals Al, Ga, In and Tl Revisited*; Aldridge, S., Downs, A. J., Eds.; Wiley-VCH: Weinheim, Germany, in preparation.
(10) Cotton, F. A. *Inorg. Chem.* **1964**, *3*, 1217.
(11) Cotton, F. A. *Q. Rev. Chem. Soc.* **1966**, *20*, 389.
(12) Schnepf, A.; Stösser, G.; Schnöckel, H. *J. Am. Chem. Soc.* **2000**, *122*, 9178.
(13) Purath, A.; Köppe, R.; Schnöckel, H. *Angew. Chem., Int. Ed.* **1999**, *38*, 2926.
(14) Tran, N. T.; Powell, D. R.; Dahl, L. F. *Angew. Chem., Int. Ed.* **2000**, *39*, 4121.
(15) Whetten, R. L.; Price, R. C. *Science* **2007**, *318*, 407.
(16) Jadzinsky, P. D.; Calero, G.; Ackerson, C. J.; Bushnell, D. A.; Kornberg, R. D. *Science* **2007**, *318*, 430.
(17) Ecker, A.; Weckert, E.; Schnöckel, H. *Nature (London)* **1997**, *387*, 379.
(18) Cotton, F. A. In *Metal Clusters in Chemistry*; Braunstein, P., Oro, L. A., Raithby, P. R., Eds.; Wiley-VCH: Weinheim, Germany, 1999; Vol. 1; p 3.
(19) Vollet, J.; Hartig, J. R.; Schnöckel, H. *Angew. Chem., Int. Ed.* **2004**, *43*, 3186.
(20) Dohmeier, C.; Robl, C.; Tacke, M.; Schnöckel, H. *Angew. Chem., Int. Ed.* **1991**, *30*, 564.
(21) Krautscheid, H.; Fenske, D.; Baum, G.; Semmelmann, M. *Angew. Chem., Int. Ed.* **1993**, *32*, 1303.
(22) Anson, C.; Eichhoefer, A.; Issac, I.; Fenske, D.; Fuhr, O.; Sevillano, P.; Persau, C.; Stalke, D.; Zhang, J. *Angew. Chem., Int. Ed.* **2008**, *47*, 1326.
(23) Müller, A.; Pope, M. T.; Todea, A. M.; Boegge, H.; van Slageren, J.; Dressel, M.; Gouzerh, P.; Thouvenot, R.; Tsukerblat, B.; Bell, A. *Angew. Chem., Int. Ed.* **2007**, *46*, 4477.
(24) Kong, X. J.; Long, L. S.; Zheng, Z. P.; Huang, R. B.; Zheng, L. S. *Acc. Chem. Res.* **2010**, *43*, 201.
(25) Simon, A. In *Molecular Clusters of the Main Group Elements*; Driess, M. Nöth, H., Eds.; Wiley-VCH: Weinheim, Germany, 2004; p 246.
(26) Braunstein, P., Oro, L. A., Raithby, P. R., Eds. *Metal Clusters in Chemistry, Vol. 1: Molecular Metal Clusters*; Wiley-VCH: Weinheim, Germany, 1999.
(27) See, for example, the following: Corbett, J. D. *Struct. Bonding (Berlin)* **1997**, *87*, 157. Corbett, J. D. *Angew. Chem., Int. Ed.* **2000**, *39*, 670. Corbett, J. D. *Inorg. Chem.* **2000**, *39*, 5178. Ponou, S.; Fässler, T. F.; Tobías, G.; Canadell, E.; Cho, A.; Sevov, S. C. *Chem.—Eur. J.* **2004**, *10*, 3615.
(28) Dong, Z. C.; Corbett, J. D. *J. Am. Chem. Soc.* **1995**, *117*, 6447.
(29) Wade, K. *Adv. Inorg. Chem. Radiochem.* **1976**, *18*, 1.
(30) Klemm, W.; Busmann, E. *Z. Anorg. Allg. Chem.* **1963**, *319*, 297.
(31) Zintl, E. *Angew. Chem.* **1939**, *52*, 1.
(32) Fässler, T. F. *Angew. Chem., Int. Ed.* **2001**, *40*, 4161.
(33) Ugrinov, A.; Sevov, S. C. *Inorg. Chem.* **2003**, *42*, 5789.
(34) Guloy, A. M.; Ramlau, R.; Tang, Z.; Schnelle, W.; Baitinger, M.; Grin, Y. *Nature* **2006**, *443*, 320.
(35) Armatas, G. S.; Kanatzidis, M. G. *Nature* **2006**, *441*, 1122.
(36) Armatas, G. S.; Kanatzidis, M. G. *Science* **2006**, *313*, 817.
(37) Sun, D.; Riley, A. E.; Cadby, A. J.; Richman, E. K.; Korlann, S. D.; Tolbert, S. H. *Nature* **2006**, *441*, 1126.
(38) Corbett, J. D. In *Zintl phases of the early p-block elements*; Kauzlarich, S. M., Ed.; VCH: New York, 1996; p 139.
(39) Li, X.; Grubisic, A.; Stokes, S. T.; Cordes, J.; Ganteför, G. F.; Bowen, K. H.; Kiran, B.; Willis, M.; Jena, P.; Burgert, R.; Schnöckel, H. *Science* **2007**, *315*, 356.
(40) Grubisic, A.; Li, X.; Stokes, S. T.; Cordes, J.; Ganteför, G. F.; Bowen, K. H.; Kiran, B.; Jena, P.; Burgert, R.; Schnöckel, H. *J. Am. Chem. Soc.* **2007**, *129*, 5969.
(41) Henke, P.; Huber, M.; Steiner, J.; Bowen, K.; Eichhorn, B.; Schnöckel, H. *J. Am. Chem. Soc.* **2009**, *131*, 5698.
(42) Wiberg, N.; Blank, T.; Westerhausen, M.; Schneiderbauer, S.; Schnöckel, H.; Krossing, I.; Schnepf, A. *Eur. J. Inorg. Chem.* **2002**, 351.
(43) Li, X.; Kuznetsov, A. E.; Zhang, H.; Boldyrev, A. I.; Wang, L. *Science* **2001**, *291*, 859.
(44) Kuznetsov, A. E.; Birch, K. A.; Boldyrev, A. I.; Li, X.; Zhai, H.; Wang, L. *Science* **2003**, *300*, 622.
(45) The calculated structure of this hypothetical $Al_4H_4^{2-}$ species is not of C_{2v} symmetry; it is a planar D_{4h} symmetric dianion, which is energetically slightly preferred. We are deeply thankful to Prof. J. Ugalde, who noticed our mistake. .
(46) Burgert, R.; Schnöckel, H.; Grubisic, A.; Li, X.; Stokes, S. T.; Bowen, K. H.; Ganteför, G. F.; Kiran, B.; Jena, P. *Science* **2008**, *319*, 438.
(47) Henke, P.; Trapp, N.; Anson, C. E.; Schnöckel, H. *Angew. Chem., Int. Ed.* **2010**, *49*, 3146.
(48) Weiss, K.; Schnöckel, H. *Z. Anorg. Allg. Chem.* **2003**, *629*, 1175.
(49) Weiss, K.; Köppe, R.; Schnöckel, H. *Int. J. Mass Spectrom.* **2002**, *214*, 383.

(50) Neumaier; M. Schnöckel, H. Personal communication.

(51) Jarrold, M. F.; Bower, J. E.; Kraus, J. S. *J. Chem. Phys.* **1987**, *86*, 3876.

(52) Jarrold, M. F.; Bower, J. E. *J. Am. Chem. Soc.* **1988**, *110*, 6706.

(53) Leuchtner, R. E.; Harms, A. C.; Castleman, A. W., Jr. *J. Chem. Phys.* **1991**, *94*, 1093.

(54) Kaya, K.; Fuke, K.; Nonose, S.; Kikuchi, N. *Z. Phys. D: At., Mol. Clusters* **1989**, *12*, 571.

(55) Bergeron, D. E.; Castleman, A. W. J.; Morisato, T.; Khanna, S. N. *Science* **2004**, *304*, 84.

(56) Bergeron, D. E.; Roach, P. J.; Castleman, A. W.; Jones, N.; Khanna, S. N. *Science* **2005**, *307*, 231.

(57) Wiberg; N. Wiberg; E. Holleman; A. F. *Lehrbuch der Anorganischen Chemie*; Walter de Gruyter: Berlin, 2007.

(58) Dohmeier, C.; Loos, D.; Schnöckel, H. *Angew. Chem., Int. Ed.* **1996**, *35*, 129.

(59) Binnewies; M. Milke; E. *Thermochemical Data of Elements and Compounds*; Wiley VCH: Weinheim, 2002; Vol. 2.

(60) Brack, M. *Rev. Mod. Phys.* **1993**, *65*, 677.

(61) de Heer, W. A. *Rev. Mod. Phys.* **1993**, *65*, 611.

(62) Knight, W. D.; Clemenger, K.; De Heer, W. A.; Saunders, W. A.; Chou, M. Y.; Cohen, M. L. *Phys. Rev. Lett.* **1984**, *52*, 2141.

(63) Knight, W. D.; De Heer, W. A.; Saunders, W. A.; Clemenger, K.; Chou, M. Y.; Cohen, M. L. *Chem. Phys. Lett.* **1987**, *134*, 1.

(64) Rao, B. K.; Jena, P. *J. Chem. Phys.* **1999**, *111*, 1890.

(65) Ahlrichs, R.; Elliott, S. D. *Phys. Chem. Chem. Phys.* **1999**, *1*, 13.

(66) Li, X.; Wu, H.; Wang, X.-B.; Wang, L.-S. *Phys. Rev. Lett.* **1998**, *81*, 1909.

(67) In the spherical jellium model, an *N* atomic cluster is approximated by a spherical drop with a radius given by the volume of *N* bulk atoms. The valence electrons are assumed to be delocalized moving in a spherical symmetrical effective potential caused by the *N* positively charged atomic cores. The positive charge distribution *N/V* is taken to be homogenous. Solving the radial Schrödinger equation leads to orbitals that are occupied according to the Pauli principle. Due to the spherical symmetry, the electronic eigenstates in this model have the same degeneracies as those of the hydrogen atom with electronic shell closings at 2, 8, 20, 34, 40, etc. valence electrons. Metal clusters with such shell closings exhibit high electronic stability. .

(68) Burgert, R.; Schnöckel, H.; Olzmann, M.; Bowen, K. H., Jr. *Angew. Chem., Int. Ed.* **2006**, *45*, 1476.

(69) Olzmann, M.; Burgert, R.; Schnöckel, H. *J. Chem. Phys.* **2009**, *131*, 174304.

(70) Baer; T. Hase; W. L. *Unimolecular Reaction Dynamics: Theory and Experiments*; Oxford University Press: New York, 1996.

(71) Olzmann, M.; Troe, J. *Ber. Bunsen-Ges. Phys. Chem.* **1992**, *96*, 1327.

(72) This is in agreement with the fact that smaller aluminum clusters exhibit weaker Al−Al bonds ($Al_{13}^- \rightarrow Al_{11}^- + 2Al$; $\Delta_R H° = 698$ kJ mol^{-1}; $Al_{11}^- \rightarrow Al_9^- + 2Al$, $\Delta_R H° = 585$ kJ mol^{-1}; $Al_9^- \rightarrow Al_7^-$ $+ 2Al$, $\Delta_R H° = 480$ kJ mol^{-1}).

(73) Bagus, P. S.; Brundle, C. R.; Illas, F.; Parmigiani, F.; Polzonetti, G. *Phys. Rev. B: Condens. Matter* **1991**, *44*, 9025.

(74) Behler, J.; Delley, B.; Lorenz, S.; Reuter, K.; Scheffler, M. *Phys. Rev. Lett.* **2005**, *94*, 036104.

(75) Batra, I. P.; Kleinman, L. *J. Electron Spectrosc. Relat. Phenom.* **1984**, *33*, 175.

(76) Sexton, J. Z.; Kummel, A. C. *J. Chem. Phys.* **2004**, *121*, 6518.

(77) Binetti, M.; Weisse, O.; Hasselbrink, E.; Katz, G.; Kosloff, R.; Zeiri, Y. *Chem. Phys. Lett.* **2003**, *373*, 366.

(78) Komrowski, A. J.; Ternow, H.; Razaznejad, B.; Berenbak, B.; Sexton, J. Z.; Zoric, I.; Kasemo, B.; Lundqvist, B. I.; Stolte, S.; Kleyn, A. W.; Kummel, A. C. *J. Chem. Phys.* **2002**, *117*, 8185.

(79) Schwarz, H. *Int. J. Mass Spectrom.* **2004**, *237*, 75.

(80) Reber, A. C.; Khanna, S. N.; Roach, P. J.; Woodward, W. H.; Castleman, A. W. *J. Am. Chem. Soc.* **2007**, *129*, 16098.

(81) As metioned earlier, these transitions are inherently slow in light atom containing species owing to their small spin−orbit coupling.[79]

(82) Adam, W. *Chem. Unserer Zeit* **1981**, *15*, 190.

(83) Greer, A. *Acc. Chem. Res.* **2006**, *39*, 797.

(84) Neumaier, M.; Köppe, R.; Schnöckel, H. *Nachr. Chem.* **2008**, *10*, 999.

(85) Lam, W. H.; Lin, Z. *Polyhedron* **2002**, *21*, 503.

(86) Pankewitz, T.; Klopper, W.; Henke, P.; Schnöckel, H. *Eur. J. Inorg. Chem.* **2008**, *2008*, 4879.

(87) Henke, P.; Pankewitz, T.; Klopper, W.; Breher, F.; Schnöckel, H. *Angew. Chem., Int. Ed.* **2009**, *48*, 7942.

(88) Uhl, W. *Z. Naturforsch.* **1988**, *43b*, 1113.

(89) Mocker, M.; Robl, C.; Schnöckel, H. *Angew. Chem., Int. Ed. Engl.* **1994**, *33*, 862.

(90) Klemp, C.; Stösser, G.; Krossing, I.; Schnöckel, H. *Angew. Chem., Int. Ed.* **2000**, *39*, 3691.

(91) Ecker, A.; Baum, E.; Friesen, M. A.; Junker, M. A.; Üffing, C.; Köppe, R.; Schnöckel, H. *Z. Anorg. Allg. Chem.* **1998**, *624*, 513.

(92) Loos, D.; Schnöckel, H.; Fenske, D. *Angew. Chem., Int. Ed. Engl.* **1993**, *32*, 1059.

(93) Köhler, S. D.; Pilawa, B.; Jauregui, D. S. d.; Fischer, G.; Köppe, R.; Schnepf, A.; Schnöckel, H.; Dormann, E. *Europhys. Lett.* **2008**, *82*, 37002.

(94) Yang, P.; Köppe, R.; Duan, T.; Hartig, J.; Hadiprono, G.; Pilawa, B.; Keilhauer, I.; Schnöckel, H. *Angew. Chem., Int. Ed.* **2007**, *46*, 3579.

(95) Breher, F. *Coord. Chem. Rev.* **2007**, *251*, 1007.

(96) Grützmacher, H.; Breher, F. *Angew. Chem., Int. Ed.* **2002**, *41*, 4006.

(97) (a) Schöller, W. W.; Begemann, C.; Niecke, E.; Gudat, D. *J. Phys. Chem. A* **2001**, *105*, 10731. (b) Niecke, E.; Fuchs, A.; Baumeister, F.; Nieger, M.; Schöller, W. W. *Angew. Chem., Int. Ed.* **1995**, *34*, 555. (c) Niecke, E.; Fuchs, A.; Nieger, M. *Angew. Chem., Int. Ed.* **1999**, *38*, 3028.

(98) (a) Rodriguez, A.; Fuks, G.; Bourg, J.-B.; Bourissou, D.; Tham, F. S.; Bertrand, G. *Dalton Trans.* **2008**, 4482. (b) Scheschkewitz, D.; Amii, H.; Gornitzka, H.; Schöller, W. W.; Bourissou, D.; Bertrand, G. *Science* **2002**, *295*, 1880. (c) Scheschkewitz, D.; Amii, H.; Gornitzka, H.; Schöller, W. W.; Bourissou, D.; Bertrand, G. *Angew. Chem., Int. Ed.* **2004**, *43*, 585. (d) Rodriguez, A.; Olsen, R. A.; Ghaderi, N.; Scheschkewitz, D.; Tham, F. S.; Müller, L. J.; Bertrand, G. *Angew. Chem., Int. Ed.* **2004**, *43*, 4880. (e) Rodriguez, A.; Tham, F. S.; Schöller, W. W.; Bertrand, G. *Angew. Chem., Int. Ed.* **2004**, *43*, 4876.

(99) Cox, H.; Hitchcock, P. B.; Lappert, M. F.; Pierssens, L. J.-M. *Angew. Chem.* **2004**, *116*, 4600.

(100) Cui, C.; Brynda, M.; Olmstead, M. M.; Power, P. P. *J. Am. Chem. Soc.* **2004**, *126*, 6510.

(101) Tacke, M.; Schnöckel, H. *Inorg. Chem.* **1989**, *28*, 2895.

(102) Chase, M. W. *NIST-JANAF Thermochemical Tables*, 4th ed.; American Chemical Society and American Institute of Physics: Washington, DC, and New York, 1998.

(103) Klemm, W.; Voss, E.; Geiersberger, K. *Z. Anorg. Chem.* **1948**, *256*, 15.

(104) Schäfer, H. *Chemische Transportreaktionen, der Transport anorganischer Stoffe über die Gasphase und seine Anwendung*; Verlag Chemie: Weinheim, Germany, 1962.

(105) Schnöckel, H. *J. Mol. Struct.* **1978**, *50*, 275.

(106) Bahlo, J.; Himmel, H.-J.; Schnöckel, H. *Angew. Chem., Int. Ed.* **2001**, *40*, 4696.

(107) Himmel, H.-J.; Bahlo, J.; Haussmann, M.; Kurth, F.; Stösser, G.; Schnöckel, H. *Inorg. Chem.* **2002**, *41*, 4952.

(108) Stösser, G.; Schnöckel, H. *Angew. Chem., Int. Ed.* **2005**, *44*, 4261.

(109) Schnöckel; H. Klemp; C. In *Inorganic Chemistry Highlights*; Meyer, G., Naumann, D., Wesemann, L., Eds.; Wiley-VCH: Weinheim, Germany, 2002; p 245.

(110) Linti, G.; Schnöckel, H. *Coord. Chem. Rev.* **2000**, *206−207*, 285.

(111) Schnöckel, H.; Köppe, R. *Silicon Chemistry*; Jutzi, P., Schubert, U., Eds.; Wiley-VCH: Weinheim, Germany, 2003; p 20.

(112) Henke, P.; Schnöckel, H. *Chem.−Eur. J.* **2009**, *15*, 13391.

(113) Schnepf, A.; Schnöckel, H. *Angew. Chem., Int. Ed.* **2001**, *40*, 712.

(114) Hartig, J.; Schnepf, A.; Jos de Jongh, L.; Bono, D.; Schnöckel, H. *Z. Anorg. Allg. Chem.* **2007**, *633*, 63.

(115) Schnepf, A.; Jee, B.; Schnöckel, H.; Weckert, E.; Meents, A.; Luebbert; Herrling, E.; Pilawa, B. *Inorg. Chem.* **2003**, *42*, 7731.

(116) Steiner, J.; Stösser, G.; Schnöckel, H. *Angew. Chem., Int. Ed.* **2003**, *42*, 1971.

(117) Hartig, J.; Klöwer, F.; Rinck, J.; Unterreiner, A.-N.; Schnöckel, H. *Angew. Chem., Int. Ed.* **2007**, *46*, 6549.

(118) Huber, M.; Henke, P.; Schnöckel, H. *Chem.−Eur. J.* **2009**, *15*, 12180.

(119) Paetzold, P. *Angew. Chem., Int. Ed.* **1991**, *30*, 544.

(120) Schulz, S.; Roesky, H. W.; Koch, H. J.; Sheldrick, G. M.; Stalke, D.; Kuhn, A. *Angew. Chem., Int. Ed.* **1993**, *32*, 1729.

(121) Weiss, J.; Stetzkamp, D.; Nuber, B.; Fischer, R. A.; Boehme, C.; Frenking, G. *Angew. Chem., Int. Ed.* **1997**, *36*, 70.

(122) Gemel, C.; Steinke, T.; Cokoja, M.; Kempter, A.; Fischer, R. A. *Eur. J. Inorg. Chem.* **2004**, 4161.

(123) Üffing, C.; Ecker, A.; Köppe, R.; Schnöckel, H. *Organometallics* **1998**, *17*, 2373.

(124) Dohmeier, C.; Krautscheid, H.; Schnöckel, H. *Angew. Chem., Int. Ed.* **1994**, *33*, 2482.

(125) Roesky, P. W. *Dalton Trans.* **2009**, 1887.

(126) Gamer, M. T.; Roesky, P. W.; Konchenko, S. N.; Nava, P.; Ahlrichs, R. *Angew. Chem., Int. Ed.* **2006**, *45*, 4447.

(127) Minasian, S. G.; Krinsky, J. L.; Williams, V. A.; Arnold, J. *J. Am. Chem. Soc.* **2008**, *130*, 10086.

(128) Minasian, S. G.; Krinsky, J. L.; Rinehart, J. D.; Copping, R.; Tyliszczak, T.; Janousch, M.; Shuh, D. K.; Arnold, J. *J. Am. Chem. Soc.* **2009**, *131*, 13767.

(129) Many attempts to isolate crystalline Al_4Cp_4 or any other metalloid Al_nCp_m ($n > m$) cluster compound at low temperatures even with the

help of sophisticated low-temperature techniques failed because of the easy formation of Al metal. Obviously there is no significant barrier for this decomposition (e.g., by very large metalloid clusters or any other kinetic hindrance). Huber, M. Diploma Thesis, University Karlsruhe (TH), 2004.

(130) Koch, K.; Burgert, R.; Stösser, G.; Schnöckel, H. *Eur. J. Mass Spectrom.* **2005**, *11*, 469.

(131) Vollet, J.; Burgert, R.; Schnöckel, H. *Angew. Chem., Int. Ed.* **2005**, *44*, 6956.

(132) These data confirm our overall conclusions: For Al₄Cp*₄, the thermodynamic barrier to the formation of Al metal and AlCp*₃ is increased via the increasing size of the metalloid clusters. On the other hand, there is no thermodynamic barrier for the decomposition of Al₄Cp₄ in the presence of AlCp.[118]

(133) Köhnlein, H.; Purath, A.; Klemp, C.; Baum, E.; Krossing, I.; Stösser, G.; Schnöckel, H. *Inorg. Chem.* **2001**, *40*, 4830.

(134) Hiller, W.; Klinkhammer, K. W.; Uhl, W.; Wagner, J. *Angew. Chem., Int. Ed.* **1991**, *30*, 179.

(135) Linti, G.; Coban, S.; Dutta, D. *Z. Anorg. Allg. Chem.* **2004**, *630*, 319.

(136) Quillian, B.; Wei, P.; Wannere, C. S.; Schleyer, P. v. R.; Robinson, G. H. *J. Am. Chem. Soc.* **2009**, *131*, 3168.

(137) Wolf, R.; Uhl, W. *Angew. Chem., Int. Ed.* **2009**, *48*, 6774.

(138) Purath, A.; Köppe, R.; Schnöckel, H. *Chem. Commun.* **1999**, 1933.

(139) Köhnlein, H.; Stösser, G.; Baum, E.; Möllhausen, E.; Huniar, U.; Schnöckel, H. *Angew. Chem., Int. Ed.* **2000**, *39*, 799.

(140) Klemp, C.; Bruns, M.; Gauss, J.; Häussermann, U.; Stösser, G.; van Wüllen, L.; Jansen, M.; Schnöckel, H. *J. Am. Chem. Soc.* **2001**, *123*, 9099.

(141) Klemp, C.; Köppe, R.; Weckert, E.; Schnöckel, H. *Angew. Chem., Int. Ed.* **1999**, *38*, 1740.

(142) Schmid, G. *Inorg. Synth.* **1990**, *27*, 214.

(143) Scheer, E.; Agrait, N.; Cuevas, J. C.; Yeyati, A. L.; Ludoph, B.; Martin-Rodero, A.; Bollinger, G. R.; van Ruitenbeek, J. M.; Urbina, C. *Nature* **1998**, *394*, 154.

(144) Xiang, H.; Kang, J.; Wei, S.-H.; Kim, Y.-H.; Curtis, C.; Blake, D. *J. Am. Chem. Soc.* **2009**, *131*, 8522.

(145) Yi, J.-Y. *Phys. Rev. B: Condens. Matter* **2000**, *61*, 7277.

(146) Schmid, G. *Clusters and Colloids: From Theory to Applications*; Wiley-VCH: Weinheim, Germany, 1994.

(147) Mocker, M.; Robl, C.; Schnöckel, H. *Angew. Chem., Int. Ed.* **1994**, *33*, 1754.

(148) Ecker, A.; Schnöckel, H. *Z. Anorg. Allg. Chem.* **1996**, *622*, 149.

(149) Ecker, A.; Schnöckel, H. *Z. Anorg. Allg. Chem.* **1998**, *624*, 813.

(150) Massey, A. G. *Adv. Inorg. Chem.* **1983**, *26*, 1.

(151) Hönle, W.; Grin, Y.; Burkhardt, A.; Wedig, U.; Schultheiss, M.; vonSchnering, H. G.; Kellner, R.; Binder, H. *J. Solid State Chem.* **1997**, *133*, 59.

(152) Morrison, J. A. *Chem. Rev.* **1991**, *91*, 35.

(153) Oganov, A. R.; Chen, J.; Gatti, C.; Ma, Y.; Ma, Y.; Glass, C. W.; Liu, Z.; Yu, T.; Kurakevych, O. O.; Solozhenko, V. L. *Nature* **2009**, *457*, 863.

(154) Matsuoka, T.; Shimizu, K. *Nature* **2009**, *458*, 186.

(155) Ma, Y.; Eremets, M.; Oganov, A. R.; Xie, Y.; Trojan, I.; Medvedev, S.; Lyakhov, A. O.; Valle, M.; Prakapenka, V. *Nature* **2009**, *458*, 182.

(156) Donchev, A.; Schnepf, A.; Stösser, G.; Baum, E.; Schnöckel, H.; Blank, T.; Wiberg, N. *Chem.—Eur. J.* **2001**, *7*, 3348.

(157) Steiner, J.; Schnöckel, H. *Chem.—Eur. J.* **2006**, *12*, 5429.

(158) Schnepf, A.; Weckert, E.; Linti, G.; Schnöckel, H. *Angew. Chem., Int. Ed.* **1999**, *38*, 3381.

(159) Schnepf, A.; Köppe, R.; Weckert, E.; Schnöckel, H. *Chem.—Eur. J.* **2004**, *10*, 1977.

(160) Steiner, J.; Stösser, G.; Schnöckel, H. *Angew. Chem., Int. Ed.* **2004**, *43*, 6549.

(161) Linti, G.; Rodig, A. *Chem. Commun.* **2000**, 127.

(162) Schnepf, A.; Stösser, G.; Schnöckel, H. *Angew. Chem., Int. Ed.* **2002**, *41*, 1882.

(163) Hartig, J.; Stösser, A.; Hauser, P.; Schnöckel, H. *Angew. Chem., Int. Ed.* **2007**, *46*, 1658.

(164) Duan, T.; Baum, E.; Burgert, R.; Schnöckel, H. *Angew. Chem., Int. Ed.* **2004**, *43*, 3190.

(165) Rodig, A.; Linti, G. *Angew. Chem., Int. Ed.* **2000**, *39*, 2952.

(166) Schnepf, A.; Köppe, R.; Schnöckel, H. *Angew. Chem., Int. Ed.* **2001**, *40*, 1241.

(167) Wilson, F. C.; Shoemaker, D. P. *Naturwissenschaften* **1956**, *43*, 57.

(168) The same is valid for the recently presented molecules exhibiting ZnZn[169] and MgMg[170,171] single bonds. .

(169) Resa, I.; Carmona, E.; Gutierrez-Puebla, E.; Monge, A. *Science* **2004**, *305*, 1136.

(170) Green, S. P.; Jones, C.; Stasch, A. *Science* **2007**, *318*, 1754.

(171) Westerhausen, M. *Angew. Chem., Int. Ed.* **2008**, *47*, 2185.

(172) Albinati, A.; Moor, A.; Pregosin, P. S.; Venanzi, L. M. *J. Am. Chem. Soc.* **1982**, *104*, 7672.

(173) Shan, H.; Yang, Y.; James, A. J.; Sharp, P. R. *Science* **1997**, *275*, 1460.

(174) Köppe, R.; Schnöckel, H. *Z. Anorg. Allg. Chem.* **2000**, *626*, 1095.

(175) Duan, T.; Stösser, G.; Schnöckel, H. *Angew. Chem., Int. Ed.* **2005**, *44*, 2973.

(176) Duan, T.; Henke, P.; Stösser, G.; Zhang, Q.; Schnöckel, H. *J. Am. Chem. Soc.* **2010**, *132*, 1323.

(177) Doriat, C. U.; Friesen, M.; Baum, E.; Ecker, A.; Schnöckel, H. *Angew. Chem., Int. Ed.* **1997**, *36*, 1969.

(178) Duan, T.; Stösser, G.; Schnöckel, H. *Z. Anorg. Allg. Chem.* **2005**, *631*, 1129.

(179) Donchev, A.; Schnepf, A.; Baum, E.; Stösser, G.; Schnöckel, H. *Z. Anorg. Allg. Chem.* **2002**, *628*, 157.

(180) Bosio, L. *J. Chem. Phys.* **1978**, *68*, 1221.

(181) On the basis of rough calculations the conversion of planar Ga₈-ring molecules to Ga-centered planar Ga₇-ring molecules should be slightly exothermic, that is, like in a substructure of γ-gallium. This reaction should be analogous to that of endohedral cage compounds. Duan, T. Dissertation, Universität Karlsruhe (TH), Cuvillier Verlag, Göttingen, 2004. Bornhauser, P.; Calzaferri, G. *J. Phys. Chem.* **1996**, *100*, 2035.

(182) There are three substructures in the γ-Ga modification: Ga₇ rings (Figure 29c); centered Gaₙ wires within these rings (Figure 29d), and a combining ladder structure. Within these three substructures, the average values of the Ga—Ga distances are 264, 260, and 268 pm. The Ga—Ga distances between these substructures are 288 pm (average), significantly larger.

(183) In β-gallium, every Ga-atom is surrounded by [2 + 2 + 2 + 2] neighbor atoms. The distances are 268.8, 276.6, 286.4, and 291.9 pm.

(184) Koch, K.; Burgert, R.; Schnöckel, H. *Angew. Chem., Int. Ed.* **2007**, *46*, 5795.

(185) Steiner, J.; Stösser, G.; Schnöckel, H. *Angew. Chem., Int. Ed.* **2004**, *43*, 302.

(186) Schulte, O.; Holzapfel, W. B. *Phys. Rev. B: Condens. Matter* **1997**, *55*, 8122.

(187) Li, Z.; Tse, J. S. *Phys. Rev. B: Condens. Matter* **2000**, *62*, 9900.

(188) Gomez, C. P.; Lidin, S. *Angew. Chem., Int. Ed.* **2001**, *40*, 4037.

(189) Mednikov, E. G.; Jewell, M. C.; Dahl, L. F. *J. Am. Chem. Soc.* **2007**, *129*, 11619.

(190) Su, J. R.; Li, X. W.; Crittendon, R. C.; Robinson, G. H. *J. Am. Chem. Soc.* **1997**, *119*, 5471.

(191) Gerlach, G.; Hönle, W.; Simon, A. *Z. Anorg. Allg. Chem.* **1982**, *486*, 7.

(192) Purath, A.; Dohmeier, C.; Ecker, A.; Köppe, R.; Krautscheid, H.; Schnöckel, H.; Ahlrichs, R.; Stoermer, C.; Friedrich, J.; Jutzi, P. *J. Am. Chem. Soc.* **2000**, *122*, 6955.

(193) Huber, M.; Hartig, J.; Koch, K.; Schnöckel, H. *Z. Anorg. Allg. Chem.* **2009**, *635*, 423.

(194) Huber, M.; Schnepf, A.; Anson, C. E.; Schnöckel, H. *Angew. Chem., Int. Ed.* **2008**, *47*, 8201.

(195) This cluster was obtained during experiments for a better synthesis of an Al₄₈R′₁₂ cluster, for which so far only a small number of crystals could be isolated. The Al₄₈ core of this cluster is similar to that of **2**, however, instead of 8 Al atoms in the center of **2** there are 6 Al atoms in the center of the Al₄₈ cluster. Hadiprono, G. Ph.D. thesis, Universität Karlsruhe (TH), Karlsruhe, Germany, 2005.

(196) Jiang, D. E.; Tiago, M. L.; Luo, W. D.; Dai, S. *J. Am. Chem. Soc.* **2008**, *130*, 2777.

(197) Koch, K. Ph. D. thesis, Karlsruhe, 2005.

(198) Hansen; M.; Anderko; K. *Constitution of Binary Alloys*; McGraw-Hill Publ. Co.: New York/Toronto/London, 1958.

(199) Cao, B.; Neal, C. M.; Starace, A. K.; Ovchinnikov, Y. N.; Kresin, V. Z.; Jarrold, M. F. *J. Supercond. Novel Magn.* **2008**, *21*, 163.

(200) Li, Z. H.; Jasper, A. W.; Truhlar, D. G. *J. Am. Chem. Soc.* **2007**, *129*, 14899.

(201) Gong, X. G.; Chiarotti, G. L.; Parrinello, M.; Tosatti, E. *Phys. Rev. B: Condens. Matter* **1991**, *43*, 14277.

(202) Martin, T. P. *Phys. Rep.* **1996**, *273*, 199.

(203) Häussermann, U.; Simak, S. I.; Abrikosov, I. A.; Lidin, S. *Chem.—Eur. J.* **1997**, *3*, 904.

(204) King, R. B.; Schleyer, P. V. R. In *Theory and Concepts in Main-Group Cluster Chemistry*; Driess, M., Nöth, H., Eds.; Wiley-VCH: Weinheim, Germany, 2004; p 1.

(205) King, R. B. *J. Organomet. Chem.* **2002**, *646*, 146.

(206) Fehlner, T.; Halet, J.-F.; Saillard, J.-Y. *Molecular Clusters*; Cambridge University Press: Cambridge, U.K., 2007.

(207) Köppe; R. Schnöckel, H. Unpublished work.

(208) Possibly fluctional structures in direction to the above mentioned C₃ᵥ structure of an Al₇ core (section 6.1.1) play a certain role. In this case, stronger cluster-to-cluster interactions may result, where the

central Al atom of one Al_7R_6 ($\sim D_{3d}$) is converted to be the capped Al atom of a new C_{3v} cluster (capped trigonal antiprism caused by an interaction with the neighbor species in the cluster chain).[144,209]

(209) Hadiprono, G. Ph. D. thesis, Karlsruhe, 2005.
(210) Krogmann, K. *Angew. Chem., Int. Ed.* **1969**, *8*, 35.
(211) Kapustinskii, A. F. *Q. Rev. Chem. Soc.* **1956**, *10*, 283.
(212) Jenkins, H. D. B.; Liebman, J. F. *Inorg. Chem.* **2005**, *44*, 6359.
(213) Glasser, L.; Jenkins, H. D. B. *Chem. Soc. Rev.* **2005**, *34*, 866.
(214) Gong, X. G.; Sun, D. Y.; Wang, X.-Q. *Phys. Rev. B* **2000**, *62*, 15413.
(215) Frenzel, J.; Gemming, S.; Seifert, G. *Phys. Rev. B* **2004**, *70*, 235404.
(216) Glaunsinger, W. S.; Sienko, M. J. *J. Chem. Phys.* **1975**, *62*, 1883.
(217) Zurek, E.; Edwards, P. P.; Hoffmann, R. *Angew. Chem., Int. Ed.* **2009**, *48*, 8198.
(218) Zaanen, J.; Sawatzky, G. A.; Allen, J. W. *Phys. Rev. Lett.* **1985**, *55*, 418.
(219) Zaanen, J.; Sawatzky, G. A. *J. Solid State Chem.* **1990**, *88*, 8.
(220) Gong, X. G.; Guido, L. C.; Parrinello, M.; Tosatti, E. *Phys. Rev. B* **1991**, *43*, 14277.
(221) Hagel, J.; Kelemen, M. T.; Fischer, G.; Pilawa, B.; Wosnitza, J.; Dormann, E.; von Löhneysen, H.; Schnepf, A.; Schnöckel, H.; Neisel, U.; Beck, J. *J. Low Temp. Phys.* **2002**, *129*, 133.
(222) Bakharev, O. N.; Zelders, N.; Brom, H. B.; Schnepf, A.; Schnöckel, H.; de Jongh, L. J. *Eur. Phys. J. D* **2003**, *24*, 101.
(223) Bakharev, O. N.; Bono, D.; Brom, H. B.; Schnepf, A.; Schnöckel, H.; de Jongh, L. J. *Phys. Rev. Lett.* **2006**, *96*, 117002.
(224) Bono, D.; Schnepf, A.; Hartig, J.; Schnöckel, H.; Nieuwenhuys, G. J.; Amato, A.; de Jongh, L. J. *Phys. Rev. Lett.* **2006**, *97*, 077601.
(225) Bono, D.; Bakharev, O. N.; Schnepf, A.; Hartig, J.; Schnöckel, H.; Jongh, L. J. d. *Z. Anorg. Allg. Chem.* **2007**, *633*, 2173.
(226) Hechtfischer, D.; Karcher, R.; Luders, K. *J. Phys. F: Met. Phys.* **1973**, *3*, 2021.
(227) Kerlin, A. L.; Clark, W. G. *Phys. Rev. B* **1975**, *12*, 3533.
(228) Magnetization measurements in the field-cooled run show the true Meissner fraction associated with the field expulsion.[225].
(229) Buckel, W.; Kleiner, R. *Superconductivity: Fundamentals and Applications*; Wiley-VCH: Weinheim, Germany, 2004.
(230) Kinsel, T.; Lynton, E. A.; Serin, B. *Phys. Lett.* **1962**, *3*, 30.
(231) The decrease of the electronic mean free path (90% c → 12% c) was measured via the $\mathbf{B}_{c2}(0)$ values of the two samples to be 1/20; consequently the coherence length ξ is reduced to $35 \times 20^{-0.5} = 7.8$ nm.[225].
(232) Dubson, M. A.; Herbert, S. T.; Calabrese, J. J.; Harris, D. C.; Patton, B. R.; Garland, J. C. *Phys. Rev. Lett.* **1988**, *60*, 1061.
(233) Friedel, J. *J. Phys. II* **1992**, *2*, 959.
(234) Already 20 years ago, L. J. de Jongh had pointed out this important aspect: de Jongh, L. J. *Nato Advanced Research Workshop: Organic and Inorganic Low Dimensional Crystalline Materials*; Plenum Press: New York, 1987; p 231.
(235) Richards, A. F.; Hope, H.; Power, P. P. *Angew. Chem., Int. Ed.* **2003**, *42*, 4071.
(236) Sekiguchi, A.; Ishida, Y.; Kabe, Y.; Ichinohe, M. *J. Am. Chem. Soc.* **2002**, *124*, 8776.
(237) Brynda, M.; Herber, R.; Hitchcock, P. B.; Lappert, M. F.; Nowik, I.; Power, P. R.; Protchenko, A. V.; Ruzicka, A.; Steiner, J. *Angew. Chem., Int. Ed.* **2006**, *45*, 4333.
(238) Prabusankar, G.; Kempter, A.; Gemel, C.; Schroter, M. K.; Fischer, R. A. *Angew. Chem., Int. Ed.* **2008**, *47*, 7234.
(239) The Zintl chemistry of Ge is not mentioned here.[240,241,242].
(240) Spiekermann, A.; Hoffmann, S. D.; Fässler, T. F.; Krossing, I.; Preiss, U. *Angew. Chem., Int. Ed.* **2007**, *46*, 5310.
(241) Esenturk, E. N.; Fettinger, J.; Eichhorn, B. *Polyhedron* **2006**, *25*, 521.
(242) Goicoechea, J. M.; Sevov, S. C. *J. Am. Chem. Soc.* **2005**, *127*, 7676.
(243) Schnepf, A.; Köppe, R. *Angew. Chem., Int. Ed.* **2003**, *42*, 911.
(244) Schnepf, A.; Drost, C. *Dalton Trans.* **2005**, 3277.
(245) Koch, K.; Schnepf, A.; Schnöckel, H. *Z. Anorg. Allg. Chem.* **2006**, *632*, 1710.
(246) Schnepf, A. *Angew. Chem., Int. Ed.* **2003**, *42*, 2624.
(247) Schenk; C. Henke; F. Neumaier; M. Olzmann; M. Schnöckel; H. Schnepf A. *Z. Anorg. Allg. Chem.* **2010**, in press.
(248) Schnepf, A. *Eur. J. Inorg. Chem.* **2008**, 1007.
(249) Schnepf, A. *Chem. Commun.* **2007**, 192.
(250) Schnepf, A.; Schenk, C. *Angew. Chem., Int. Ed.* **2006**, *45*, 5373.
(251) Schrenk, C.; Schellenberg, I.; Pöttgen, R.; Schnepf, A. *Dalton Trans.* **2010**, *39*, 1872.
(252) Guloy, A. M.; Ramlau, R.; Tang, Z. J.; Schnelle, W.; Baitinger, M.; Grin, Y. *Nature* **2006**, *443*, 320.
(253) Fässler, T. F. *Angew. Chem., Int. Ed.* **2007**, *46*, 2572.
(254) Schenk, C.; Schnepf, A. *Chem. Commun.* **2008**, 4643.
(255) Teo, B. K.; Shi, X.; Zhang, H. *J. Am. Chem. Soc.* **1992**, *114*, 2743.
(256) Schmid, G. *Chem. Soc. Rev.* **2008**, *37*, 1909.
(257) Schmid, G.; Pfeil, R.; Böse, R.; Bandermann, F.; Meyer, S.; Calis, G. H. M.; Vandervelden, W. A. *Chem. Ber.* **1981**, *114*, 3634.
(258) However, although there are a great number of chemical and physical methods proving this structure, a precise structure determination via X-ray experiments is missing so far.[256]
(259) Smaller metalloid Au clusters with similar AuSAu bonding motifs are not discussed here.[260−263].
(260) Donkers, R. L.; Lee, D.; Murray, R. W. *Langmuir* **2004**, *20*, 1945.
(261) Donkers, R. L.; Lee, D.; Murray, R. W. *Langmuir* **2008**, *24*, 5976.
(262) Pei, Y.; Gao, Y.; Shao, N.; Zeng, X. C. *J. Am. Chem. Soc.* **2009**, *131*, 13619.
(263) Heaven, M. W.; Dass, A.; White, P. S.; Holt, K. M.; Murray, R. W. *J. Am. Chem. Soc.* **2008**, *130*, 3754.
(264) A comparison of their structures with the structure of the metalloid cluster Si@$Al_{56}R_{12}$, **46**, has already been published[194] and is briefly mentioned in section 6.2.3 (Figure 36).
(265) Schnöckel, H.; Schnepf, A.; Whetten, R. L.; Schenk, C.; Henke, P. *Z. Anorg. Allg. Chem.* (in preparation).
(266) Though this approach has been successful, however, unexpected for the chemical community in the beginning, for the metastable fullerenes, that is, for naked clusters of the nonmetallic element carbon, it is music of the future to get crystals of monodispersed particles of precious metals; for base metals, it seems to be more utopian. Furthermore, the bonding and structure of both hypothetical and real nanoscaled species (e.g., Au_n and C_n) are completely different from those of the metalloid clusters with their highly complex bonding and unexpected properties discussed here. .
(267) Simon, A. *Coord. Chem. Rev.* **1997**, *163*, 253.
(268) The situation strongly reminds one of the high sophisticated investigations of the boranes by Alfred Stock nearly 100 years ago.[269,270] However, the importance of these results for the development of the entire chemistry, and especially of general bonding principles, was only realized after the essential investigations by scientists like W. N. Lipscomb some decades later.[271]
(269) Stock, A.; Massenez, C. *Ber. Dtsch. Chem. Ges.* **1912**, *45*, 3539.
(270) Stock, A. *Hydrides of Boron and Silicon*; Cornell University Press: Ithaca, NY, 1933.
(271) Lipscomb, W. N. *Angew. Chem.* **1977**, *89*, 685. See also http://nobelprize.org/chemistry/laureates/1976/lipscomb-lecture.pdf, accessed 2005.
(272) Steiner, J.; Stösser, G.; Schnöckel, H. *Z. Anorg. Allg. Chem.* **2004**, *630*, 1879.